TRANSITIONS IN BULK POLYMERS

by

Ian Harvey Hillier, B.Sc., A.R.C.S.

A Thesis submitted for the degree of
Doctor of Philosophy
of the University of London

Department of Chemistry,
Imperial College of Science and Technology,
London, S.W.7.

June 1964

ACKNOWLEDGEMENTS

It is with gratitude that I acknowledge the neverfailing advice and encouragement of my supervisor, Professor Manfred Gordon.

I would also like to thank members of the University of London Computer Unit for their helpful discussions on the numerical and programming methods employed.

Thanks are also due to the D.S.I.R. for a Research Studentship.

Abstract

The bulk crystallization kinetics of polymethylene, polystyrene, poly-(ethylene oxide), polypropylene and polybutene have been studied dilatometrically. Extensive use of computers has made possible improvements in the statistical analysis.

The kinetics of polymethylene crystallization in the absence of the usual secondary crystallization have been fitted to variants of a single-crystal folded-chain platelet model. Non-coherent, secondary nucleation leading to spherulitic growth is rejected. The detailed morphology of crystalline polymers is notoriously complex, but certain broad features of the crystallization process are supported by this work. Thus, there appear to be two kinds of coherent, secondary two-dimensional nucleation acts, one associated with the corner sites and another with the face sites on the growing platelet. A single rate equation covering both the primary and secondary crystallization has been deduced and amply verified. The secondary process, which can be kinetically isolated is fitted to an equation by Eyring, which generalizes Maxwell's treatment for the relaxation of matter. Electron microscopy supports the existence of lamellae in polymethylene.

This single crystal platelet model which can also describe spherulitic crystallization is further shown to fit the

crystallization of polystyrene, and poly-(ethylene oxide). When the crystallization kinetics of these polymers, and polymethylene are analysed according to this model, a number of similarities become apparent. The temperature dependence of the rate constants associated with the model is very similar for all three polymers, and the residual deviations from the model are strikingly similar for polymethylene and poly-(ethylene oxide).

The crystallization kinetics of polybutene and polypropylene are described by the simple Avrami picture of the radial growth of spherulites. This radial growth rate is constant for polybutene, and diffusion controlled for polypropylene.

By iterative methods of solving difference equations (or by a Monte Carlo method) statistical parameters are calculated for a number of models concerned with the progressive random occupation of sites on a linear lattice subject to specified restrictions. Examples of applications are cited from the field of crystallization or chemical reactions of chain polymers, sorption in graphite, and the close packing of hard spheres in one dimension.

INDEX

Introduction 1

Chapter I
The Experimental Determination of the Crystallization Rate 4

1.1 Sample Preparation 4
1.2 Dilatometer Construction 6
1.3 Temperature Stability during Isothermal Runs 8
1.4 Execution of Kinetic Runs 9
1.5 Melting Point Determination 11
1.6 Microscopic Investigations 13

Chapter II
Interpretation of Dilatometric Data 14

2.1 Derivation of General Rate Equation 14
2.2 Particular Cases of the General Rate Equation 17
2.3 The Avrami Equation 19
2.4 Deviations from the General Rate Equation 20
2.5 Temperature Dependence of Growth Rate 22
2.6 Crystallization after Partial Melting 26
2.7 Statistical Analysis of Dilatometric Data 27

Chapter III
The Kinetics of Bulk Crystallization of Polymethylene 35

3.1 Morphology of Solution and Bulk Crystallized Polyethylene 35
3.2 Previous Kinetic Studies 41
3.3 A Single Crystal Model for the Primary Crystallization of Polymethylene 44
3.4 The Secondary (Post-Avrami) Crystallization of Polymethylene 77
3.5 Crystallization after Partial Melting('Seeding') 96

Chapter IV
The Crystallization of Polypropylene, Polybutene, Poly-(ethylene oxide) and Polystyrene 99

4.1 Morphology 99
4.2 The Crystallization of Polypropylene 100
4.3 The Crystallization of Polybutene 108
4.4 The Crystallization of Poly-(ethylene oxide) 115
4.5 The Crystallization of Polystyrene 121

Chapter V
Statistics of Random Placement, Subject to Restrictions, on a Linear Lattice 136

References 156

Appendix (Tabulated Results) 160

INTRODUCTION

The kinetic crystallization process which occurs when a molten polymer is cooled below its melting temperature is rate determined by the nucleation and growth of the crystalline bodies, and their subsequent impingement to fill part or whole of the available space. The growth rate must be related to the shape, and growth mechanism of the crystalline regions.

Crystallization kinetics of polymers have been traditionally interpreted (Mandelkern 1956, 1958) although with limited success, in terms of the nucleation and growth of spherulites. These are spherical crystalline bodies, which are observed by optical microscopy in most bulk polymers. A typical structure of this type might have a diameter of $\sim$ 0.1 mm. On a molecular level, the spherulite structure is usually described in terms of the 'fringed micelle' model (Flory 1953, Fig.1). The crystallites are indicated by a parallel array of portions of polymer chains. The ordered regions are randomly arranged relative to one another, and are connected by portions of the chains passing through amorphous or disordered regions.

When observed under the polarizing microscope, between crossed Nicols, spherulites exhibit a range of birefringent structures. Apart from the usual Maltese cross, zig-zag and ring-shaped extinction lines are found (Keller 1955a, 1955b, 1955c). These are interpreted in terms of particular orientations of the

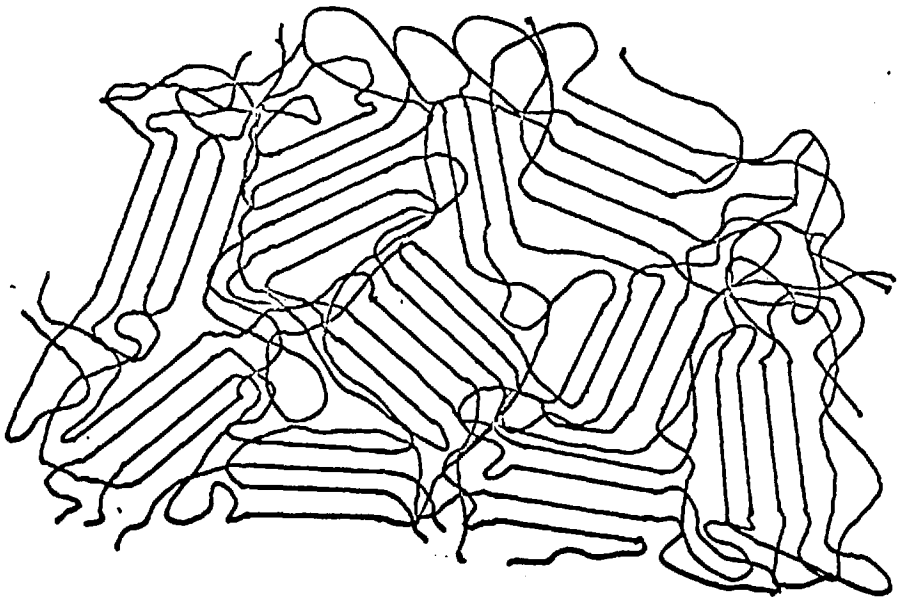


Fig 1. Schematic representation of fringed micelle structure.

crystallites. The common feature of all arrangements is that molecular chains are perpendicular to the radii of the spherulite.

One of the most important discoveries in polymer science during the last decade is the existence of single polymer crystals (Keller 1962). In these, a polymer chain does not pass through a number of separate crystalline and amorphous regions, but is completely contained in a single crystalline entity. The structure of these single crystals, their occurence in the bulk, and their relationship to spherulites, will be used to interpret kinetic data, and forms a central theme of this thesis.

CHAPTER I

The Experimental Determination of the Crystallization Rate

The crystallization rate is measured by following the contraction of the sample at a constant temperature below its melting point, as a function of time. In this work, the dilatometer has been designed for smaller samples than are normally used. This has the advantage that rapid temperature equilibration takes place (less than 1 min.) when the sample is transferred from one thermostat bath to another. This is especially important when 'seeded' runs (section 2.6) are being carried out. The various aspects of the dilatometer construction will now be described.

1.1 Sample Preparation

The samples used in this work were obtained from various commercial sources in the form of powders or 'shavings', and were used without any further purification. The polymer was compressed into a cylinder, approximately 3 mm.diameter, and 1 - 1.5 cm.long, weighing less than 100 mg in a spring-loaded steel vacuum press (see Fig.1.1). The press was then heated to 20 ^{o}C above the melting temperature of the polymer in vacuo ($< 10^{-4}$ mm.mercury) for 15 minutes and allowed to cool in vacuo. The furnace used consisted of a glass tube, slightly larger than the press, the outside being wound with nichrome wire, and covered with asbestos cement. The moulded cylinder of polymer, thus freed from any air, was weighed, and sealed in the dilatometer.

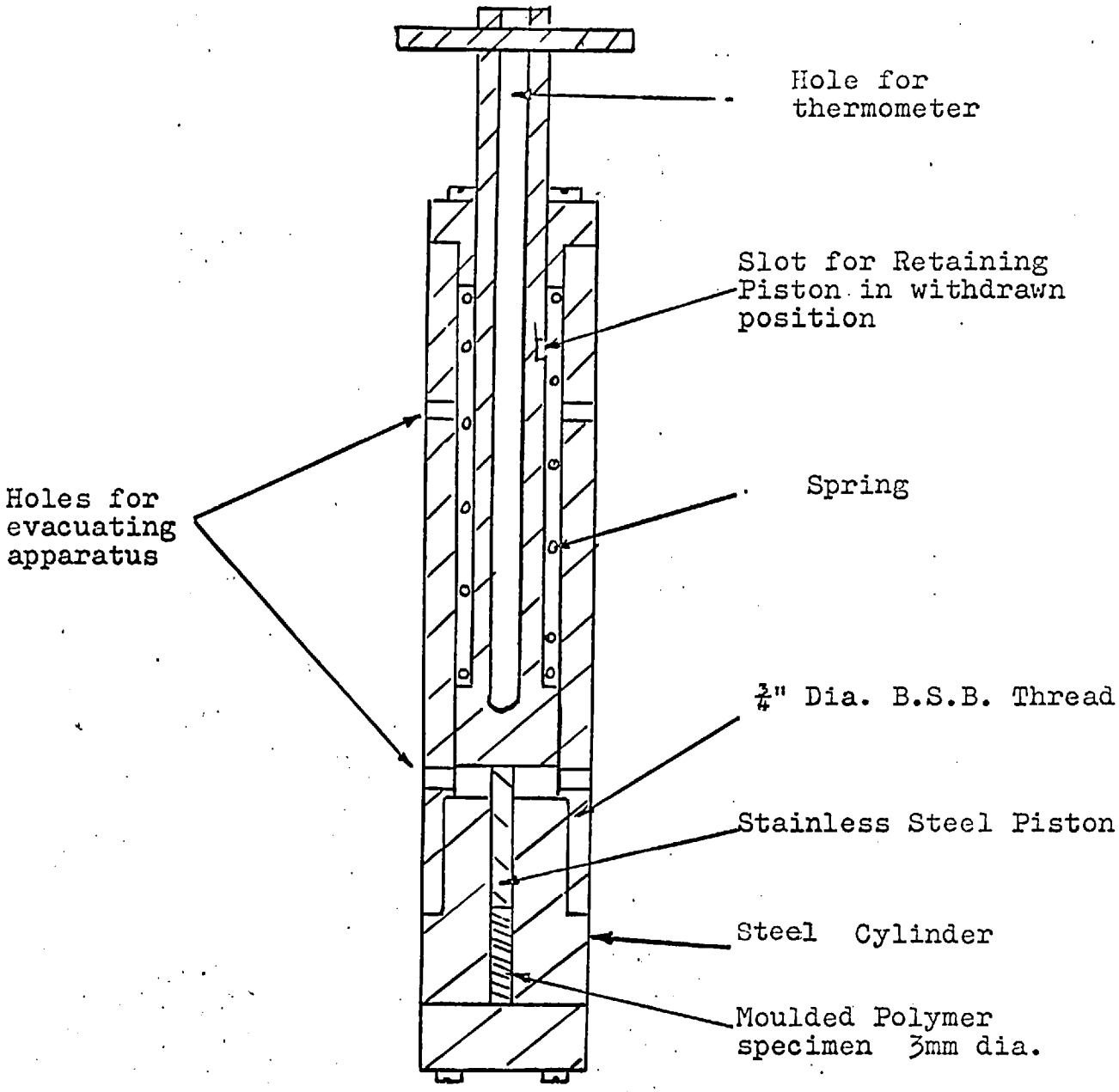


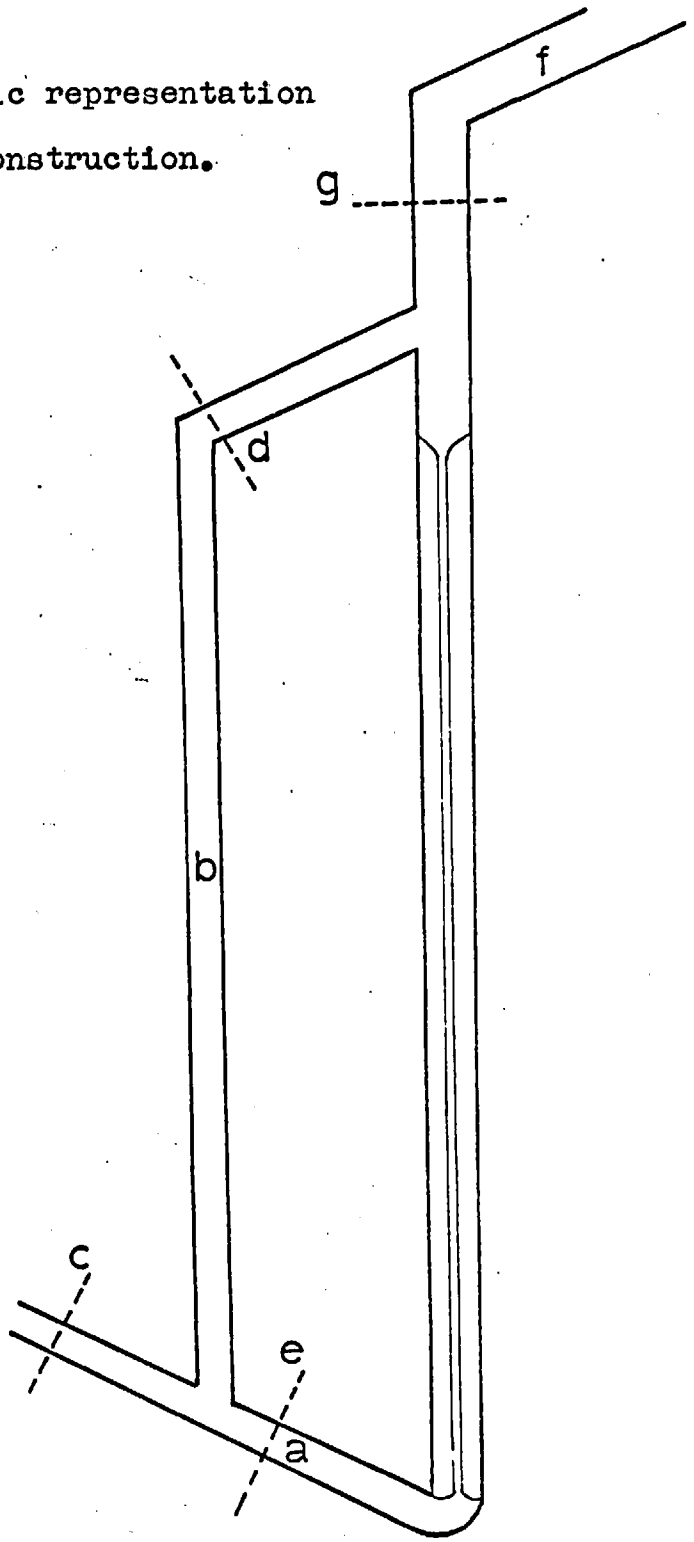
FIGURE1.1

SKETCH OF MOULDING PRESS

1.2 Dilatometer Construction

The measuring capillaries (~ 20 cm.long) in all the dilatometers constructed consisted of 'Veridia' precision bore tubing. A sample was checked for uniformity of bore by measuring a length of mercury thread. It was found that the variations along its length was only ±0.1%. The glass system from which the dilatometer is finally constructed is shown in Fig.1.2. The sample is to be contained in the tube a, the diameter of which is only slightly greater than that of the polymer sample. This tube is inclined at about 45°, to prevent the molten polymer from blocking the measuring capillary. The by-pass tube b, connecting the sample holder to the top of the measuring capillary is necessary for evacuation of the dilatometer, owing to the small bore of the capillary used (approximately 0.38 mm). The glass system, after cleaning with nitric acid, and sealing at c, is evacuated (less than 10^{-4} mm.mercury) and 'flamed' to remove sorbed gases from the walls of the capillary and sample holder. It is then opened at c, the polymer sample inserted into a and resealed. After re-evacuation, the dilatometer is sealed at d and e, thus removing the by-pass link. The dilatometer is then filled with mercury. It was found necessary to distil the mercury twice in the same vacuum system to prevent gas bubbles forming later during the heating and cooling cycles associated with the kinetic measurements. The second distillation

Fig.1.2- Schematic representation of dilatometer construction.



condensed the mercury above the dilatometer in f, which filled the space surrounding the polymer sample via the capillary. When the dilatometer was full of mercury to the top of the capillary the dead space above the mercury was filled with 1/2 atmosphere of dry, oxygen-free nitrogen and the dilatometer finally sealed at g. During the subsequent kinetic runs, the mercury height was adjusted by using the side-arm which remained after sealing at d as a mercury reservoir. The nitrogen pressure above the capillary was designed to minimize variations in the meniscus height caused by the pressure fluctuations of any small gas bubbles which might form during kinetic runs, due to incomplete degassing of sample, mercury or dilatometer.

1.3 Temperature Stability during Isothermal Runs

The extreme sensitivity of the crystallization rate to crystallization temperature (section 2.5) necessitates a high degree of temperature stability being maintained during the isothermal crystallization runs. Large (13 ℓ) Dewar vessels, completely silvered except for two vertical observation slits opposite one another, and containing polyethylene glycol, with 2-mercapto-benzolthiazole added as an anti-oxidant, were used for all runs below 180 ^{o}C. In the case of the crystallization of polystyrene (Chapter 4) some runs were carried out above this temperature. A thermostated aluminium block (constructed by

Mr.G.R.Scantlebury) was used for this purpose. The bath heaters were made from Thermocoax heating wire consisting of nichrome wire contained in a stainless steel sheeth; insulation is by a layer of magnesium oxide between these. The wattage necessary to maintain a bath at a given temperature was shared between two such heaters. One was permanently on, giving approximately 80% of the power needed, the secondary heater being switched by means of a mercury contact regulator. The Dewars were covered with asbestos lids containing holes for the heaters, stirrer, thermometer and temperature regulator. An asbestos plug with a vertical stainless steel rod attached to it, fitted into a further hole. The dilatometer, attached to this rod with stainless steel clips could be rapidly transferred between thermostated tanks at different temperatures. The bath temperature was measured by Beckmann thermometers calibrated against National Physical Laboratory calibrated thermometers. Temperature stability of $\pm 0.01\ ^{o}C$ was achieved in the thermostat baths. Variations of meniscus height due to thermal fluctuations can be neglected under these conditions.

1.4 Execution of Kinetic Runs

The dilatometer, attached to a stainless steel rod is immersed in a bath maintained at approximately 20 ^{o}C above the melting temperature of the polymer for 15 minutes to melt the

sample completely. It has been shown (Banks, Gordon, Roe and Sharples 1963a) for polyethylene, that a melt temperature ranging from 0.9° to 70° above the melting temperature has no effect on the subsequent kinetic behaviour. Consequently, the persistence of nuclei above the melting point can be excluded. After the sample has been melted, the dilatometer is rapidly transferred to a bath, regulated at a temperature below its melting point, where the subsequent isothermal crystallization is followed, by observing the mercury meniscus height as a function of time through a cathetometer. A micrometer attachment allowed the height to be measured to ±0.001 cm. The total contraction obtained with 50 - 100 mg. of sample was 3 - 10 cms, depending on the polymer studied. The dilatometric data obtained are of sufficient accuracy to allow a critical assessment of the validity of the various models tested. To this end, the statistical analysis of the data has been improved by fitting various rate equations to the data using computers (section 2.7).

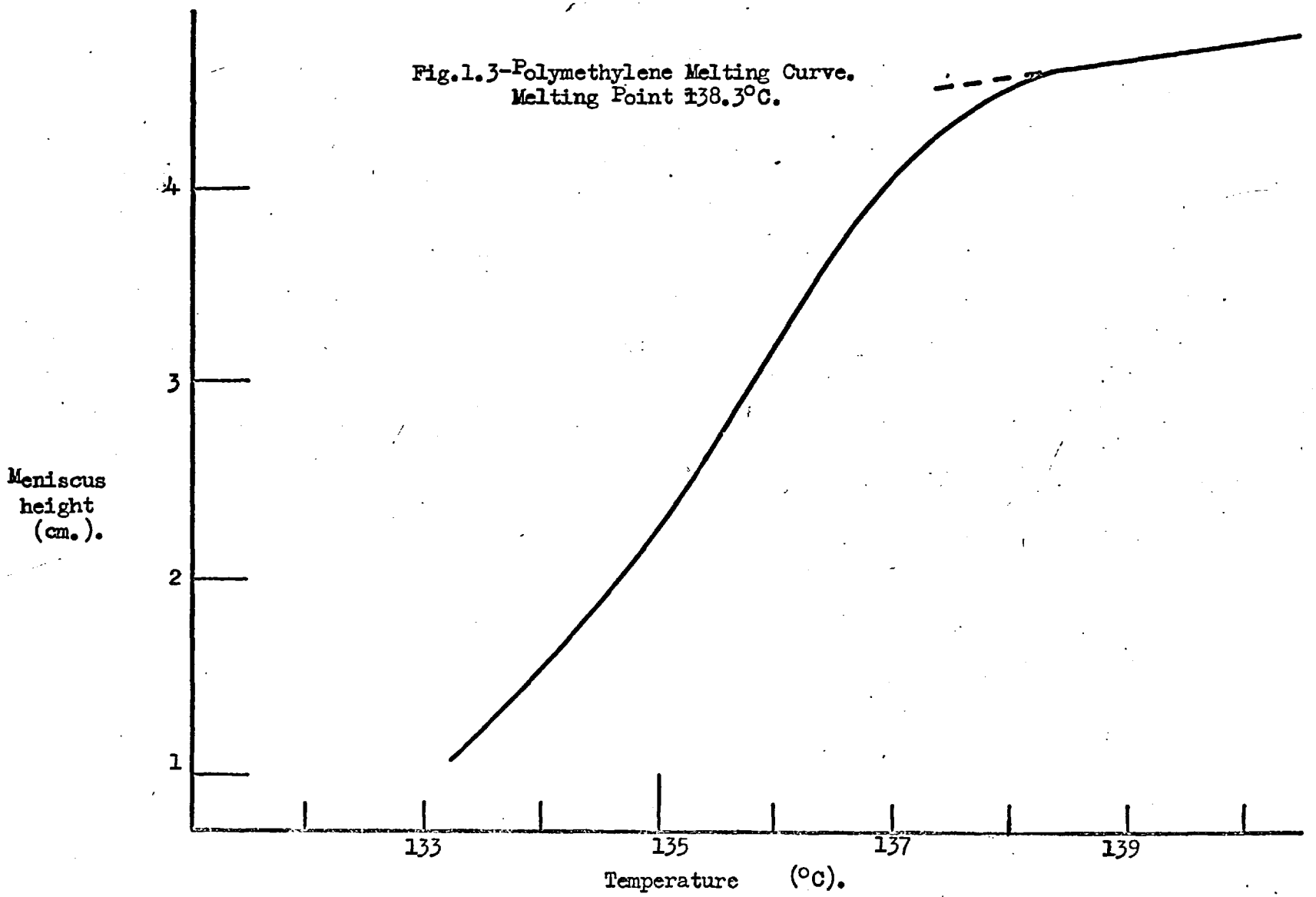
'Seeded' runs (section 2.6) are carried out by holding the crystallized sample at a temperature below the melting point to leave a (metastable) equilibrium degree of 'seed' crystallinity. The dilatometer is then transferred to a bath at a lower temperature where further isothermal crystallization is observed.

1.5 Melting Point Determination

The analysis of the temperature dependence of the crystallization rate constants requires a knowledge of the melting temperature of the polymer (section 2.5). The main features of melting in polymers, which differs from that for low molecular weight solids is the wide temperature range over which melting occurs. This effect is usually (Gubler and Kovacs 1959) attributed to the difference in stability of the crystals, arising from their size variation, and hence surface to volume ratio. Furthermore, at a given temperature, the expansion which accompanies the melting is not instantaneous, being much slower than the rate of heat transfer to the bulk material.

The mechanism of melting will be further discussed in section 3.5. At this point, the effect that the wide melting range and non-instantaneous expansion has on the melting-point determination is discussed. The melting point was found by progressively raising the temperature of a crystallized sample, until its volume was linearly dependent upon temperature. At this stage, the polymer will have completely melted. The temperature at which the volume vs. temperature curve departs from linearity gives the melting point. In the initial stages, the heating rate must be sufficiently high to avoid any recrystallization (section 3.4) while in the latter stages it must be slow enough to allow the volume relaxation to occur. Fig.1.3 shows such an

Fig.1.3-Polymethylene Melting Curve.
Melting Point 138.3°C.



equilibrium melting curve for polymethylene. The heating rate varied from 4×10^{-4} deg.sec.$^{-1}$ at the lower temperatures to 5×10^{-5} deg.sec.$^{-1}$ near the melting point.

1.6 Microscopic Investigations

Examination of thin films of polymer was carried out using a Cook Troughton and Simms polarizing microscope fitted with long working distance objectives. The sample between glass cover slips, was contained in a well in a copper hot-stage attached to the microscope. Temperature stability of ± 0.02 °C was maintained using a proportional temperature controller, with a platinum resistance thermometer as the sensing element.

Dispersed samples (section 3.1) were investigated using a Phillips 100 desk model electron microscope, the sample being deposited from aqueous suspension upon formvar supports.

CHAPTER II

Interpretation of Dilatometric Data

2.1 Derivation of General Rate Equation (Gordon 1963)

When a bulk polymer is cooled to below its melting point, the rate equation describing the crystallization is derived assuming that all the crystalline bodies growing in the melt are:-

1. randomly placed; and
2. grow with identical growth laws.

We define an entity as a crystalline body which has not impinged with any other. The crystalline bodies are taken as having a higher density than the amorphous polymer. The problem is to relate the overall volume contraction of the sample at time t which is proportional to the total volume of the crystalline bodies (growing with impingement) to the volume of an entity which has been in existence for this time. At time t, the overall degree of crystallinity (χ_t) is

$$\chi_t = \chi_\infty \left[1 - p\right] \qquad 2.1$$

where χ_∞ is the fractional crystallinity of a body, and (1 - p) is the fraction of the total volume occupied by the bodies. If the total volume is V, and the volume of the individual n entities is $V_1, V_2, \ldots\ldots, V_n$, then the chance p_i that a chosen point is not in the entity i is -

$$p_i = 1 - \frac{V_i}{V} \qquad 2.2$$

The chance p, that the point is not in any of the n entities is therefore:

$$p = \prod_{i=1}^{n} p_i = \prod_{i=1}^{n} (1 - V_i/V) \qquad 2.3$$

i.e.

$$\ln p = \sum_{i=1}^{n} \ln(1 - V_i/V) \qquad 2.4$$

If all the entities are small ($V_i \ll V$) compared to the total volume, $\ln(1 - \frac{V_i}{V})$ may be expanded as $-\frac{V_i}{V}$, when eq.24 becomes:

$$\ln p = -\sum_{i=1}^{n} (V_i/V) = -\rho(t)\,\bar{V}(t) \qquad 2.5$$

where $\rho(t)$ is the number per unit volume and $\bar{V}(t)$, the mean size of the entities at time t.

Eq.2.5 gives

$$p = \exp\left[-\rho(t)\,\bar{V}(t)\right] \qquad 2.6$$

The quantity p, the chance that a chosen point is not in any entity, is taken to be the chance p' that it is not in any body. This is exact for spheres growing linearly in radius with time, since a point which belongs to a given entity then lies either in the corresponding body, or in one of the bodies with which the entity overlaps. In cases involving discs or rods, identifying p and p' is an approximation as fragmentation of the growing entities may occur owing to impingement (section 3.3). Assuming

p and p' to be equal, equation 2.6 gives the chance that the chosen point is not in any body, which is also the amorphous fraction $(1 - \chi_t/\chi_\infty)$. Equations 2.1 and 2.6 give:

$$\chi_t = \chi_\infty[1 - \exp - \rho(t)\,\bar{V}(t)] \qquad 2.7$$

If all the bodies are born instantaneously, then $\rho(t)$ is constant (= c) and

$$\bar{V}(t) = V(t) \qquad 2.8$$

then $$\chi_t = \chi_\infty\,[1 - \exp - cV(t)] \qquad 2.9$$

where V(t) is the volume of an entity that has been in existence for time t. If nucleation is not instantaneous, then $\bar{V}(t)$ is given by:

$$\bar{V}(t) = \left[\int_0^t V(t-\tau)\left[d\rho(\tau)/d\tau\right]d\tau\right] \Big/ \left(\int_0^t \left[d\rho(\tau)/d\tau\right]d\tau\right) \qquad 2.10$$

This expression is the chance that an entity was born at time τ, multiplied by its volume at time t, when it has been in existence for time $(t - \tau)$ integrated from time zero to t.

As $$\int_0^t \left[d\rho(\tau)/d\tau\right]d\tau = \rho(t) \qquad 2.11$$

equation 2.10 becomes

$$\rho(t)\bar{V}(t) = \int_0^t V(t-\tau)\left[d\rho(\tau)/d\tau\right]d\tau \qquad 2.12$$

and substituting this in eq.2.7, the general rate equation

$$\chi_t = \chi_\infty\left[1 - \exp - \left\{\int_0^t V(t-\tau)\left[d\rho(\tau)/d\tau\right]d\tau\right\}\right] \qquad 2.13$$

is obtained. Using this equation, dilatometric data can be

fitted to various forms of the nucleation [$\rho(t)$] and growth [$V(t)$] rate laws. Special cases of eqs.2.9 and 2.13 which arise when the entities are of simple shape will now be considered.

2.2 Particular Cases of the General Rate Equation

The special forms of the rate equations (2.9 and 2.13) when the entities are rods, discs and spheres, will now be derived. In all these cases it is assumed that the growth rate (k_g) (radial for discs and spheres) is constant. This implies that the rate of inclusion of new material in the growing entity is proportional to the area of the growth front. Thus, for instantaneous nucleation, eq.2.8 becomes (Gordon 1963):

1. For rods of constant cross-sectional area A

$$V(t) = k_g A t \qquad 2.14$$

2. For discs of constant thickness d

$$V(t) = \pi d k_g^2 t^2 \qquad 2.15$$

3. For spheres

$$V(t) = 4\pi k_g^3 t^3/3 \qquad 2.16$$

For sporadic nucleation, when the number of nuclei $\rho(t)$ increases linearly with time

$$\rho(t) = k_n t \qquad 2.17$$

where k_n is the nucleation rate. The quantity $\rho(t)\bar{V}(t)$ must be evaluated using eq.2.10. Thus for sporadically

nucleated spheres

$$\rho(t)\bar{V}(t) = \int_0^t 4\pi[k_g(t-\tau)]^3 k_n/3 \quad d\tau \qquad 2.18$$

$$= \pi k_g^3 k_n t^4/3 \qquad 2.19$$

For sporadically nucleated rods and discs, the corresponding equations are:

$$\rho(t)\bar{V}(t) = Ak_g k_n t^2/2 \qquad 2.20$$

$$\rho(t)\bar{V}(t) = d\pi k_g^2 k_n t^3/3 \qquad 2.21$$

A second possible growth rate arises for diffusion controlled growth, when the radial growth rate is proportional to $1/t^{1/2}$ It can be readily shown that for spheres, eqs.2.16 and 2.19 become:

$$V(t) = 4\pi k_g^3 t^{3/2}/3 \qquad 2.22$$

and

$$\rho(t)\bar{V}(t) = 8\pi k_g^3 k_n t^{5/2}/15 \qquad 2.23$$

Corresponding equations may be derived for rods and discs. For all these examples, eq.2.7 can be written

$$\chi_t = \chi_\infty[1 - \exp - z t^n] \qquad 2.24$$

when n is an integer between 1 and 4 (or multiples of 1/2 between 1/2 and 5/2) and z is a constant depending upon the nucleation and growth rates. Assuming that the crystallinity at time t is proportional to the dilatometric contraction observed [h(o) - h(t)] eq.2.24 becomes

$$\frac{h(o) - h(t)}{h(o) - h(\infty)} = 1 - \exp(-zt^n) \qquad 2.25$$

where $h(o)$ and $h(\infty)$ are the initial and final dilatometric heights respectively. In terms of these measurements, the more general equation (2.7) becomes

$$\frac{h(o) - h(t)}{h(o) - h(\infty)} = 1 - \exp - [\rho(t)\overline{V}(t)] \qquad 2.26$$

A novel graphical representation of the variation of $\rho(t)\overline{V}(t)$ with time can be obtained by using eq.2.26 and plotting

$$-\ln\left[1 - \frac{h(o) - h(t)}{h(o) - h(\infty)}\right] = \rho(t)\overline{V}(t) \qquad 2.27$$

against time. This often provides useful guidance as to the form of the rate equation needed to fit the dilatometric data (Chapter 3).

2.3 The Avrami Equation

In the majority of examples found in the literature, dilatometric results are interpreted in terms of eq.2.25, which was first used by Avrami (1939) (by whose name it is generally known) to describe crystallization in metals. In the majority of polymers, optically resolveable spherulites are found, leading to an expected value of the Avrami exponent n (eq.2.25) of 3 or 4. Although no detailed fitting of this equation to experimental data was attempted, values of n of 4 for polyethylene (Tung and Buckser 1959) and polybutene (Boor and Mitchell 1963) and 3 for polypropylene (Griffith and Ranby 1959), have been

claimed. Recent work on polyethylene (Banks et al. 1963a) and poly-(decamethylene terephthalate) (Sharples and Swinton 1963), has cast doubt as to whether integral values of n are in fact found, and emphasizes the need for rigorous statistical analysis of the dilatometric data (section 2.7).

2.4 Deviations from the General Rate Equation

The derivation of the general Avrami equation (2.25) using eqs.2.1 and 2.5 assumes that the total volume V of the system is constant throughout the crystallization. However, owing to the difference in density between the liquid phase, and the crystalline bodies, this volume will decrease as crystallization proceeds, owing to the higher density of the crystalline regions.* A further approximation is introduced by equating the volume fraction of amorphous material $(1 - \chi_t/\chi_\infty)$ to the dilatometric measurements $1 - [h(o) - h(t)]/[h(o) - h(\infty)]$ (eq.2.25). This latter approximation will be discussed first. Let

ρ_l be the density of the liquid phase

ρ_c be the density of the crystalline bodies

$V_l(t)$ be the volume of the liquid phase at time t

$V_c(t)$ be the volume of the crystalline bodies at time t

V_o be the volume of the system at zero time

V_∞ be the volume of the system at infinite time

V_t be the volume of the system at time t

* Professor F.C. Frank has pointed out that this derivation due to Price is incorrect as the positions of the bodies will no longer be uncorrelated when the sample contracts.

The volume fraction of amorphous polymer (θ) is given as

$$\theta = V_l(t)/V_t \qquad 2.28$$

Also,

$$V_t = V_l(t)[1 - \rho_l/\rho_c] + V_o\rho_l/\rho_c \qquad 2.29$$

giving

$$V_l(t) = (V_t - V_o\rho_l/\rho_c)/(1 - \rho_l/\rho_c) \qquad 2.30$$

Substitution of eq.2.30 into eq.2.28 gives

$$\theta = [1 - (V_o/V_t)(\rho_l/\rho_c)] / (1 - \rho_l/\rho_c) \qquad 2.31$$

It can be readily shown that the experimentally measured quantity $[h(t) - h(\infty)] / [h(o) - h(\infty)]$ is related to θ by the expression

$$[h(t) - h(\infty)] / [h(o) - h(\infty)] \quad (V_o/V_t) = \theta \qquad 2.32$$

The effect of the first approximation, that of assuming the volume (V_t) of the polymer to be constant, for use in

$$(1 - \theta) = 1 - \exp - (\sum_{i=1}^{n} V_i/V_t) \quad \text{(eqs. 2.1, 2.5)} \qquad 2.33$$

may be seen by inserting V_t from eq.2.31 into eq.2.33, giving

$$(1 - \theta) = 1 - \exp -\left\{(\sum_{i=1}^{n} V_i/V_o)/ \ (\rho_l/\rho_c)[1 - \theta(1 - \rho_l/\rho_c)]^{-1}\right\} \qquad 2.34$$

For the simple Avrami model,

$$(\sum_{i=1}^{n} V_i/V_o) = kt^n \text{ (section 2.2)} \qquad 2.35$$

when eq.2.34 becomes

$$(1 - \theta) = 1 - \exp -\left\{(kt^n)/ \ (\rho_l/\rho_c)[1 - \theta(1 - \rho_l/\rho_c)]^{-1}\right\} \qquad 2.36$$

which can be compared to the simple Avrami equation (2.24).

This equation (2.36) cannot be solved analytically for θ, but Price (1964) has estimated the error which will be incurred by using eq.2.25 in place of eq.2.36. He estimates that for $0.95 > \rho_l/\rho_c > 0.85$, n will be increased by less than 0.1 over 80% of the crystallization. This change is so small that in the analysis of our kinetic data we use the approximate Avrami equation (2.25). In two further cases, the general rate equation (2.7) is approximate. The first, which arises owing to the possible fragmentation when the entities are rods or discs is discussed fully when a single crystal platelet model is fitted to the crystallization of polymethylene (section 3.3). A second approximation is introduced when nucleation is not instantaneous, as eq. 2.7 implies that a fictitious entity nucleated and growing inside another can never outgrow the bounds of its host, and cannot therefore encroach on the amorphous space. This is geometrically exact for spheres with a constant radial growth rate, but never exact for discs and rods. Eq.2.7 therefore overestimates the crystallinity at all times in these two cases. These two approximations will be discussed further when the kinetics of polyethylene crystallization are interpreted (Chapter 3).

2.5 Temperature Dependence of Growth Rate

The crystallization rate of all polymers is extremely sensitive to the crystallization temperature. Thus for

polyethylene (Tung and Buckser 1959, Banks et al. 1963a) z (eq.2.25) changes by a factor of 10^3 for a temperature change of only 3 °C. This sensitivity to crystallization temperature has been explained on the assumption that growth of the crystalline bodies proceeds by a process of secondary nucleation at the growth front (Mandelkern 1958). The nucleation theory of Turnbull (1949) gives the steady state nucleation rate ($\dot{N}$) for a condensed system as

$$\dot{N} = K\frac{NkT}{h} \exp\left(\frac{\Delta S^*}{k}\right) \exp\left(\frac{-\Delta H^*}{kT}\right) \exp\left(\frac{-\Delta \phi^*}{kT}\right) \qquad 2.37$$

where ΔH^* is the heat of activation of the elementary jump rate process at the supercooled liquid - nucleus interface;

ΔS^* is the corresponding entropy of activation; and

$\Delta \phi^*$ is the free energy of formation of a nucleus of critical size.

$\Delta \phi^*$ is determined by the balance between the surface free energies (σ) associated with the particular model, and the bulk free energy of fusion (Δf). At this stage, we shall discuss only the simple three-dimensional bundle-like nucleus (Fig.2.1), a two-dimensional chain-folded nucleus, applicable to single crystals, will be discussed in relation to polyethylene in Chapter 3. For the three dimensional nucleus, the free energy of formation ($\Delta \phi$) is:

$$\Delta \phi = 2ab\sigma_e + 2al\sigma + 2bl\sigma - abl(\Delta f) \qquad 2.38$$

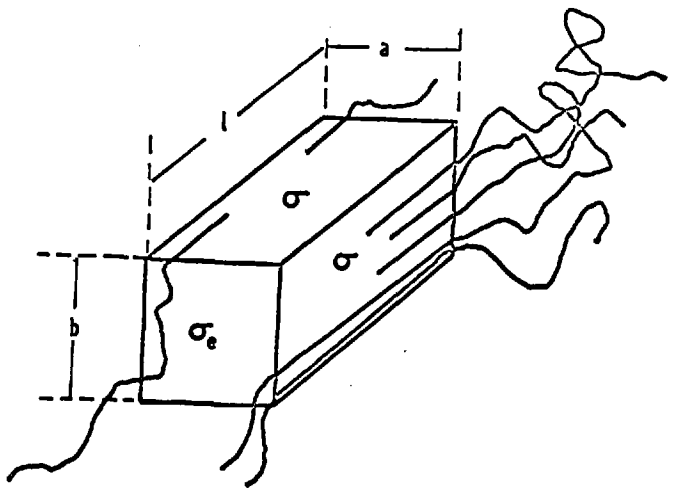


Fig.2.1.- Bundlelike nucleus.

Ordinary symbols are used to denote the dimensions a,b, and l, and the lateral and the end surface free energies, σ and σ_e.

$\Delta\phi^*$ corresponds to the saddle point of the free energy surface and is found by putting

$$\left(\frac{\partial \Delta\phi}{\partial a}\right)_{b,\,l} \quad \left(\frac{\partial \Delta\phi}{\partial b}\right)_{a,\,l} \quad \text{and} \quad \left(\frac{\partial \Delta\phi}{\partial l}\right)_{a,\,b} \quad \text{equal to zero.}$$

The dimensions of the critical nucleus, (a^*, b^*, l^*) and the free energy of formation ($\Delta\phi^*$) are then found to be:

$$a^* = 4\sigma / \Delta f \qquad 2.39$$

$$b^* = 4\sigma / \Delta f \qquad 2.40$$

$$l^* = 4\sigma_e / \Delta f \qquad 2.41$$

$$\Delta\phi^* = 32\,\sigma^2\,\sigma_e / (\Delta f)^2 \qquad 2.42$$

At the melting-point (T_m),

$$\Delta S_{fusion} = \Delta H_{fusion} / T_m \qquad 2.43$$

With the assumption that ΔS does not vary with temperature near the melting-point, the free energy of fusion at temperature T, may be approximated by

$$\Delta f = \Delta H_{fusion} \left[1 - \frac{T}{T_m}\right] \qquad 2.44$$

$$= \Delta H_{fusion} (\Delta T)/T_m \qquad 2.45$$

where $\Delta T = T_m - T$ 2.46

Eqs.2.42 and 2.45 give

$$\Delta\phi^* = 32\,\sigma^2\,\sigma_e T_m^{\,2} / \Delta H_{fusion}^2 (\Delta T)^2 \qquad 2.47$$

Eqs.2.47 and 2.37 give

$$\dot{N} \propto \exp - (32\,\sigma^2\,\sigma_e T_m^{\,2}) / [\Delta H_{fusion}^2 (\Delta T)^2\, kT] \qquad 2.48$$

i.e. $\ln(\dot{N}) \propto -1/(\Delta T)^2$ 2.49

Eq.2.48 assumes that the temperature dependence of $\dot{N}$ is determined predominantly by the variation of the quantity $\Delta\phi^*/T$ with temperature. This will be true near the melting point, when the value of $^1/\Delta T$ will change more rapidly than $^1/T$. At low temperatures, the $^1/T$ value may become the most important. This can result in a maximum in the crystallization rate vs temperature plot, which is found in the case of polystyrene (Chapter 4). However, for polyethylene, the crystallization rate is only measurable within about 10 ^oC of the melting point, where the predominant term is $^1/(\Delta T)^2$.

The temperature dependence of the Avrami rate constant Z (eq.2.25) has been interpreted in terms of such a three-dimensional bundle-like nucleus, as this leads to a 'fringed-micelle' structure, which is used to describe the intra-spherulitic structure. Polyethylene (Banks et al.1963a) poly-(decamethylene sebacate) (Flory and McIntyre 1955) and poly-decamethylene terephthalate (Sharples et al.1963) are examples of polymers whose Avrami rate constant (Z) fit this $^1/(\Delta T)^2$ relationship.

2.6 Crystallization after Partial Melting

The overall rate of crystallization (eq.2.13) depends upon the nucleation [ρ (t)] and growth [V(t)] rates. The determination of the appropriate growth law is facilitated if

these two steps can be separated. This is attempted by incompletely melting the sample to leave 'seeds', and following the subsequent crystallization when the temperature is lowered. Hoffman, Weeks, and Murphy (1959) using poly (chlorotrifluorethylene) suggested that on partial melting, the growth from primary nuclei is reversed until at least some of the original nuclei remain. These were assumed to be capable of acting as 'seeds' when the polymer is again crystallized at a lower temperature. If the crystallization in the absence of 'seeds' is described by the Avrami equation (2.24), then the Avrami exponent n, on crystallization from 'seeds', would be expected to remain constant, or decrease by unity, depending on whether the nucleation in the unseeded crystallization was instantaneous, or sporadic. Hoffman et al.(1959) found that for poly (chlorotrifluorethylene) a decrease in n from 2 to 1 was found on 'seeding'. This result was interpreted in terms of one-dimensional growth of rods, sporadically nucleated in the unseeded experiments. It will be seen that in the polymers investigated here, a decrease in n is generally found on seeding, but in no case does a decrease by unity occur.

2.7 Statistical Analysis of Dilatometric Data

The kinetic data are traditionally interpreted in terms of the Avrami equation (2.25).

$$[h(o) - h(t)] / [h(o) - h(\infty)] = 1 - \exp - zt^n \qquad 2.50$$

by plotting (e.g. Parrini and Corrieri 1963)

$$\ln - \left[\ln\left(1 - [h(o) - h(t)]/[h(o) - h(\infty)]\right)\right] \quad \text{vs. } \ln(t)$$

The slope of this double logarithmic plot gives the value of the Avrami exponent n. This plot does not give a true indication of the goodness of fit of eq.2.50 mainly owing to the extreme sensitivity of the points at high values of t to the value of $h(t) - h(\infty)$. An improved method (Banks et al.1963a) involves the differentiation of eq.2.50 with respect to time to give

$$n = -t[dh(t)/dt]/\left([h(t) - h(\infty)]\ln [h(o) - h(\infty)]/[h(t) - h(\infty)]\right) \qquad 2.51$$

As dh(t)/dt can be calculated from successive pairs of results, n can be obtained for every stage of the crystallization as a function of the crystallinity [taken as proportional to $h(o) - h(t)$]. The rate constant z can then be calculated from the half-life $t_{1/2}$, and the average value of n,

$$z = \ln(2)/t^n_{1/2} \qquad 2.52$$

In the work presented here models are fitted which lead to more complex forms of the general rate equation (2.13) than the simple Avrami equation (2.24). A method of analysing the data is used which is not dependent upon the nucleation [$\rho(t)$] or growth [V(t)] rates having a simple form. Extensive use is made of electronic computers, all programs being written in Mercury

Autocode, and run on the Mercury Computer of London University or the Atlas Computer of Manchester University.

The general problem of curve fitting is to find the functional relationship between a quantity A (in this case the crystallinity χ), which can be measured, and a further quantity x (in this case the time) from a number of empirical data. If a functional relationship

$$A = A(x, \theta_1, \ldots\ldots, \theta_n) \qquad 2.53$$

is assumed, the problem is to evaluate the unknown parameters, $\theta_1, \ldots\ldots \theta_n$, from N values of A_i^{obs}. The most frequently used method for the solution of this problem is the principle of least squares, which states that the best estimates of the parameters are the values of θ which minimize the n-variable function,

$$Y(\theta_n) = \sum_{i=1}^{N} [A_i^{obs} - A_i(x_i, \theta_1, \ldots, \theta_n)]^2, \quad N \geqslant n \qquad 2.54$$

This equation can only be solved analytically if A is linear in $\theta_1, \ldots \theta_n$. In none of the examples encountered here is this the case, and iterative methods must be used. The considerations which influence the choice of the actual method used to minimize $Y(\theta_n)$, and hence to find $\theta_1, \ldots \theta_n$, are as follows:

(a) The method should converge from a starting vector θ_n, which may be a considerable distance from the minimum. In many cases, it has been found to be difficult to obtain good estimates

of a starting value for θ_n, especially when there are a large number of parameters.

(b) The optimum value of θ_n should be found with the minimum number of iterations or cycles. This is particularly important if $Y(\theta_n)$ contains functions requiring lengthy machine computation, such as integrals which have to be evaluated numerically.

(c) A minimum number of auxiliary functions associated with $Y(\theta_n)$ should be needed. Some methods require the derivatives of $Y(\theta_n)$ with respect to θ_n

Three methods of minimization have been examined and are now discussed very briefly.

1. The Newton-Raphson method (Strand, Kohl and Bonham 1963) is an extension to many variables of the well-known Newton method used for a single variable. It is used to find the zero of a function $F_k(\theta_1, \ldots \theta_n)$, which in this case is the derivative of $Y(\theta_n)$ with respect to θ_n

$$F_k(\theta_1, \ldots \theta_n) = \partial Y(\theta_1, \ldots \theta_n)/\partial \theta_k = 0 \qquad 2.55$$

$$k = 1, \ldots\ldots, n \qquad 2.56$$

This method expands eq.2.55 in a first-order Taylor series. The correction vector $\Delta\theta_n$ is then given in matrix notation as:

$$\Delta\theta_j = -[\partial F_k(\theta_n)/\partial \theta_j]^{-1} F_k(\theta_n) \qquad 2.57$$

$$k = 1, \ldots\ldots n$$

$$j = 1, \ldots\ldots n$$

This method has the disadvantage that it only converges if the starting vector θ_n is a good approximation. It also requires the derivatives of the function with respect to θ_n.

2. Fletcher and Powell's method (1963) uses the method of steepest descent when the function is far from the minimum. In this region the correction vector is

$$\Delta\theta_k \propto [-\partial Y(\theta_n)/\partial\theta_k] \Big/ \sum_{k=1}^{n} [\partial Y(\theta_n)/\partial\theta_k]^2 \qquad 2.58$$

the magnitude of $\Delta\theta_k$ being found by a process of trial and error. In the vicinity of the minimum, the function is expanded in a Taylor series and truncated after the second derivative which results in quadratic convergence in this region. This method is very powerful as it converges with a starting vector θ_n, which is far from the minimum.

3. Rosenbrock's method (1960) uses the method of steepest descent, modified to take account of the interaction between the variables. It also converges from a starting vector some distance from the minimum and does not use analytical expressions for the derivatives of the function, although they are numerically estimated.

There is little to choose between the methods 2 and 3, Rosenbrock's method is used for all the curve fitting presented here. In Chapter 3, examples are given showing the convergence of this method.

Numerical Integration

If the birth of nuclei is taken as neither sporadic nor instantaneous, but follows some other rate law, then in many cases the integral which occurs in the general rate equation (2.13) cannot be evaluated analytically, but must be estimated numerically. In this work, the Gauss integration formulae (Hildebrand 1956) have been used, which are especially suitable for machine computation. Their superiority over the well-known Simpson's rule arises as an n-point Gauss formula is equivalent to approximating the function by a 2n - 1 polynomial, while Simpson's rule is only exact if the expression is cubic within the step length.

Presentation of Results

The computer was programmed to present results in the form of optimum parameters, with the associated standard deviation, between the calculated and experimental dilatometer heights. The experimental and calculated heights, and the difference between these quantities were also tabulated for each experimental point. The results are presented graphically in the form of difference plots, i.e., percentage difference, calculated on the total range of shrinkage covered by a given run, between calculated and observed shrinkage at the experimental times. The regions in which the model fits the data well, can be readily seen from such a graph.

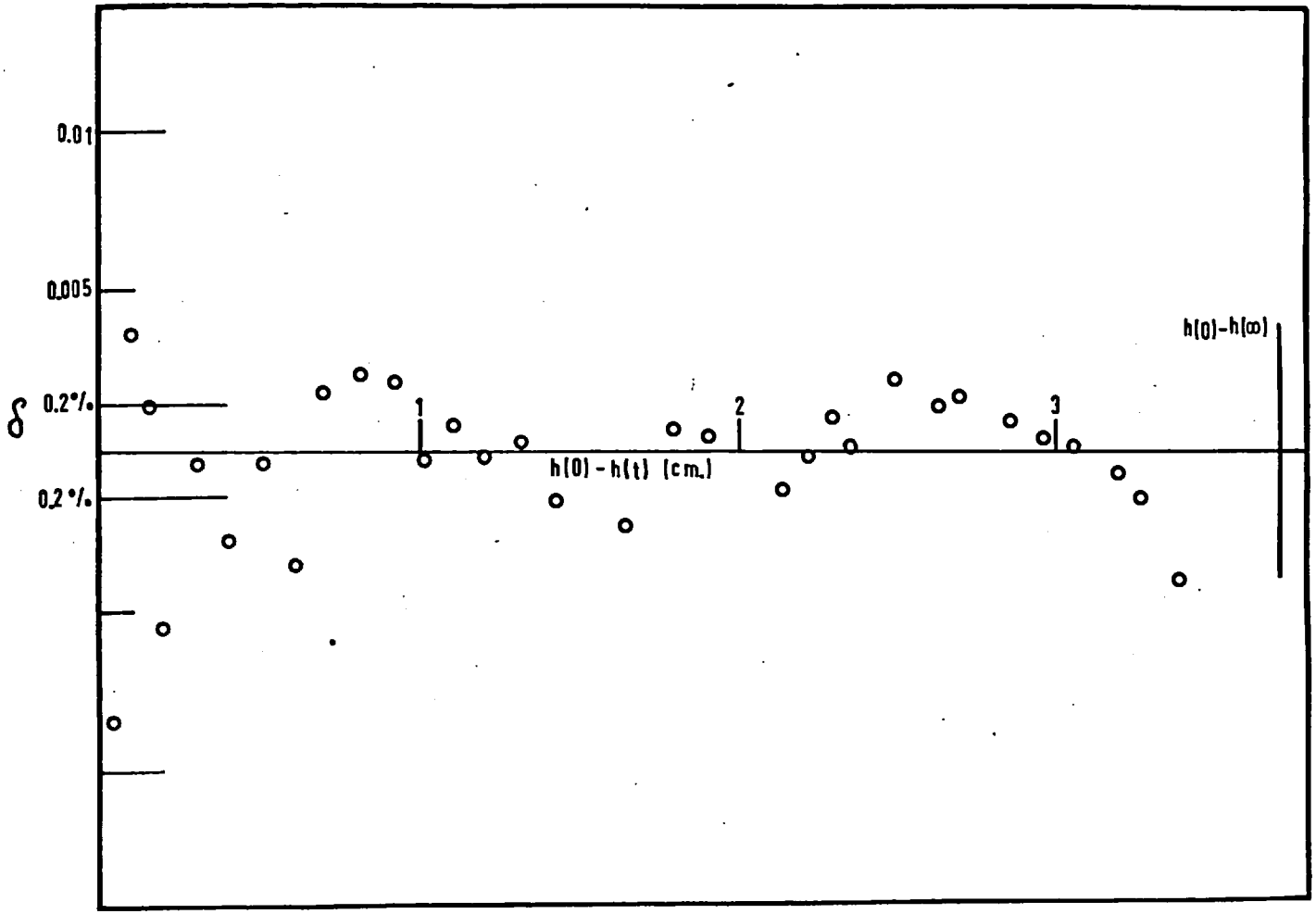
To establish a criterion for the goodness of fit of any model to the data, a representative run (run C, polymethylene, Chapter 3) was fitted to the empirical 16-parameter equation:

$$\left[\frac{h(o) - h(t)}{h(o) - h(\infty)}\right] / \left[1 - \exp -(2 \times 10^{-6} t^{2.8})\right] - \sum_{i=0}^{15} a_i T_i(\ln t) = \delta \qquad 2.59$$

where $T_i(x)$ is the i^{th} Tchebichev polynomial. The best values of the sixteen a_i were found by a least-square method to give a standard deviation $\sigma = 0.25\%$. The plot of δ versus $h(0) - h(t)$ is shown in Fig.2.2. Better agreement than a standard deviation of 0.2 per cent is not to be sought from any model, since even 'swamping' the measurements with sixteen adjustable parameters produces a 'scatter' of this order. This must be regarded as the approximate magnitude of the experimental scatter, though the difference plot reveals that this is not entirely random scatter. (It may contain some short-range systematic errors, e.g., due to sticking of the mercury thread in the dilatometer stem).

It seems doubtful if models with more than five parameters could be convincingly fitted, and a three parameter fit to about 1-2 per cent standard deviation is worth considering.

Fig. 2.2 - Difference plot of statistical variation of experimental points. (eq. 2.59).



CHAPTER III

The Kinetics of Bulk Crystallization of Polymethylene

3.1 Morphology of Solution and Bulk Crystallized Polyethylene

Recent work on the morphology of solution and bulk crystallized polyethylene indicates that a striking similarity exists between the structural unit present in both cases. The main features of this work are now reviewed, and in later sections used to formulate a new model which satisfactorily describes the kinetics of bulk crystallization of polymethylene.

Morphology of Solution Crystallized Polyethylene

When polyethylene is crystallized from an organic solvent such as xylene, single crystals are formed. They consist of lamellae of uniform thickness in the range 100 $\overset{o}{A}$. The crystals thicken via a screw dislocation growth mechanism which leads to a spiral terraced structure. Electron diffraction shows that the polymer chains are approximately normal to the face of the platelet. As the length of the polymer molecule is many times greater than the lamellar thickness, it must fold back on itself to be accommodated (Keller 1962). The fold length is found to be characteristic of the temperature at which crystallization occured, ranging from 90 - 155 $\overset{o}{A}$ for temperatures between 50 ^{o}C and 90 ^{o}C. If crystals formed at one temperature are heated to a higher temperature, the layer thickness is found to increase.

The degree of sharpness of the folds at the lamellae face is at present the subject of some controversy. Kawai and Keller (1963) find that the density of solution grown crystals is close to the ideal crystallographic density, and argue that the molecular folds are sharp, and that there is no appreciable amorphous content. Jackson, Flory and Chaing (1963) on the other hand, find a disparity between the specific volume for single crystals, and the crystallographic value, leading to about 20% amorphous polymer, which is assumed to be situated at the lamellar faces. Repeated passage of the same molecule through the lamella requires the amorphous layer to consist of chain loops connecting successive crystalline sequences formed from the same molecule. The 20% amorphous fraction requires the loop to be about 20 carbon atoms in length. Flory argues that there are thus no grounds for supposing that successive crystalline sequences from the same molecule are juxtaposed and connected by a regular fold in the growth plane. A more random array of interconnections between crystalline sequences is more plausible, and leads to a 'switch-board' picture at the face of the platelet (Flory 1962).

Morphology of Bulk Crystallized Polyethylene

The problem of examining the submicroscopic morphology of the interior of the bulk polymer presents formidable difficulties. However, lamellar structures have been observed

along fracture surfaces (Geil 1960, Fischer 1957). It has been shown that the low angle X-ray spacing of approximately 100 Å found for solution growth polyethylene reflects the lamellar thickness (Geil 1962). Similar low angle spacings are well established in the bulk polymer and provide additional grounds for suspecting that the morphological unit in the bulk resembles single crystals (Keller 1962).

A powerful technique has been developed by Palmer and Cobbold (1964) which allows the morphology of the bulk sample to be directly investigated. Digestion of polyethylene with concentrated nitric acid at approximately 70 °C is found to result in the complete fragmentation of the sample. Examination of the debris under the electron microscope reveals the presence of lamellae of thickness 100 - 200 Å. Density measurements of polyethylene crystallized within about 10° of the melting temperature shows that there is an amorphous content of up to 60%. It is supposed that the nitric acid preferentially attacks the amorphous polymer which is taken to be situated at the lamellar faces, resulting in fragmentation. In the formation of single crystals from dilute solution, a given molecule can participate in only one crystallite. In the melt, however, a molecule can involve itself in several different, or in the same crystallite, represented by the Flory (1962) switch-board model. Keller and Sawada (1964) have further shown the analogy between

solution grown single crystals and the lamellae found in the bulk, by showing that in the latter, the chains are also normal to the face of the platelet.

Examination of Samples used for Kinetic Measurements

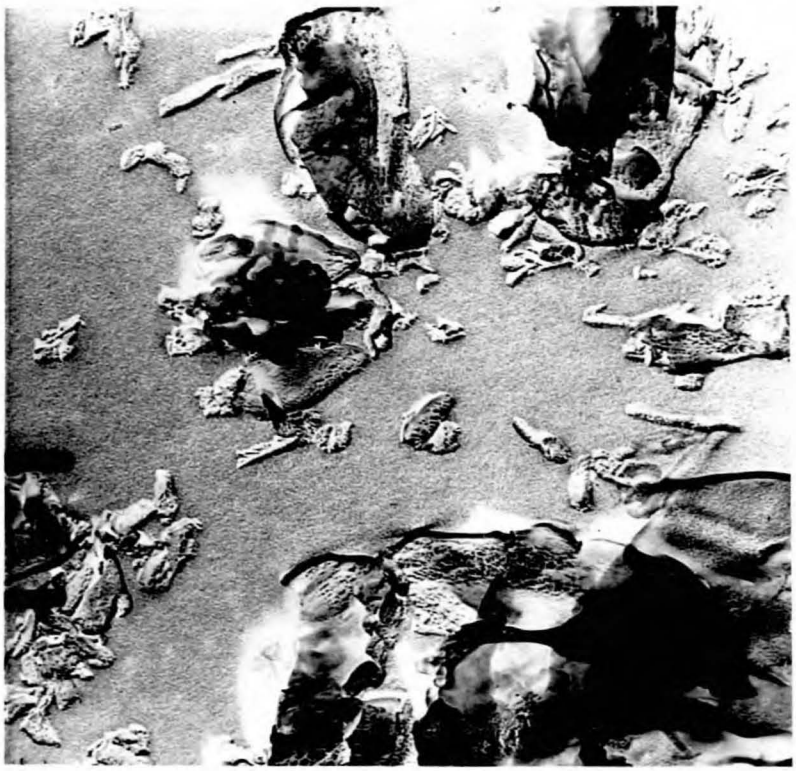
A high molecular weight polymethylene (P_v = 26 000; from Dist.Anal.Inc., Baton Rouge, Louisiana) was used in the kinetic investigations. Dr.R.Palmer kindly submitted a sample of this polymethylene to his nitric acid etching technique. Fig.3.1a shows lamellar structures of thickness approximately 200 Å. (The scale corresponds to 1 μ). The sample had originally been crystallized at 126.92 °C to give a final crystallinity of 43.7% at that temperature, the crystallization being well into the post-Avrami stage (section 3.4) at this point. However, on cooling to room temperature more crystallization occured since the crystallinity (found by Miss A.Turner-Jones) using the X-ray method, was 65 - 68%. We have used Palmer's etching technique with ozone as the oxidising agent. This has the advantage that attack occurs at room temperature, thus removing any danger of recrystallization or melting. After 2 days' treatment with ozone (produced by a silent discharge from an induction coil) a film of Philips polyethylene (M.W. = 6 800) became brittle. The film was dispersed in water using ultrasonics (Mr.Parott of the Physics Department of this College kindly allowed his apparatus to be used)

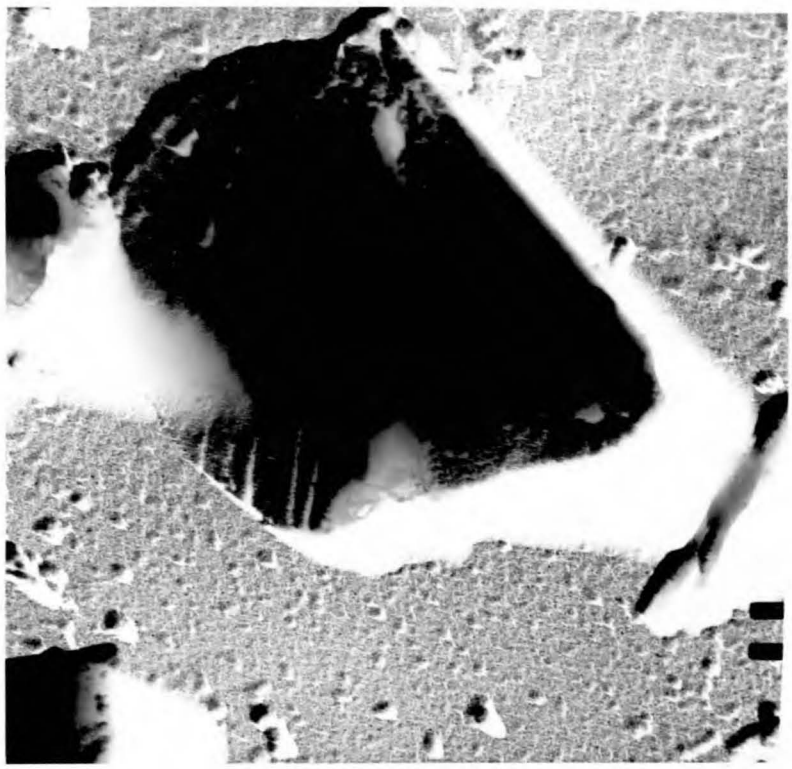
Figure 3.1

Photomicrographs

(a): Top - Photomicrograph of polymethylene. The sample was digested in nitric acid. The scale represents 1 μ. Note the lamellar structure.

(b): Bottom - Photomicrograph of polyethylene degraded by ozone, showing typical rhomb-like structure with steps near the bottom left edge. (Original negative × 12,000)





and the resulting suspension examined using the electron microscope. Fig.3.1b shows an object after shadowing with gold and palladium at $\tan^{-1}3$. (Original negative × 12 000.) It has a rhomb-like structure with steps near bottom left edge, of height (100 - 200 Å) which is further evidence for a lamellar structure. A sample of polypropylene has also been examined using this technique, the results being discussed in Chapter 4.

Single Crystals and Spherulites

A major problem in present morphological studies is the relationship between these lamellae and the microscopically observed spherulites. Keller and Sawada (1964) have observed lamellae in the form of 'air-screws' and equate the pitch of these with the distance between successive concentric bands seen in polyethylene spherulites. The detailed manner in which these lamellae are arranged within the spherulite is undecided but a 'splaying book' arrangement has been suggested (Hoffman and Lauritzen 1961). This space-filling problem is naturally important in the formulation of models to interpret the kinetic behaviour.

3.2 Previous Kinetic Studies

It is well established (Banks et al.1963a, Peterlin and Roeckl 1963) that the rate curve for the crystallization of polyethylene from the bulk shows two distinct portions. The earlier ('primary') crystallization has usually been analysed

in terms of the Avrami equation (2.24)

$$\chi_t = \chi_\infty [1 - \exp - zt^n] \qquad 3.1$$

The latter ('secondary') crystallization approximately obeys a χ vs.log(t) relationship, and has not been interpreted in detail, mainly owing to the uncertainty in separating it from the primary process. It has been suggested (Banks et al.1963a) that this secondary crystallization can be described by the Hirai and Eyring (1958) equation, for the bulk relaxation in glasses, fibres and metals. This equation approximates to the log (time) relationship, but no detailed fitting of experimental data was attempted. In particular, any overall rate equation must accurately fit the transition region between these two rate processes.

Tung and Buckser (1959) found that the best integral value of the Avrami exponent (n) to fit the primary crystallization was 4. The temperature dependence of the Avrami rate constants z, obtained using this value of n was interpreted in terms of the $1/\Delta T^2$ relationship (eq.2.48) corresponding to three dimensional secondary nucleation. Banks et al. (1963a) have investigated samples of Phillips polyethylene of varying molecular weights. The criterion used for the separation of the primary and secondary crystallization was that the exponent n should be constant throughout the primary process. This method of analysis (using eq.2.51) yielded values of n which were

non-integral, and were temperature and molecular weight dependent. The value of n varied from 2.70 ($\overline{P}_v$ = 18 500, T_c = 128.60 °C) to 3.87 ($\overline{P}_v$ = 1 800, T_c = 130.00 °C). These results cannot be explained by the simple Avrami model. The Avrami rate constants also fitted the $^1/\Delta T^2$ relationship, especially when allowance was made for the variation of n with temperature, by plotting

$$\log (z) \quad \text{vs.} \quad n/\Delta T^2 \qquad 3.2$$

Using the double logarithmic plot to evaluate n, Banks, Gordon and Sharples (1963b) found that it was reduced to 1.2 - 1.6 on 'seeding'; its value again varied with molecular weight, but not with the degree of 'seed' crystallinity, provided this exceeded about 4%. Although optically resolvable spherulites are not normally found in polyethylene thermal treatment (heating to 300 °C in vacuum) is found to produce spherulites about 10^{-2} cm in diameter (Banks, Hay, Sharples and Thomson 1962). Banks et al.(1963b) have followed a 'seeded' run under the polarizing microscope with a specimen treated in this way. They find that the birefringence disappears uniformly, on partial melting, and comes back uniformly within the outline of the original spherulite, on cooling. However, the original structure is not reformed, the new structure being granular in form. The process of partial melting followed by recrystallization is thus not completely reversible. However,

a certain degree of reversibility was indicated by the equality of the temperature dependence of the Avrami rate constants for the 'seeded' and 'unseeded' experiments.

3.3 A Single Crystal Model for the Primary Crystallization of Polymethylene

Introduction

In the interpretation of the dilatometric data, the discovery that specific thermal treatment of a sample of high molecular weight polymethylene can destroy the secondary or post-Avrami process has enabled a detailed interpretation of both these processes to be carried out. A kinetic run was carried out at 127.18 ^{o}C until no further crystallization occurred, which took six weeks. On subsequent melting, and again crystallizing at the same temperature, it was found that the secondary crystallization had been completely suppressed (Fig.3.2). Evidence confirming the supposition that this thermal treatment has removed the secondary crystallization will be discussed in section 3.4, where the post-Avrami crystallization is interpreted. That this kinetic isolation of the primary crystallization is not fortuitous is attested by a similar independent observation on a fraction of Phillips polyethylene (Sharples 1963). To the Avrami process thus isolated, variants of a new model are fitted whose basic features (including chain-folding) are inspired by previous work on crystallization of polyethylene from dilute solution. To this end, the statistical methods of fitting and

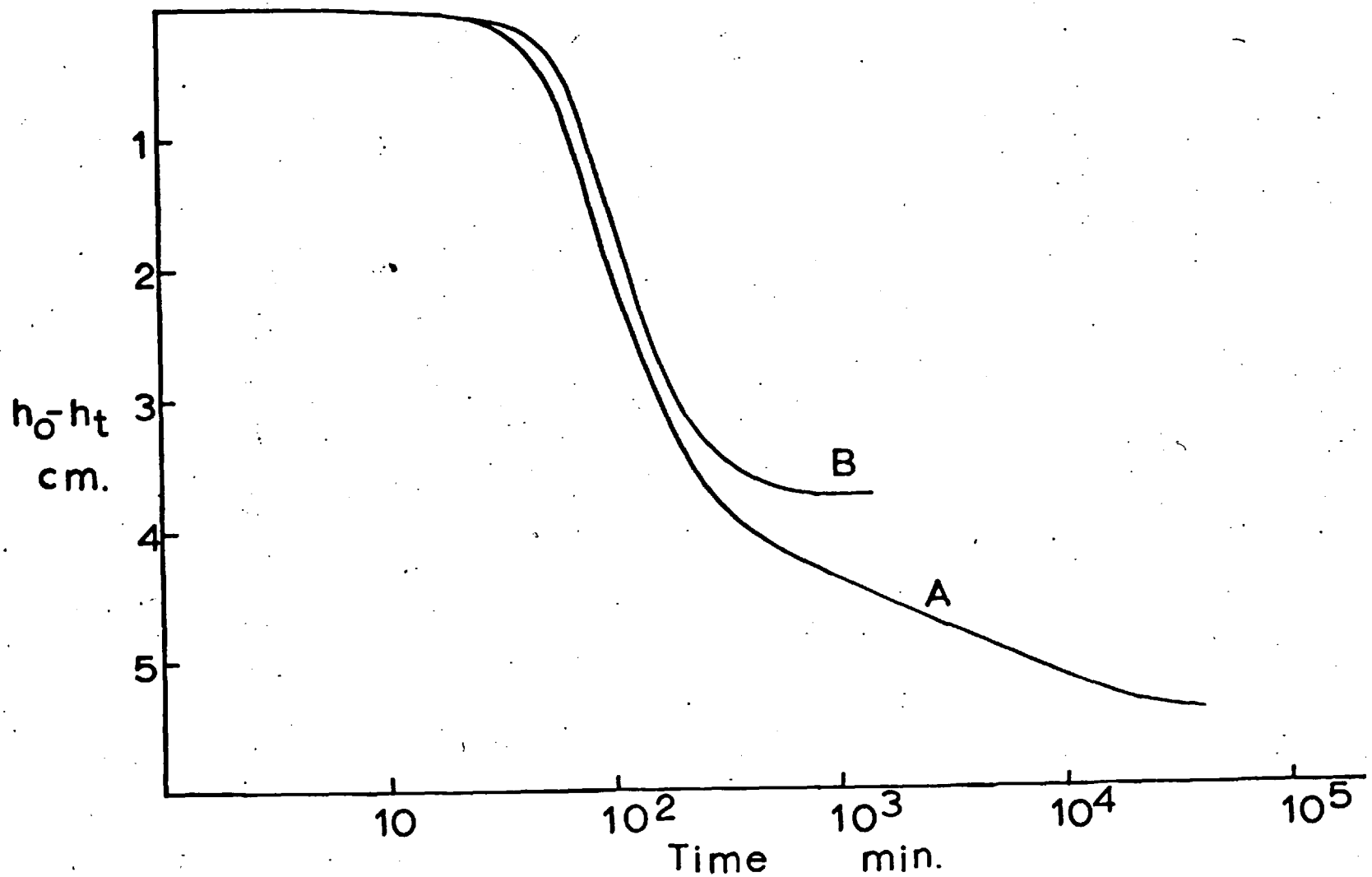


Fig3.2- Crystallization of polymethylene (127.18°C).

(A) Secondary crystallization present.

(B) Secondary crystallization absent.

presenting experimental curves has been improved (see section 2.7.) All the experimental runs are tabulated in Appendix ..

The Avrami Model

For application to dilatometry, the Avrami equation (eq.2.24) becomes

$$\frac{h(0) - h(t)}{h(0) - h(\infty)} = 1 - \exp(-zt^n) \qquad 3.3$$

This equation does not assume that the degree (χ_∞) of crystallinity at infinite time is unity. It is, indeed, found to be approximately only 0.3 (Table 3.1) for polymethylene deprived of its post-Avrami shrinkage. The conversion formulae of dilatometric shrinkage to degree of crystallinity used were those of Swan (1960) and Chiang and Flory (1961) respectively:

$$\bar{V}_l - \bar{V}_c = 0.1420 + 0.6434 \times 10^{-3}t - 0.443 \times 10^{-6}t^2 \qquad 3.4$$

$$\bar{V}_l - \bar{V}_c = 0.159 + 0.58 \times 10^{-3}t \qquad 3.5$$

where t is the temperature in degrees C, and $\bar{V}_l$ and $\bar{V}_c$ are the specific volumes of the liquid and crystalline phases respectively. Eq.3.3 does assume (see section on 'single crystals and spherulites') that the degree of crystallinity of the growing bodies has the constant value χ_∞ at all times (Banks et al.1963a).

All experimental runs are now analysed (Table 3.2) in relation to various models. All the fits were based on

Table 3.1

Final Crystallinities as Function of Temperature

Run (see Fig.3.4)	Temp. ^{o}C	Percentage Crystallinity (χ_{∞})	
		Swan's formula Eq.3.4	Flory's formula Eq.3.5
A	125.79	34.7	32.3
B	125.92	38.4	35.8
C	127.18	35.2	32.8
D	127.61	32.9	30.6
E	128.26	32.8	30.5
F	129.12	33.3	31.0

Table 3.2/

Analysis of Polymethylene runs

Run (see Fig.3.4)	Temp. °C	No.of points	Avrami model			Folded chain + inst.birth			Folded chain + first-order birth			
			n	z	σ %	$k_1 min^{-1}$	k_2	σ %	$k_1 min^{-1}$	k_2	$k_1^* min^{-1}$	σ %
A	125.79	69	1.81	1.04,-3	2.73	3.39,-3	212	2.44	4.97,-3	106	1.22, 0	2.35
B	125.92	64	1.81	8.27,-4	3.48	3.71,-3	132	3.43	5.84,-3	76.9	1.87, 0	2.33
C	127.18	76	1.99	5.34,-5	2.64	1.29,-3	129	2.70	2.95,-3	32.7	9.57,-2	1.96
D	127.61	58	2.28	6.28,-6	2.06	9.93,-4	120	3.24	1.03,-3	151	3.47,-2	1.52
E	128.26	54	2.29	1.37,-6	1.75	7.78,-4	46.8	3.34	8.47,-4	80.3	1.09,-2	1.10
F	129.12	23	2.55	2.85,-8	1.72	4.27,-4	23.0	1.38	3.81,-4	36.2	-	0.77

/ In Tables, 1.04,-3 means 1.04×10^{-3} etc.

'measured' values of $h(\infty)$. If, instead, $h(\infty)$ is made an adjustable parameter, the fittings are not significantly improved (Table 3.3). The least-square fit of the general (2-parameter) Avrami equation gives standard deviations in the range 1.7 - 3.5% and a representative difference plot (run D ; Fig.3.3, plot c) shows that the deviations are highly systematic: there are only three changes of sign in the sequence of deviations, while for random deviations the expected number of changes is 29. The reasonably low standard deviations suggest that there may be enough truth in the model underlying the Avrami equation to refine it by adding a further parameter. The value of n appears to increase with increasing temperature, and generally does not fit the simple variants of the Avrami model normally considered. The embarrassment of fractional n values has repeatedly been commented on (Banks et al.1963a, Sharples and Swinton 1963). The kernel of truth in the Avrami picture is probably the essentially random spacing and constant density of the growing bodies, while other assumptions, especially the linear growth rate are more suspect. If this is correct eq.2.26 may be used:

$$\frac{h(0) - h(t)}{h(0) - h(\infty)} = 1 - \exp - \rho \bar{V} \qquad 3.6$$

here $\rho = \rho(t)$ designates the number per unit volume of growing bodies, and $\bar{V}$ [$= \bar{V}(t)$] the volume of the growing entities.

Table 3.3

Effect on the fit of the three models of allowing $h(o) - h(\infty)$ to be an adjustable parameter (Run D).

Avrami model (eq.3.3)

n	z	$h(o)-h(\infty)$	σ (%)
2.28	6.28,-6	3.495	2.06 [$h(o)-h(\infty)$ constant]
2.29	6.23,-6	3.427	1.88 [$h(o)-h(\infty)$ allowed to vary]

Folded model + inst.birth (eq.3.16)

k_1 (min^{-1})	k_2	$h(o)-h(\infty)$	σ (%)
9.93,-4	120	3.495	3.24 [$h(o)-h(\infty)$ constant]
9.66,-4	118	3.608	2.99 [$h(o)-h(\infty)$ allowed to vary]

Folded model with first order birth (eq.3.21)

k_1 (min^{-1})	k_2	k_1^* (min^{-1})	$h(o)-h(\infty)$	σ (%)
1.03,-3	151	3.47,-2	3.495	1.52 [$h(o)-h(\infty)$ constant]
1.04,-3	152	3.47,-2	3.458	1.45 [$h(o)-h(\infty)$ allowed to vary]

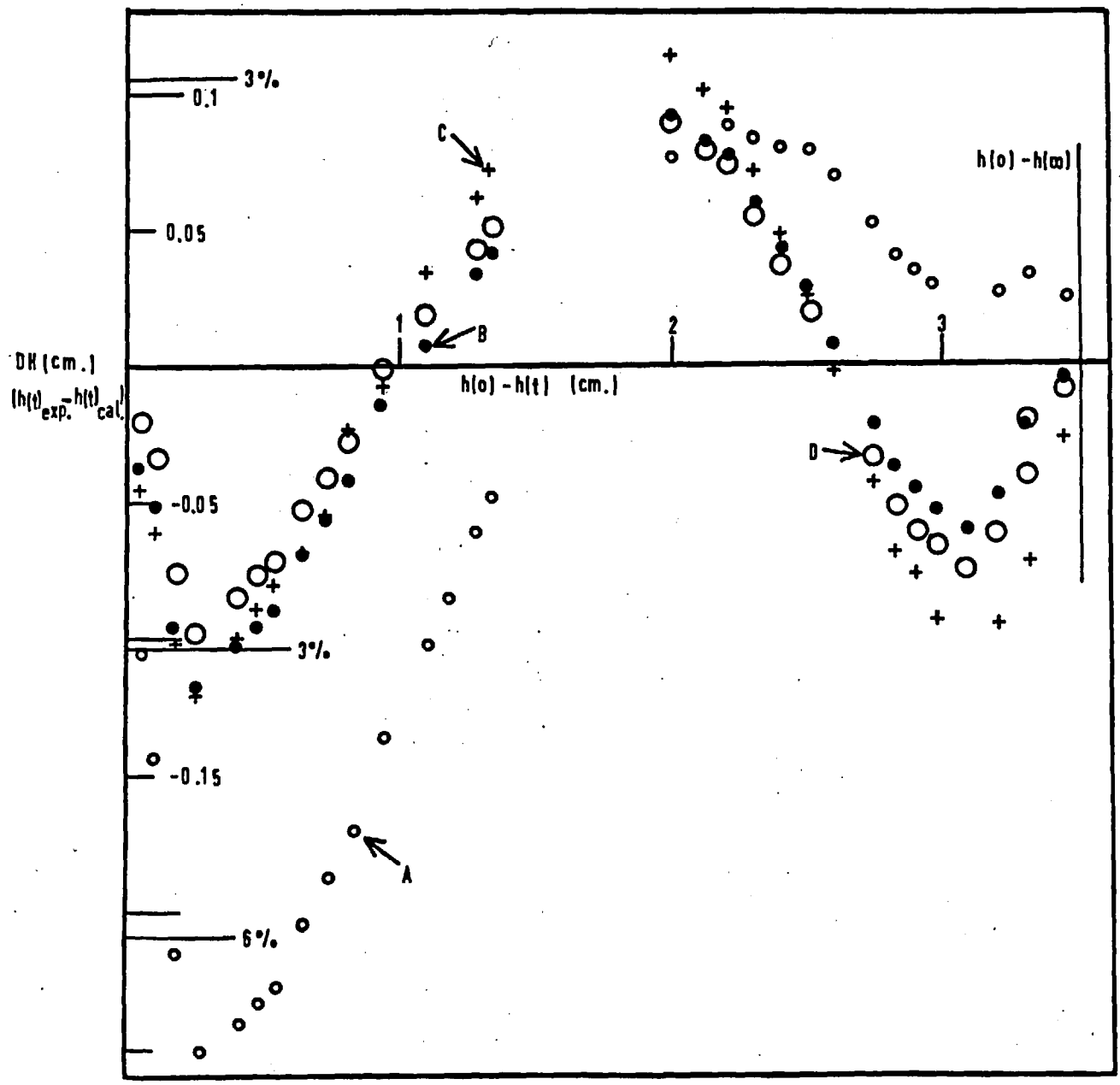


Fig. 3.3-Difference plots showing fits of four models considered.
A, folded chain model with instantaneous birth (eq. 3.16)
B, folded chain model with varying fold length (eq. 3.19)
C, Avrami model (eq. 3.3)
D, folded chain model with first order birth (eq. 3.21)

If the entities are born instantaneously, then ρ is constant; if sporadically, then ρ is proportional to time

$$\rho = ct \qquad 3.7$$

Assuming further that all the entities have the same growth law (once they are nucleated), then, for instantaneous birth, one plots against time the quantity $\rho\bar{V}$ given by:

$$\rho\bar{V} = -\ln[h(t) - h(\infty)]/[h(o) - h(\infty)] \qquad 3.8$$

Again, for sporadic birth, one plots against time the quantity cV, given formally by the derivative with respect to t of the right hand side of eq.3.8:

$$cV = -\frac{d}{dt}\left[\ln[h(t) - h(\infty)]/[h(o) - h(\infty)]\right] \qquad 3.9$$

Here V is the volume of any entity which has been growing for time t, and obviously in eq.3.8 we have for instantaneous birth:

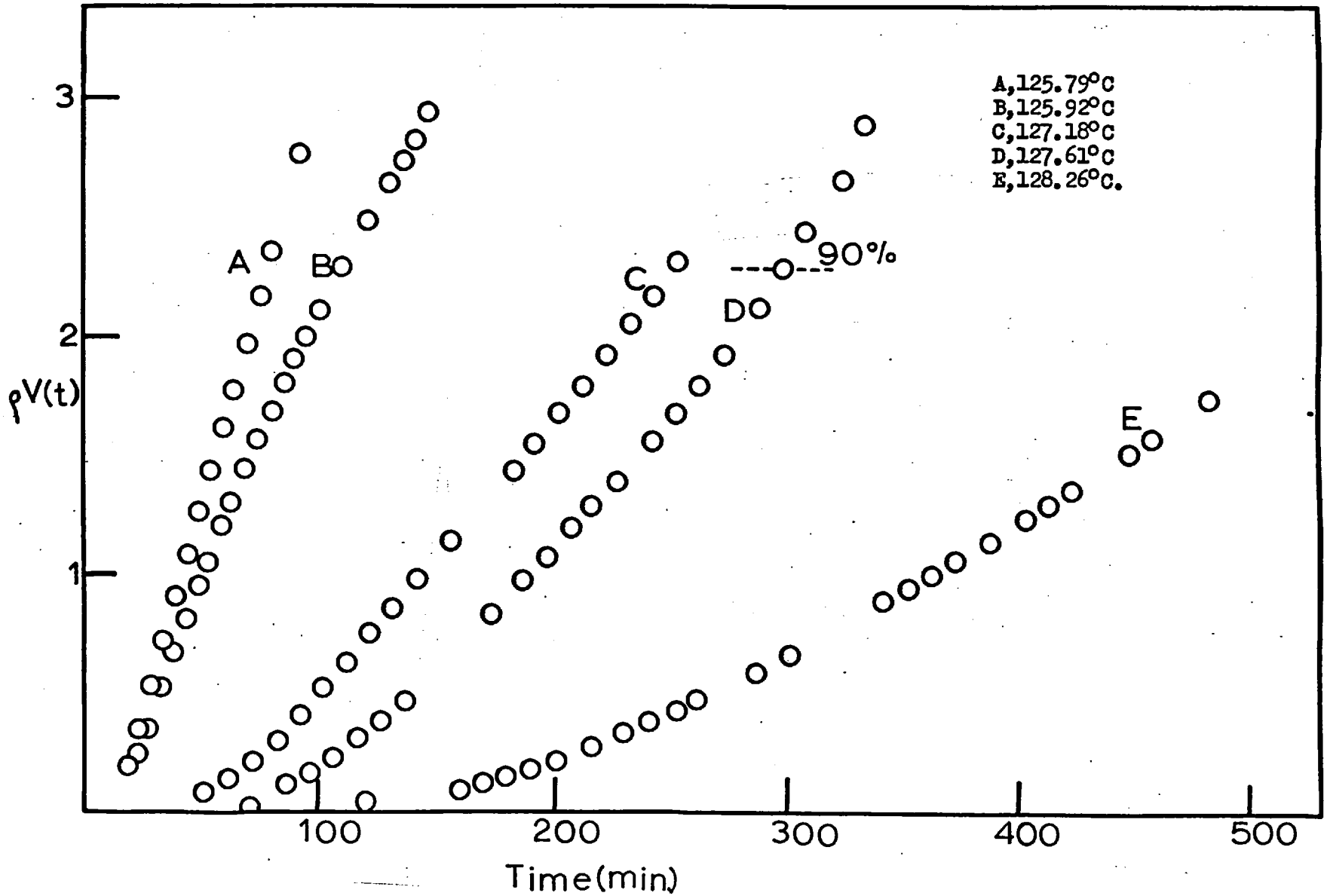
$$\bar{V} = V \qquad 3.10$$

For any other birth law, $\bar{V}$ is required in eq.3.6 and is given by eq.2.12

$$\rho\bar{V} = \int_o^t V(t - \tau)(d\rho(\tau)/d\tau)\, d\tau \qquad 3.11$$

The plots in Fig.3.4 are based on eq.3.8 for instantaneous birth. Plots according to eq.3.9 were not promising because they led to V approaching a limit with time, which militates strongly against the notion of sporadic birth. Fig.3.4 refers to one sample at various temperatures and suggests that the volume V of an

Fig 3.4- Growth of entities against time. At conversions more than 90%, the plot becomes too sensitive to the experimental value of h(o)-h(∞) to be reliable.



isolated entity increases linearly with time after an initial non-linear acceleratory period. The later portions of the plots, being linear, correspond to the ordinary Avrami equation with n = 1.

Single Crystals and Spherulites

Each of these plots (Fig.3.4) when conventionally analysed, would correspond to an Avrami exponent n which decreases with time towards a final value n = 1 (final linear portion). This behaviour can be shown to fit the type of model previously used by other workers (Keller 1962) for crystallization from dilute solutions, rather than in the bulk, and the data is now fitted to the folded-chain model of Hoffman and Lauritzen (1961). This finding extends the work of other teams in the field of morphology and physical properties who have recently concluded (Keller 1962; Eppe, Fischer and Stuart 1959; Fischer 1957; Stuart 1959) that the basic morphological unit in bulk polyethylene resembles single crystals grown from solution, especially with regard to chain folding and even the fold-lengths observed. The two main radical changes implied in using this type of model for bulk crystallization are:

(a) non-coherent secondary nucleation on the surface of the growing bodies is abolished. In other words, we turn from the notion of a spherulite to that of a 'single crystal'.

Microscopic examination of the polymethylene does not, in fact, reveal resolvable spherulites, except after thermal degradation (heating in air to about 350 °C). This agrees with findings of (Banks et al.1962) on samples of polyethylene. It is concluded that under normal conditions, the number of primary nuclei per unit volume is so high, that secondary non-coherent nuclei do not grow on the surfaces of the small faces of these nuclei.

(b) Inside a spherulite, the existence of a substantial constant amorphous fraction has been accepted on the basis of the fringed-micelle model for the local intraspherulitic structure. The single crystal models similarly involve constant amorphous fraction associated with each single crystal, in terms of Flory's (1962) concept of an amorphous 'interfacial layer'. This layer, which occurs on the surfaces containing the chain folds, must have a constant thickness, here about equal to that of the thickness of the central crystalline part of the platelet, (Fig.3.5) since the overall crystallinity of the platelet is only about 1/3 (Table 3.1). In the present work, it is postulated that neither nucleation nor growth occurs in the interfacial layer; but evidence will be presented (section 3.4) that the secondary or post-Avrami stage, which is absent in the present experiments, does consist of ordering processes occurring within this layer. Palmer (1964) has shown by his etching

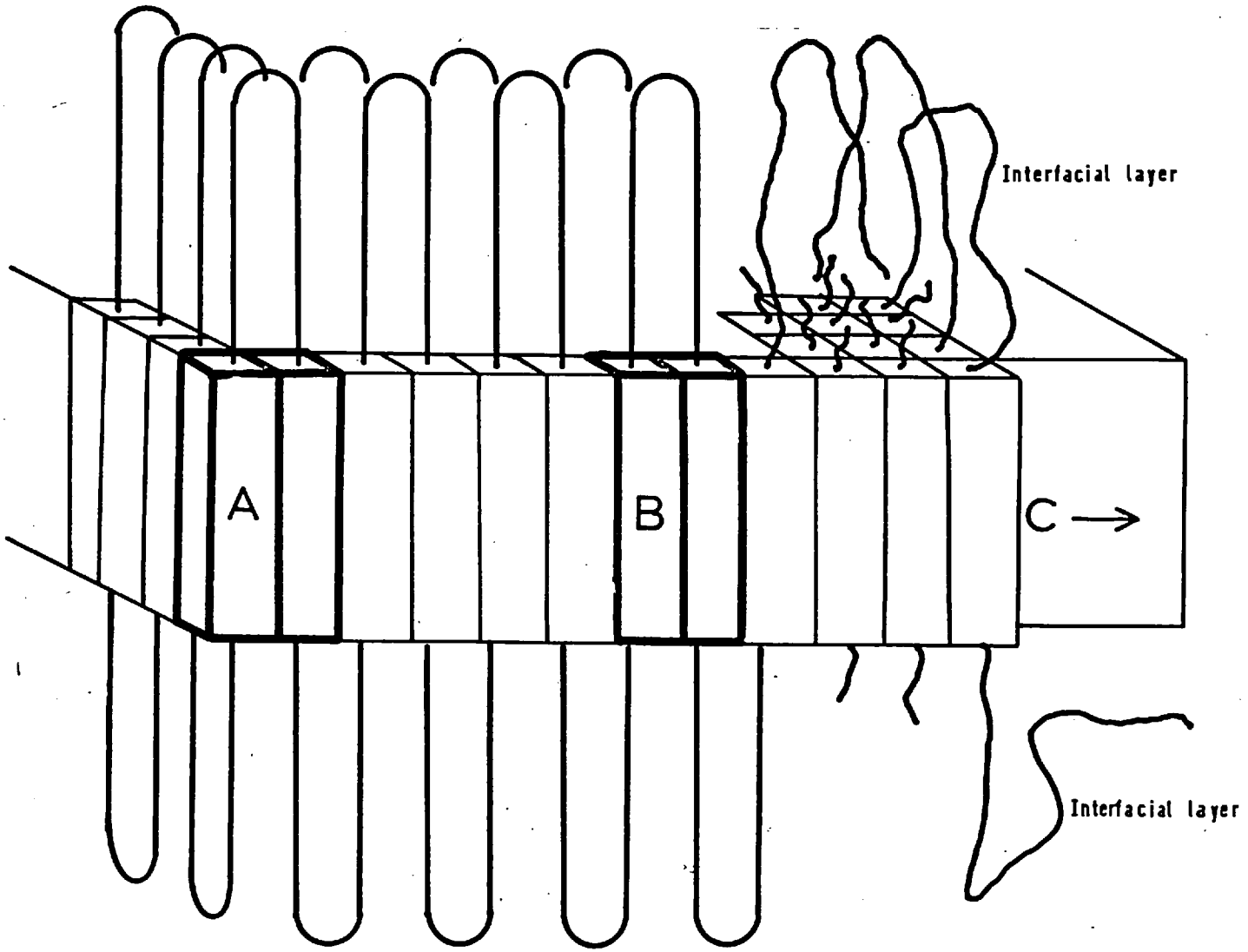


Fig.3.5-Schematic representation of growing platelet with interfacial layers:left,regular pleating; right,Flory's "switchboard " model.
A,corner nucleus; B,face nucleus; C, growth front.

technique using nitric acid, that the amorphous fraction in bulk-crystallized linear polyethylene can be accounted for by an amorphous layer lying between crystallites.

Two-parameter folded-chain model

Essentially similar models have been examined theoretically by a number of workers (Hoffman and Lauritzen 1961; Flory 1962; Frank and Tosi 1961; Price 1961) in which crystallization is treated as a sequential process. Each individual stage in the sequence comprises the attachment of several 'successive pleat segments of one long-chain molecule to the side surface of a plate-like crystal when the molecule has just turned a corner of the plate and is starting a new side face. The transition from one stage to the next occurs when the chain bends back on itself and begins to attach the next pleat segment in an adjacent parallel position to the previous one' (Frank and Tosi 1961). Fig.3.5 illustrates this model. It is based on Fig.1 of Hoffman and Lauritzen, and like theirs, it must not be considered necessarily restricted to rectangular cross section of the plates, which could be 'a parallelogram, hexagon or other polygon' (Hoffman and Lauritzen 1961).

Flory (1962) has generalized this picture with special reference to passing from solution to bulk crystallization; thus he abandons the regular folding in favour of the 'switchboard' model (right of Fig.3.5).

The main point of previous theories has been the persistence or otherwise of the pleat length during the growth process. From the point of view of kinetics, and assuming the pleat length to be constant, one discerns two regions of the rate curve to be expected for an isolated plate: initially the rate will be controlled by the process of transition from one stage to the next, i.e., when the chain is at a corner of the plate. Later, when the plate is large, the waiting period at a corner plays a subordinate part, and the rate is controlled by the attachment of a large number of successive pleat segments across the large face. If ρ of these plates are placed <u>at random</u> in unit volume, growing until they impinge, it is readily seen that the Avrami analysis will lead to an apparent n value falling from a two in the initial region of the rate curve, to unity at the end. This is shown quantitatively below.

$\overline{V} = \overline{V}(t)$, and $\rho = \rho(t)$, are now computed (for insertion in eq.3.6), for various versions of the folded chain model. For convenience, the sequential model described above is generalized without affecting the kinetics by introducing a second nucleation step or waiting period (Fig.3.5). Thus each individual stage of adding pleat segments across a face of the platelet is sub-divided into a number of bursts of activity alternating with a period of waiting for renucleation. It is thought that this process arises from certain faults occasionally preventing the immediate deposition of a pleat. Such a fault

may stem from a chain-end, or from a failure of supply of suitable chain segments emanating from the local 'switchboard' arrangement. When the chain currently being pleated reaches such a fault, a waiting period intervenes, until an end or suitable segment belonging to another chain arrives, and a critical coherent two-dimensional nucleus consisting of a few pleats of the new chain is built up. The chance of a chain running out just when it has reached the corner of the platelet may be neglected, and there are therefore just two kinds of nucleation acts (or waiting periods):

(a) a waiting period τ_c for renucleation when a chain turns the corner of the platelet;

(b) a waiting period τ_f, the mean waiting time for laying down a pleat on the growing face of the platelet.

However, any rate equation based on the Avrami model, which is 'space filling', in the sense that any point is eventually engulfed by the growing crystalline bodies, is only approximate for rods and discs. The discussion is restricted to instantaneous birth. For rods and discs growing with any growth law, this model implies that a body that has grown out from one centre, occurs in several unconnected pieces (see Fig.3.6). It is not realistic to expect that in a real polymer system any but the central fragment (A in Fig.3.6) of a formally fragmented body would be actually present. The other fragments

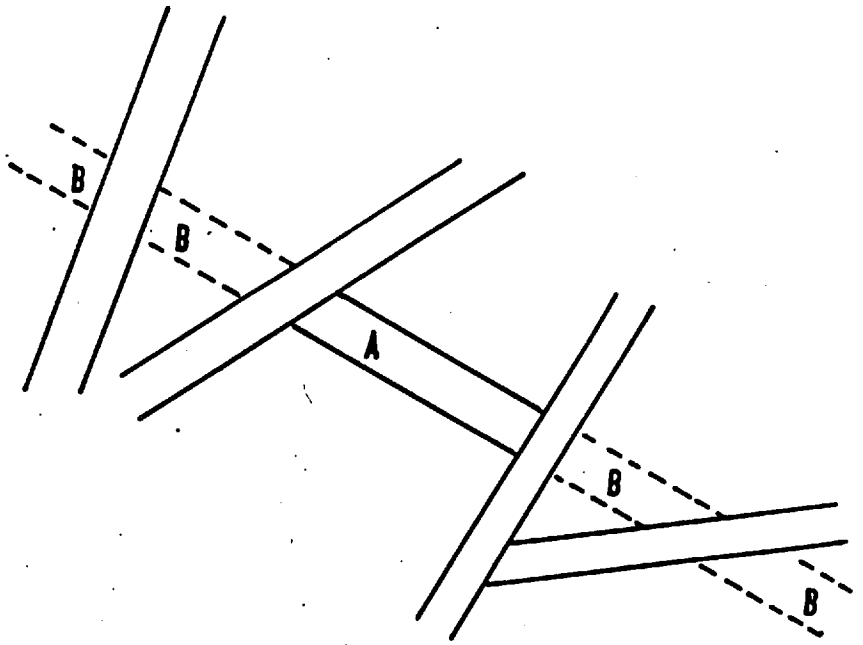


Fig.3.6-Schematic representation of fragmentation of growing body.

A -actual body present.

B -fragmented pieces of body which are considered present by the Avrami model, but which may not be present in reality.

(B in Fig.3.6) would not form in practice, so that the sample would retain amorphous regions in their place. Thus, in these cases, a space filling model is not realistic, but may serve as an approximation. For spheres growing linearly in radius with time, fragmentation does not occur, and the Avrami model is quite realistic.

The single crystal model attributes all the final amorphous content of the sample to the growth of amorphous interlayers on both faces of the disc-like bodies. The model is essentially space filling in discounting the presence of amorphous regions arising form the formal fragmentation of the discs during growth. In fitting kinetic data the true amorphous content of the sample is underestimated at all times. However, much of this error will be 'corrected' by the implied adjustment of the thickness of the interlayer. (In the real crystal, the amorphous regions due to fragmentation are completely enclosed by amorphous interlayers).

It will be seen in Chapter 4 that the rate law to be derived for the growth of individual platelets applies under certain conditions if these platelets are grouped together to form spherulites, as is suggested by morphological investigations (section 3.1). In this case, the underestimation of the amorphous content may be more serious as the degree of fragmentation may be increased.

Computation of $\bar{V}(t)$

Let N be the number of chain loops contained in a single platelet at time t. Then the model leads to the following rate equation in terms of the two parameters just defined:

$$dN = \left[\frac{\tau_c}{\tau_c+(N^{1/2}-1)\tau_f}\ \frac{1}{\tau_c} + \frac{\tau_f(N^{1/2}-1)}{\tau_c+(N^{1/2}-1)\tau_f}\ \frac{1}{\tau_f}\right] dt \qquad 3.12$$

The number dN of pleats laid down in time dt consists of two terms: one term represents the ratio of dt to the waiting time at a corner-site multiplied by the chance of finding the chain at a corner-site; the other term arises analogously from the renucleation sites on the face of the platelet. Eq.3.12 uses the fact that for a square platelet there are $N^{1/2} - 1$ pleats along the face for each corner pleat. Cancelling redundant factors in eq.3.12 and integrating, one finds:

$$N = \left(\frac{\tau_c-\tau_f}{\tau_f}\right)^2\left[2+\frac{\tau_f t}{[\tau_c-\tau_f]^2}-2\left(1+\frac{\tau_f t}{[\tau_c-\tau_f]^2}\right)^{1/2}\right] \qquad 3.13$$

The volume v_p of one pleat is given by

$$v_p = 2a^2 l$$

where a^2 is the cross sectional area associated with one chain-strand in the crystal (about 20Å in polymethylene), and l is the pleat length (which is a function of temperature). Hence the volume of the platelet is

$$V = 2Na^2 l \qquad 3.14$$

with N given by eq.3.13. The dilatometric rate law is then derived as follows for instantaneous birth of platelets, using eqs.3.6, 3.10, 3.14, 3.13:

$$\frac{h(o)-h(t)}{h(o)-h(\infty)} = 1-\exp\left\{-2\rho a^2 l\left(\frac{\tau_c-\tau_f}{\tau_f}\right)^2\left[2+\frac{\tau_f t}{(\tau_c-\tau_f)}-2\left(1+\frac{\tau_f t}{(\tau_c-\tau_f)}\right)^{1/2}\right]\right\} \qquad 3.15$$

For computational purposes this becomes the two-parameter equation:

$$\frac{h(o)-h(t)}{h(o)-h(\infty)} = 1-\exp -k_2[2+k_1 t-2(1+k_1 t)^{1/2}] \qquad 3.16$$

On physical grounds it is expected that $\tau_c \gg \tau_f$; on this assumption

$$k_1 k_2^{\frac{1}{2}} = a\sqrt{2\rho l}/(\tau_c-\tau_f) \simeq a\sqrt{2\rho l}/\tau_c \qquad 3.17$$

Also,
$$k_1 k_2 = 2\rho a^2 l/\tau_f \qquad 3.18$$

Table 3.2 shows least-square fittings of the runs at six different temperatures to eq.3.16; standard deviations are seen to vary between 1.38 and 3.43 per cent. The run at 127.61 °C with standard deviation 3.24 per cent was chosen as representative for further investigation, and Fig.3.3 shows the corresponding difference plot A. By far the most serious deviations of the data from the model equation are seen to occur during the first third or so of the process, where the observed rate of crystallization lags behind the calculated. Two different attempts were made at altering the model to slow down the initial crystallization. Thus plot B presents the optimum fit

(σ = 1.84%) of the five-parameter equation in which the fold length is allowed to increase towards a limiting value as number N of pleats in the platelet increases; and plot D represents the optimum fit (σ = 1.52) for the three-parameter equation when the birth process of the platelet is changed from the instantaneous regime (plot A) to a first-order process. These fittings are now discussed further.

Folding-chain model with variable fold length

It was deduced by Price (1961) that when a platelet grows, the pleat length would initially vary monotonically but level off as the platelet grows larger. This leads to various possible single-crystal profiles shown as his Fig.4. It is clear that to improve the fit of our kinetic data, we require an increasing fold-length as in his curve C. The shape of this curve may be simulated by the equation (with three parameters l_o, l_∞ , and b):

$$l = l_o + (l_\infty - l_o)(1 - \exp - bN^{1/2}) \qquad 3.19$$

where $N^{1/2}$ is the number of pleats per crystal edge (more exactly $N^{1/2} - 1$). Using N from eq.3.13, and substituting for l from eq.3.19 in 3.15, a five-parameter dilatometric rate law is obtained. The optimum parameters for the least-square fit (Fig.3.3, plot B) were:

$$b = 0.18,\ \frac{l_\infty}{l_o} = 3.4,\ k_2 = 8.9 \times 10^{-4}\ [\ \frac{\tau_c - \tau_f}{\tau_f}\ ]^2 = 8.4 \times 10^3,$$

$k_1 = 49.9$. The ratio l_∞ / l_o is thus 3.4 which is approximately the value suggested in Price's plot.

Folding-chain model with first order birth of nuclei

It was observed experimentally by Banks et al.(1962) that samples of a polyethylene fraction after thermal pre-treatment could produce microscopically resolvable spherulites. The thermal pre-treatment is deemed to destroy most of the primary nuclei. (It is postulated that platelets grow from these nuclei when they are present in large concentration, while they develop into spherulites by secondary nucleation when present in small concentration, i.e., when the platelets develop large surfaces). Banks et al (1964) observed, as shown in their Fig.4, that the birth of the primary nuclei was intermediate between instantaneous and sporadic, increasing from zero to a fixed value rapidly at the beginning of each run. This behaviour can be incorporated into this model by assuming the nuclei to be born in random positions at a rate governed by the law of mass action. Rate equations governing this type of behaviour are well known (Jacobs and Tompkins 1955) for the conventional type of simple Avrami processes. The unimolecular rate law for the birth of the nuclei is given by

$$\rho(t) = \rho(\infty) [1 - \exp(-k_1 * t)] \qquad 3.20$$

Substituting this in eq.311, and substituting the result in eq.3.6 and using eq.3.16, yields

$$\frac{h(o)-h(t)}{h(o)-h(\infty)} = 1-\exp-\left(k_1^* k_2(\exp-k_1^* t)\int_o^t [2+k_1 u-2(1+k_1 u)^{1/2}]\exp k_1^* u\,du\right) \qquad 3.21$$

This is a three-parameter equation depending on k_1^*, k_1 and k_2. The least-square fit of the data, was programmed on the basis of approximating to the integral on the right of eq.3.21 with the eight-point Gauss formula; this procedure is amply accurate enough, as no significant change was noticed on passing to the twelve-point formula. A least-square fit of eq.3.21 to 70 experimental points takes about one minute on the Atlas computer. Eq.3.21 slightly overestimates the crystallinity at all times because of an approximation. The derivation implies (Gordon 1963) that a fictitious entity nucleated and growing inside another can never outgrow the bounds of its host and cannot, therefore, encroach on the amorphous space. This is geometrically exact for spheres with a constant radial growth rate, but never exact for discs. The approximation is adequate here, however, because the calculated first-order birth process is more than half completed (half-life = 20 min for run D) before the first experimental point is reached.

Critical evaluation for various models tested

The information on the four models tested in Fig.3.3 and Table 3.2 is now discussed. Of the two-parameter models

tested in Fig.3.3, the standard Avrami equation (3.3) gives comparable standard deviations to the folded-chain model with instantaneous birth of nuclei (Table 3.2). The latter is the better model for further refinement, since the standard Avrami model has known physical meaning only for selected values of n, i.e., multiples (Morgan 1954) of 1/2 or in the range 1.1 - 1.2 (Ham 1958; Jaycock and Parfitt 1961). On the other hand, the folded-chain model incorporates only features which have specifically arisen from morphological studies of the crystallization of polyethylene. Most of these admittedly refer to crystallization from dilute solutions rather than the bulk state, but there is increasing evidence (section 3.1) that similar features are present here.

Of the two refinements of the chain-folding model, the first-order birth of nuclei (Fig.3.3, plot D) is somewhat more attractive because it only involves three parameters, while the varying-fold-length model (plot B) contains five parameters. Inspection of the plots shows that discrimination between such refinement on the basis of dilatometry is not conclusive. In fact the residual deviations in all four plots are similar and follow the same pattern in the six runs analysed, which might indicate a small departure from an assumption common to all four models. This departure might, for example, arise from slight variations of τ_f close to a

region of impingement of two bodies. Effects of this kind have not been included in our models. Barnes, Luetzel and Price (1961) have observed visually a deceleration of the growth of spherulites of polyethylene oxide in regions of impingement. Plot A of Fig.3.3 might be explained in terms of acceleration of growth of single crystals near regions of impingement. All four plots of this figure may possibly be explained in terms of non-random placement of the nuclei, in the sense of a slight clustering together. The fit of these four models to run (D) is tabulated in tables 3.4, 3.5, 3.6 and 3.7. These tables correspond to the difference plots of Fig.3.3. The rapid convergence of the method of curve fitting used is well demonstrated by the small number of cycles needed. The iterative procedure was terminated when the standard deviations of two successive cycles differed by less than 0.1%.

Temperature Dependence of Rate Constants

The single crystal model assumes that the rate determining step is the formation of a coherent surface nucleus of monomolecular thickness a, length l, and width b, on the substrate crystal (Fig.3.7). This model postulates that there are two types of nuclei, one formed at the face of the growing platelet, the other at the corner. The end surface free energy of such nuclei is σ_e, and the lateral surface free energy is σ. The free energy of formation is $\Delta\phi_c$ for the corner nucleus, and $\Delta\phi_f$ for the face nucleus. It readily follows that

Table 3.4

Fit of run (D) to Avrami equation (3.3).

	n	z	h(o)-h(∞)	σ (%)
Initial parameters	2.200, o	6.000, -6		
	2.280, o	6.275, -6	3.495, o	2.060, o
	2.280, o	6.275, -6	3.495, o	2.060, o

T	Ho-HT(EX)	Ho-HT(CAL)	DH
35	0.014	0.034	-0.0196
40	0.053	0.097	-0.0441
50	0.100	0.160	-0.0599
60	0.152	0.239	-0.0875
65	0.184	0.285	-0.1014
70	0.225	0.335	-0.1103
75	0.268	0.389	-0.1212
80	0.334	0.447	-0.1127
85	0.408	0.508	-0.0999
90	0.484	0.572	-0.0885
95	0.559	0.640	-0.0812
100	0.655	0.711	-0.0560
105	0.745	0.785	-0.0395
110	0.838	0.861	-0.0225
115	0.947	0.939	0.0083
123	1.102	1.068	0.0342
125	1.140	1.101	0.0392
127	1.181	1.134	0.0471
130	1.237	1.184	0.0530
133	1.281	1.218	0.0634
135	1.340	1.268	0.0717
138	1.914	1.898	0.1162
140	2.130	2.039	0.1013
143	2.165	2.061	0.1042
145	2.204	2.108	0.0955
147	2.239	2.140	0.0991
150	2.275	2.187	0.0884
153	2.303	2.232	0.0705
155	2.337	2.286	0.0643
158	2.400	2.351	0.0488
160	2.460	2.423	0.0375
163	2.517	2.491	0.0256
165	2.556	2.545	0.0113
170	2.607	2.609	-0.0020
175	2.656	2.671	-0.0147
185	2.742	2.786	-0.0439
190	2.785	2.839	-0.0543
195	2.822	2.890	-0.0681
200	2.861	2.938	-0.0771
205	2.901	2.989	-0.0884
210	2.936	3.036	-0.0900
215	2.973	3.086	-0.0940
220	3.004	3.105	-0.0994
225	3.093	3.201	-0.1081
230	3.158	3.255	-0.0970
235	3.206	3.301	-0.0948
240	3.238	3.331	-0.0928
245	3.270	3.356	-0.0859
250	3.313	3.395	-0.0780
255	3.345	3.409	-0.0638
260	3.369	3.425	-0.0557
265	3.396	3.446	-0.0475
270	3.435	3.469	-0.0344
275	3.449	3.476	-0.0269
280	3.465	3.481	-0.0159
285	3.477	3.485	-0.0077
290	3.495	3.490	0.0053
295	3.495	3.492	0.0031

Table 3.5.

Fit of run (D) to folded chain model + inst. birth. (eq. 3.16

	k_1	k_2	$h(0)-h(\infty)$	σ (%)
Initial parameters	1.000, -3	1.200, 2		
	1.003, -3	1.205, 2	3.495, 0	3.30
	9.944, -4	1.197, 2	3.495, 0	3.24
	9.933, -4	1.200, 2	3.495, 0	3.24

T	(Ho-HT)EX.	(Ho-HT)CAL.	DH
25	0.014	0.063	-0.0493
40	0.053	0.159	-0.1057
50	0.100	0.244	-0.1436
60	0.152	0.344	-0.1917
65	0.184	0.399	-0.2150
70	0.225	0.457	-0.2324
75	0.268	0.519	-0.2506
80	0.334	0.583	-0.2485
85	0.408	0.649	-0.2408
90	0.484	0.717	-0.2332
95	0.559	0.788	-0.2285
100	0.655	0.859	-0.2045
105	0.745	0.933	-0.1878
110	0.838	1.007	-0.1692
115	0.947	1.083	-0.1356
123	1.102	1.204	-0.1024
125	1.140	1.235	-0.0950
127	1.181	1.266	-0.0847
130	1.237	1.312	-0.0747
132	1.281	1.342	-0.0614
135	1.340	1.388	-0.0483
172	2.014	1.938	0.0764
180	2.130	2.048	0.0816
182	2.165	2.076	0.0895
185	2.204	2.116	0.0883
187	2.239	2.142	0.0968
190	2.275	2.181	0.0936
193	2.303	2.220	0.0830
195	2.327	2.245	0.0816
201	2.400	2.320	0.0801
206	2.460	2.380	0.0801
211	2.517	2.438	0.0790
215	2.556	2.483	0.0728
220	2.607	2.538	0.0692
225	2.656	2.591	0.0655
235	2.742	2.690	0.0519
240	2.785	2.737	0.0481
245	2.822	2.782	0.0403
250	2.861	2.825	0.0364
255	2.901	2.866	0.0354
260	2.936	2.905	0.0312
265	2.972	2.942	0.0300
270	3.004	2.977	0.0265
285	3.093	3.073	0.0196
295	3.158	3.129	0.0289
305	3.206	3.179	0.0272
310	3.238	3.201	0.0366
320	3.270	3.243	0.0272
330	3.313	3.279	0.0339
340	3.345	3.311	0.0341
347	3.369	3.331	0.0382
360	3.396	3.363	0.0333
385	3.435	3.409	0.0257
395	3.449	3.423	0.0256
405	3.465	3.435	0.0296
415	3.477	3.446	0.0314
435	3.495	3.461	0.0336
450	3.495	3.470	0.0249

	$\left(\frac{\tau_e-\tau_s}{\tau_s}\right)^2$	b	(L_∞/L_0-1)	k_2	k_1	$h(0)-h(\infty)$
Initial parameters	3.000, 4	1.000, 0	5.000, 0	8.000, −4	5.000, 1	
	1.200, 4 σ = 2.836, 0	4.000, −1	2.000, 0	9.010, −4.	4.990, 1	3.495, 0
	1.157, 4 σ = 2.763, 0	4.070, −1	1.961, 0	8.968, −4	4.983, 1	3.495, 0
	8.365, 3 σ = 1.836, 0	1.761, −1	2.416, 0	8.917, −4	4.988, 1	3.495, 0
	8.414, 3 σ = 1.836, 0	1.758, −1	2.420, 0	8.913, −4	4.987, 1	3.495, 0

T	Ho-HT(C)	Ho-HT(E)	DH
35	0.030	0.0140	0.0158
40	0.090	0.0530	0.0367
50	0.152	0.1000	0.0518
60	0.232	0.1530	0.0805
65	0.286	0.1840	0.0957
75	0.387	0.2250	0.1623
75	0.387	0.2680	0.1193
80	0.447	0.3340	0.1134
85	0.511	0.4080	0.1032
90	0.579	0.4840	0.0949
95	0.650	0.5590	0.0909
100	0.724	0.6350	0.0888
105	0.801	0.7450	0.0555
110	0.880	0.8380	0.0415
115	0.961	0.9470	0.0136
120	1.094	1.1000	−0.0083
125	1.137	1.1400	−0.0125
127	1.161	1.1810	−0.0196
130	1.213	1.2370	−0.0244
130	1.247	1.2810	−0.0248
135	1.298	1.3400	−0.0417
140	1.922	2.0140	−0.0913
180	2.049	2.1300	−0.0809
180	2.080	2.1650	−0.0850
185	2.126	2.2040	−0.0783
187	2.156	2.2390	−0.0832
190	2.200	2.2750	−0.0749
192	2.244	2.2030	−0.0592
195	2.272	2.3270	−0.0546
201	2.356	2.4000	−0.0439
206	2.423	2.4600	−0.0368
211	2.488	2.5170	−0.0292
215	2.538	2.5560	−0.0183
220	2.598	2.6070	−0.0093
225	2.655	2.6560	−0.0008
235	2.762	2.7420	0.0204
240	2.812	2.7850	0.0272
245	2.859	2.8220	0.0375
250	2.904	2.8610	0.0433
255	2.947	2.9010	0.0456
260	2.987	2.9360	0.0507
265	3.024	2.9720	0.0524
270	3.060	3.0040	0.0558
285	3.154	3.0930	0.0606
295	3.206	3.1580	0.0485
305	3.252	3.2060	0.0463
310	3.272	3.2380	0.0349
320	3.310	3.2760	0.0395
330	3.341	3.3100	0.0308
340	3.367	3.3450	0.0285
347	3.384	3.3690	0.0146
360	3.409	3.3960	0.0129
385	3.444	3.4350	0.0086
395	3.454	3.4490	0.0045
405	3.462	3.4650	−0.0033
415	3.468	3.4770	−0.0087
435	3.478	3.4950	−0.0169
450	3.483	3.4950	−0.0119

Table 3.6

Fit of run (D) to folded chain model with varying fold length. (eq.3.19).

Table 3.7

Fit of run (D) to folded chain model with first order birth. (eq.3.21)

	k_1^*		k_2		k_1		$h(0)-h(\infty)$		σ (%)	
Initial parameters	2.000,	-2	1.200,	2	1.000,	-3				
	2.517,	-1	1.261,	2	1.015,	-3	3.495,	0	3.094,	0
	1.978,	-1	1.256,	2	9.981,	-4	3.495,	0	2.716,	0
	1.535,	-1	1.272,	2	1.000,	-3	3.495,	0	2.578,	0
	9.629,	-2	1.313,	2	1.006,	-3	3.495,	0	2.243,	0
	7.303,	-2	1.349,	2	1.010,	-3	3.495,	0	2.001,	0
	5.549,	-2	1.396,	2	1.017,	-3	3.495,	0	1.756,	0
	4.426,	-2	1.446,	2	1.023,	-3	3.495,	0	1.592,	0
	3.923,	-2	1.478,	2	1.028,	-3	3.495,	0	1.538,	0
	3.639,	-2	1.500,	2	1.031,	-3	3.495,	0	1.522,	0
	3.501,	-2	1.512,	2	1.032,	-3	3.495,	0	1.519,	0
	3.475,	-2	1.514,	2	1.033,	-3	3.495,	0	1.519,	0

T	(H0-HT)Ex.	(H0-HT)C.	DH
25	0.014	0.021	-0.0066
40	0.053	0.074	-0.0214
50	0.100	0.134	-0.0338
60	0.152	0.213	-0.0610
65	0.184	0.260	-0.0759
70	0.225	0.312	-0.0866
75	0.264	0.368	-0.0998
80	0.334	0.428	-0.0942
85	0.408	0.493	-0.0848
90	0.484	0.561	-0.0771
95	0.559	0.633	-0.0739
100	0.655	0.708	-0.0528
105	0.745	0.786	-0.0405
110	0.838	0.866	-0.0276
115	0.947	0.948	-0.0009
123	1.102	1.083	0.0192
125	1.140	1.117	0.0229
127	1.181	1.151	0.0295
130	1.237	1.203	0.0336
132	1.281	1.238	0.0429
135	1.340	1.290	0.0497
172	2.014	1.924	0.0902
180	2.130	2.052	0.0779
182	2.165	2.083	0.0816
185	2.204	2.130	0.0742
187	2.239	2.160	0.0787
190	2.275	2.205	0.0697
193	2.303	2.250	0.0534
195	2.327	2.279	0.0483
201	2.400	2.364	0.0364
206	2.460	2.432	0.0283
211	2.517	2.497	0.0198
215	2.556	2.548	0.0082
220	2.607	2.609	-0.0016
225	2.656	2.667	-0.0109
235	2.742	2.775	-0.0334
240	2.785	2.826	-0.0407
245	2.822	2.873	-0.0515
250	2.861	2.919	-0.0577
255	2.901	2.961	-0.0604
260	2.936	3.002	-0.0656
265	2.972	3.040	-0.0675
270	3.004	3.075	-0.0711
285	3.093	3.169	-0.0759
295	3.158	3.221	-0.0635
305	3.204	3.267	-0.0608
310	3.238	3.287	-0.0490
320	3.270	3.323	-0.0529
330	3.313	3.353	-0.0404
340	3.345	3.379	-0.0341
347	3.369	3.395	-0.0256
360	3.396	3.419	-0.0226
385	3.436	3.451	-0.0159
395	3.449	3.460	-0.0109
405	3.465	3.467	-0.0023
415	3.477	3.473	0.0039
435	3.495	3.482	0.0134
450	3.495	3.486	0.0091

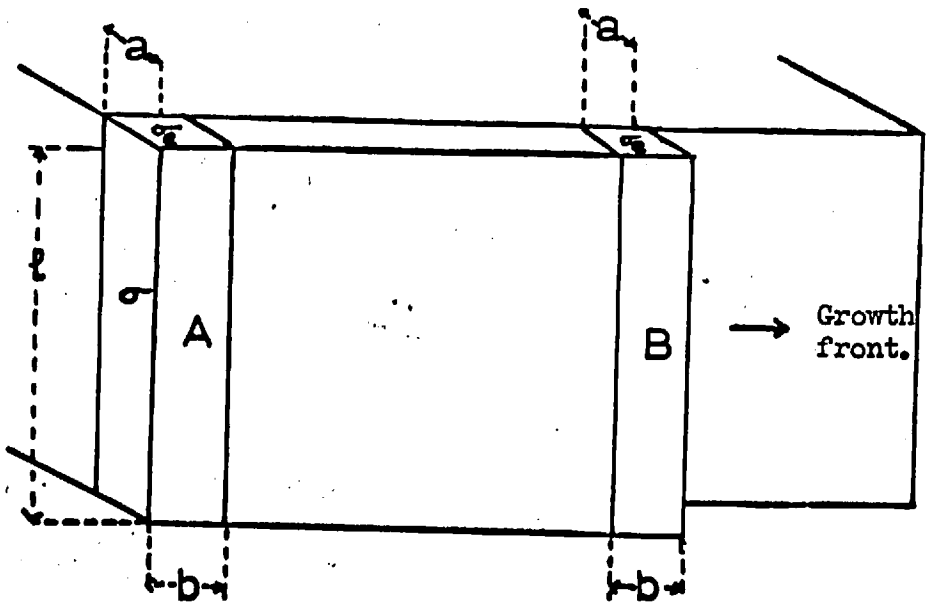


Fig.3.7- Schematic representation of face (B), and corner(A) coherent two-dimensional nuclei.

$$\Delta\phi_c = 2ba\,\sigma_e + 2\,l\,a\sigma - ab\,l\,(\Delta f) \qquad 3.22$$

$$\Delta\phi_f = 2ba\,\sigma_e + \epsilon l a\sigma - ab\,l\,(\Delta f) \qquad 3.23$$

where Δf is the bulk free energy of fusion, and ϵ is a parameter which depends upon the fraction of new face which has to be formed when the fault occurs, and a new face nucleus is built up. At the saddle-points, which correspond to the critical free energies of nucleation ($\Delta\phi_c^*$, $\Delta\phi_f^*$), the dimensions of the critical nuclei can be easily shown to be

$$l^* = 2\,\sigma_e/\Delta f \qquad 3.24$$

For the corner nucleus:

$$b_c^* = 2\sigma/\Delta f \qquad 3.25$$

$$\Delta\phi_c^* = 4a\,\sigma\,\sigma_e/\Delta f \qquad 3.26$$

For the face nucleus:

$$b_f^* = \epsilon\,\sigma\,/\Delta f \qquad 3.27$$

$$\Delta\phi_f^* = 2\,\epsilon\,a\,\sigma\,\sigma_e/\Delta f \qquad 3.28$$

We use the approximation (eq.2.44)

$$\Delta f = \Delta H_f(\Delta T)/T_m \qquad 3.29$$

giving

$$\Delta\phi_c^* = 4a\,\sigma\,\sigma_e T_m/\Delta H_f(\Delta T) \qquad 3.30$$

$$\Delta\phi_f^* = 2\,\epsilon\,a\,\sigma\,\sigma_e T_m/\Delta H_f(\Delta T) \qquad 3.31$$

Hence, plots of $\ln(1/\tau_c)$ and $\ln(1/\tau_f)$ vs. $1/\Delta T$ should be linear. Following eqs.3.17, 3.18, Fig.3.8 shows plots of $\ln k_1 k_2$ and of $\ln k_2^{1/2} k_1$ against $1/\Delta T$. The equilibrium melting point determined by melting at a rate of about

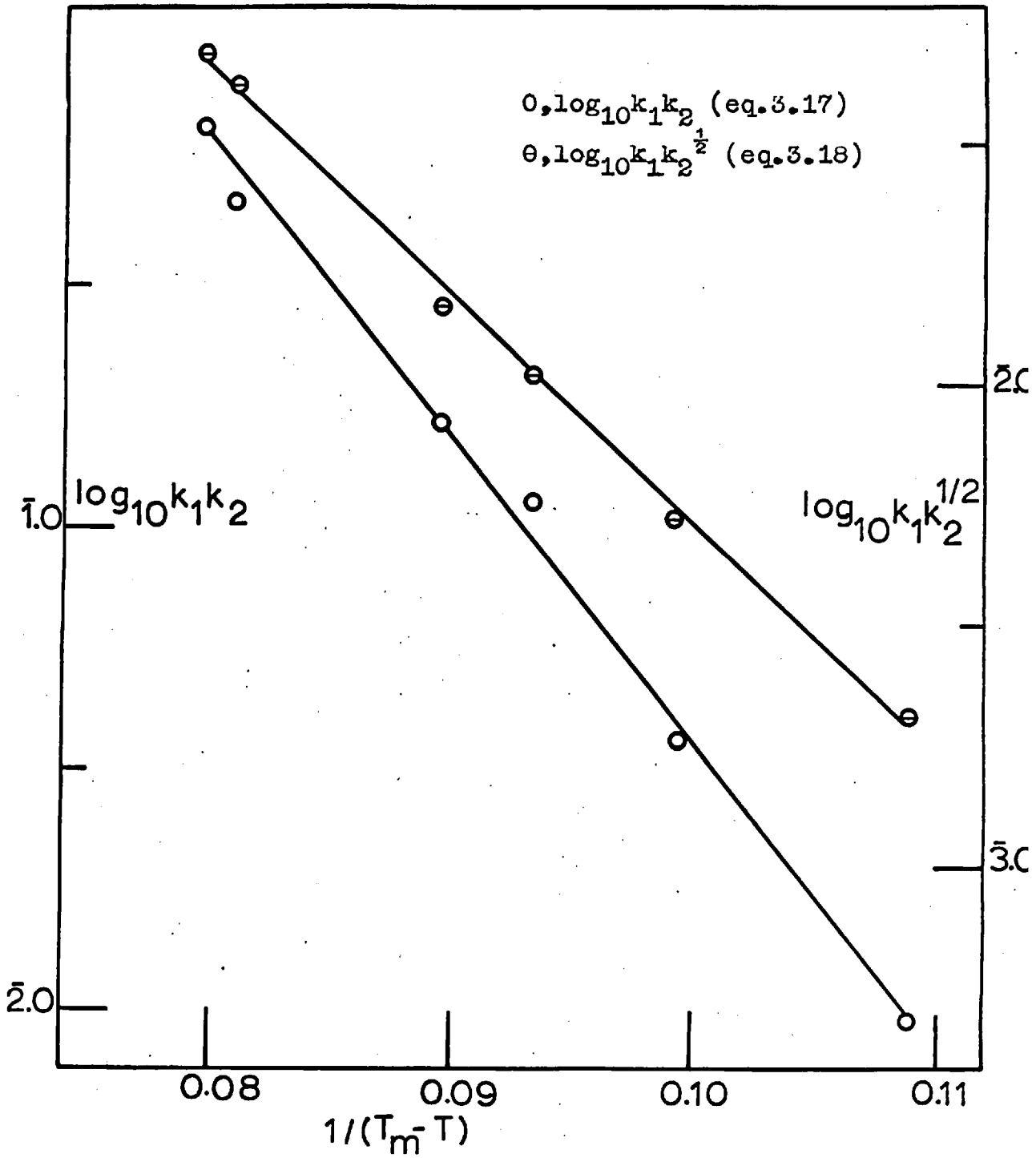


Fig.3.8-Temperature dependence of growth and nucleation parameters with instantaneous birth.

1×10^{-4} °C/sec was 138.3 °C. The linearity of the plots supports the postulate of two-dimensional nucleation in the basic rate-determining steps. Previous investigators have obtained good linear plots of $\ln(z)$ against $1/(\Delta T)^2$ (cf. eq.2.48) when analysing their data according to the unrefined Avrami model (Tung and Buckser 1959; Banks et al. 1963a) especially when allowance (Banks et al.1963a) was made for the variations of n with temperature (cf. Table 3.2). The more detailed chain-folding model splits the overall temperature dependence ($1/\Delta T^2$) corresponding to a single three-dimentional act into two two-dimensional acts ($1/\Delta T$) exactly as postulated (Fig.3.5). The slopes of the plots in Fig.3.8 throw some light on the energetics of the process, but a detailed discussion is not justified. Thus the slopes of the plots in Fig.3.8 include (eqs.3.17, 3.18) contributions from the temperature dependence of the density ρ of primary nuclei and the fold length l. The linearity of the plot implies that over the temperature range tested neither $\ln(l)$ nor $\ln(\rho)$ vary with temperature more sharply than $1/\Delta T$. On the assumption that $1/\ln l$ can be expanded as $a_1 \Delta T + a_2 \Delta T^2 \ldots$, then near the melting point, $\ln l$ will vary as $1/\Delta T$. The temperature dependence of $\ln(\rho)$ just deduced implied that the birth of primary nuclei does not involve spontaneous nucleation in more than two dimensions. In fact, applying the analysis of

temperature dependence to the model involving first order birth of primary nuclei (Fig.3.9), the logarithm of this first order rate constant again appears to vary linearly with $1/\Delta T$ (corresponding to two-dimensional nuclei) though the experimental scatter of the three relevant plots in this figure is somewhat increased in this more refined model.

3.4 The Secondary (Post-Avrami) Crystallization of Polymethylene

In this section it will be shown that a general equation for the bulk relaxation of matter derived by Hirai and Eyring (1958) satisfactorily describes the secondary crystallization of polymethylene. The secondary and primary crystallizations are combined to give an overall rate equation which gives a good fit over the whole of the crystallization process.

To gain the maximum information on the secondary process, a run was carried out until no further contraction occurred (Fig.3.2A) which took six weeks. This thermal treatment was found to suppress the secondary process, allowing the isolated primary process to be interpreted (Fig.3.2B) (Section 3.3).

The Hirai-Eyring Rate Equation

Hirai and Eyring (1958) have derived a rate equation for the bulk relaxation of matter which considers that the activation energy of the relaxation process varies linearly with

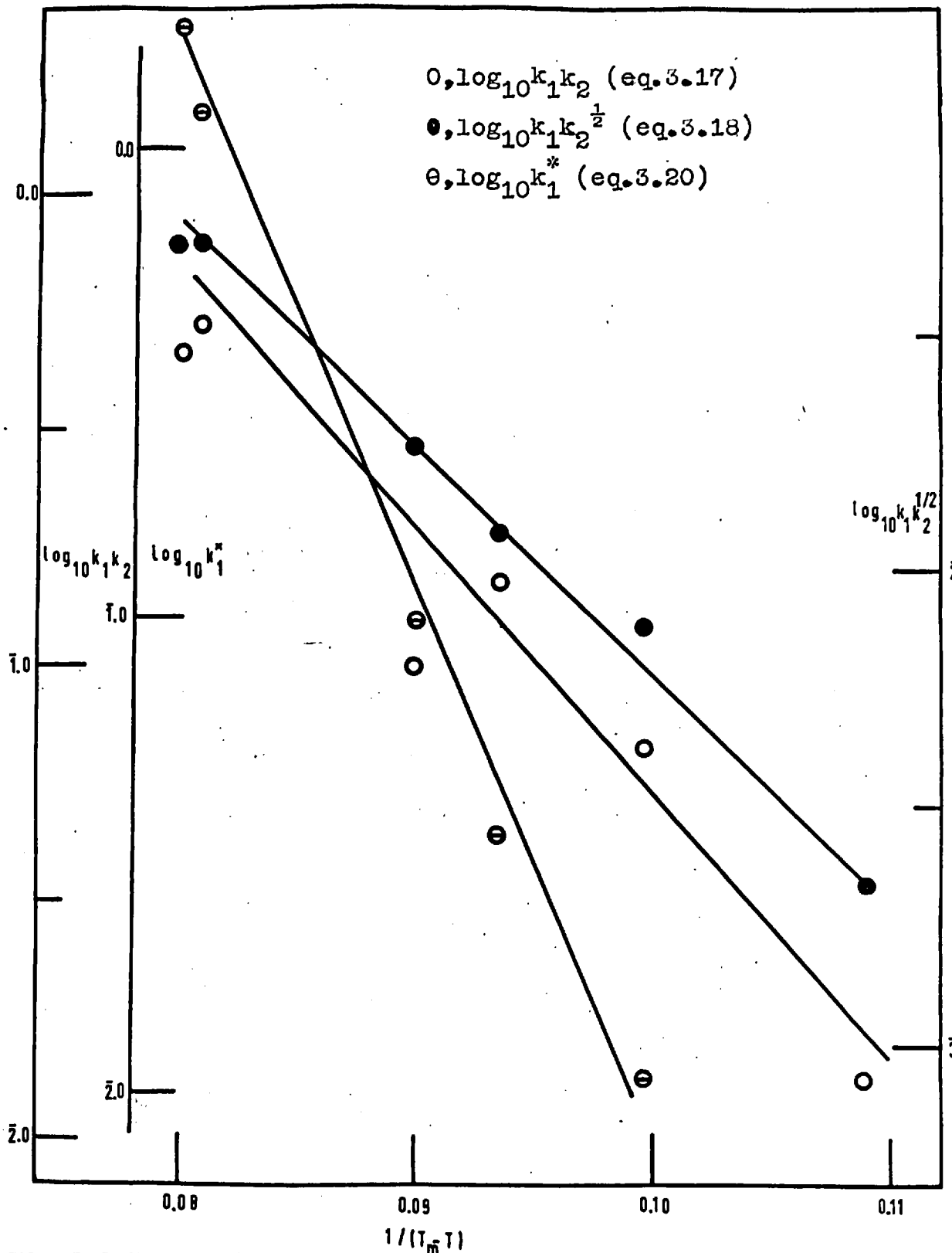


Fig.3.9-Temperature dependence of growth and nucleation parameters with first-order birth of nuclei.

the distance from equilibrium. This is in contrast to Maxwell's treatment for the relaxation of matter which assumes a constant activation energy. The differential equation describing the volume contraction is given as

$$-\frac{1}{V}\frac{dV}{dt} = \frac{kT}{h}\exp -\left(\frac{\Delta F^{\neq}}{kT}\right) 2 \sinh \left(\frac{a}{2}\,\frac{V - V_{\infty}}{V_{\infty}}\right) \qquad 3.32$$

where V_{∞} is the volume at $t = \infty$, and a is a constant, related to the molar volume V_m of the kinetic unit, and the difference between the compressibilities $\Delta\beta$ of the liquid and the glass by the equation

$$a = V_m / 6RT\,\Delta\beta \qquad 3.33$$

$\Delta F^{\neq}$ is the energy of activation of the forward and backward reactions at equilibrium, where they are taken as equal.

The solution of eq.3.32 is

$$\tanh \frac{a}{2}\left(\frac{V - V_{\infty}}{V_{\infty}}\right) = \tanh \frac{a}{2}\left(\frac{V_o - V_{\infty}}{V_{\infty}}\right) \exp - t/\tau \qquad 3.34$$

where τ is a relaxation time. This treatment has been shown to describe relaxation processes in a variety of materials, such as glasses fibres and metals (Ree, Hahn and Eyring 1955).

In terms of crystallinity, eq.3.34 becomes

$$\tanh \frac{a}{2}\left(\frac{\chi_{\infty} - \chi_{s,\,t}}{M - \chi_{\infty}}\right) = \tanh \frac{a}{2}\left(\frac{\chi_{\infty} - \chi_{s,\,0}}{M - \chi_{\infty}}\right)\exp - t/\tau \qquad 3.35$$

where M is related to the specific volumes of the crystalline and amorphous phases V_c, V_a, by the expression

$$M = V_a/(V_a - V_c)$$

and where $\chi_{s,\,t}$ is the degree of crystallinity of a volume

element which has been in existence for time t, its crystallinity being $\chi_{s,\,0}$ at t = 0. It can be seen as follows that this equation approximates to the linear χ vs. $\ln(t)$ plot to which the secondary crystallization also approximates.

Expanding the left hand side of eq.3.35 for large values of the argument, retaining the first two terms, and expanding exp $- t/\tau$ for $\tau \gg t$, gives

$$1 - 2\exp - a\left(\frac{\chi_\infty - \chi_{s,\,t}}{M - \chi_\infty}\right) = \tanh \frac{a}{2}\left(\frac{\chi_\infty - \chi_{s,\,0}}{M - \chi_\infty}\right)(1 - t/\tau) \qquad 3.36$$

$$\approx 1 - t/\tau \qquad 3.37$$

giving

$$\ln(t/2\tau) = -a\left(\frac{\chi_\infty - \chi_{s,\,t}}{M - \chi_\infty}\right) \qquad 3.38$$

$$\text{i.e.} \qquad \chi_\infty - \chi_{s,\,t} \propto \ln(t) \qquad 3.39$$

This approximation fails as $t \to \infty$, when eq.3.35 approximates to a Maxwellian (first-order) relaxation law. Thus, expanding $\tanh \frac{a}{2}\left(\frac{\chi_\infty - \chi_{s,\,t}}{M - \chi_\infty}\right)$ for small arguments (i.e., as $\chi_{s,\,t} \to \chi_\infty$), equation 3.35 becomes

$$\frac{a}{2}\left(\frac{\chi_\infty - \chi_{s,\,t}}{M - \chi_\infty}\right) = \tanh \frac{a}{2}\left(\frac{\chi_\infty - \chi_{s,\,0}}{M - \chi_\infty}\right) \exp - t/\tau \qquad 3.40$$

$$\text{i.e.,} \qquad \chi_\infty - \chi_{s,t} \propto \exp - t/\tau \qquad 3.41$$

Derivation of Overall Rate Equation

The proposed model combining the two rate processes is now described. Crystalline entities grow in the supercooled melt according to a rate equation describing the primary (Avrami) crystallization, the total crystallinity at time t due to this process alone is given by $\chi_{a,t}$. Thus, when a volume element is incorporated in the growing entity, its crystallinity 'jumps' from zero to $\chi_{a,\infty}$, the final degree of crystallinity approached by the Avrami process alone. Immediately after a volume element has attained this degree of crystallinity, a further process begins in it, whereby its crystallinity increases from $\chi_{a,\infty}$ to $\chi_{s,T}$. Here T is the time measured from the moment the element was incorporated in the growing entity. The exact form of these two rate equations need not be specified for the present, but that for the Avrami process has been discussed fully in section 3.3.

The combined crystallinity $\chi_{c,t}$ at time t due to the Avrami process (χ_a) and the secondary process (χ_s) is given by

$$\chi_{c,t} = \int_0^t \frac{\chi_{a,t}}{\chi_{a,\infty}} \cdot \frac{\frac{d}{d\theta}(\chi_{a,\theta})}{\chi_{a,t}} \cdot \chi_{s,(t-\theta)}\, d\theta \qquad 3.42$$

The first two terms give the probability that a volume element had been incorporated in a growing entity at time θ, the final term giving the crystallinity of this element which has been in

existence for time $(t - \theta)$ at time t. When suitable rate laws for $\chi_{a,t}$ and $\chi_{s,T}$ are substituted in eq.3.42, $\chi_{c,t}$ can be compared with that measured dilatometrically.

Integrating 3.42 by parts gives

$$\chi_{c,t} = \frac{1}{\chi_{a,\infty}} \left[\chi_{a,\theta} \cdot \chi_{s,(t-\theta)}\right]_0^t - \int_0^t \left(\frac{\chi_{a,\theta}}{\chi_{a,}}\right) \frac{d}{d\theta} \chi_{s,(t-\theta)} d\theta \qquad 3.43$$

At $\theta = 0$, $\chi_{a,\theta} = 0$

At $\theta = t$, $\chi_{s,(t-\theta)} = \chi_{a,\infty}$

Eq.3.43 becomes

$$\chi_{c,t} = \chi_{a,t} - \int_0^t \left(\frac{\chi_{a,\theta}}{\chi_{a,\infty}}\right) \frac{d}{d\theta} \left[\chi_{s,(t-\theta)}\right] d\theta \qquad 3.44$$

Evaluation of dilatometric data

The two runs, with and without the secondary crystallization process present are now used to test various forms of the overall rate equation 3.44. As before (section 3.3) equations having a number of adjustable parameters are fitted to the experimental rate curves (using a least squares procedure) on the Mercury Computer. Results of such fittings are presented in the form of 'difference' plots, and standard deviations. This presentation allows critical evaluation of the merit of the various rate equations used. The overall rate equations corresponding to various forms of the primary and secondary rate processes are now derived and fitted to the dilatometric

measurements. The secondary crystallinity ($\chi_{s,t}$) is given by the Hirai-Eyring equation (3.35) as:-

$$\chi_{s,t} = \chi_{\infty} - [\frac{2}{a}(M - \chi_{\infty})] \tanh^{-1}[(\tanh C)\exp - t/\tau] \qquad 3.45$$

where $C = a\chi_{s,\infty} / 2(M - \chi_{\infty})$ 3.46

$\chi_{s,\infty}$ is the total additional crystallinity added during the secondary crystallization process, i.e., the difference between the final crystallinity χ_{∞} , and that of $\chi_{a,\infty}$ due to the primary crystallization alone. Using eqs.3.44 and 3.45 the integrated rate equation becomes

$$\chi_{c,t} = \chi_{a,t} + \frac{\chi_{s,\infty}}{C} \int_{\exp -t/\tau}^{1} \frac{\chi_{a,\theta}}{\chi_{a,\infty}} \frac{\tanh C}{1-u^2\tanh^2 C}\, du \qquad 3.47$$

where

$$\theta = \tau \ln(u) + t \qquad 3.48$$

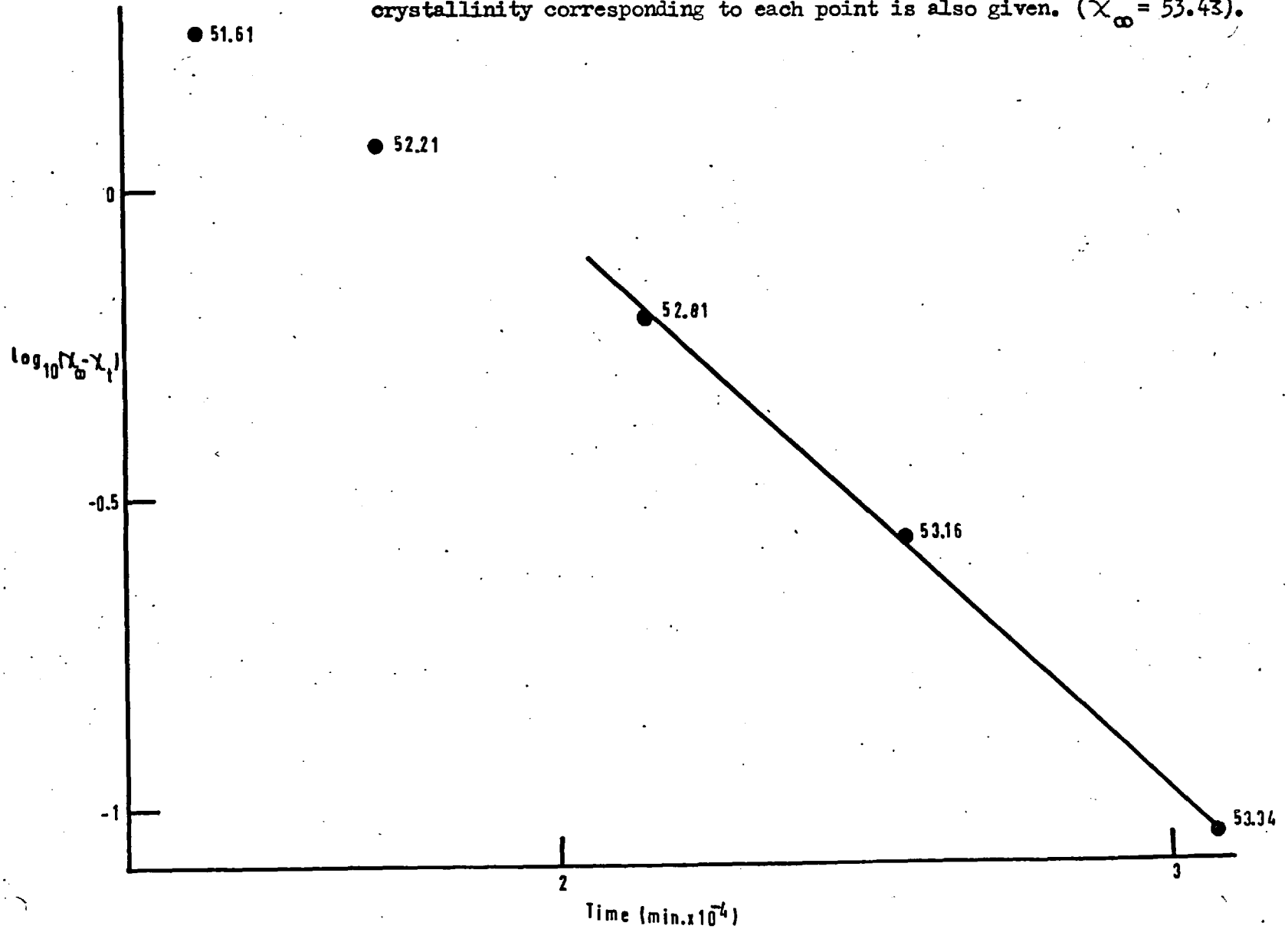
This equation (3.47) is insensitive to the value of τ except at high times. Thus τ is best found by applying the first order decay law (eq.3.41)

$$(\chi_{\infty} - \chi_{c,t}) \propto \exp - t/\tau \qquad 3.49$$

to the final experimental points (Fig.3.10) giving a value of of 4,300 mins. The value of χ_{∞} was taken, when no further contraction occurred after 4 days.

Eq.3.47 will have various forms depending on the rate equation used to describe the primary crystallization process.

Fig.3.10- Final points of Fig.3.2(A),plotted as first order decay law. The percentage crystallinity corresponding to each point is also given. (χ_∞ = 53.43).



Two examples will now be examined.

(1) In the absence of the secondary crystallization, the isolated primary process can be fitted to the Avrami equation with the following parameters: $n = 1.99$, $z = 5.34 \times 10^{-5}$ with standard deviation 2.64% (Table 3.2). The small standard deviation suggests that an overall rate equation with the Avrami equation representing the primary process may give a good fit to the experimental rate curve. The overall rate equation now becomes in terms of dilatometric measurements:

$$[h(o) - h(c,t)] = [h(o) - h(a,\infty)]\,(1 - \exp - zt^n) \quad + \quad \frac{2}{a}\,[M - \chi_\infty]\int_{\exp -t/\tau}^{1} (1 - \exp - z\theta^n)\,\frac{\tanh C}{(1 - u^2\tanh^2 C)}\,du \qquad 3.50$$

with the six adjustable parameters

$$[h(o) - h(a,\infty)];\quad [h(o) - h(s,\infty)];\quad z;\quad n;\quad \frac{a}{2(M - \chi_\infty)};\quad \tau$$

The integral in equation 3.50 could not be evaluated analytically, and was approximated by the 12 point Gauss formula. The best fit to the experimental data (76 points) was obtained with the parameters $h(o) - h(a,\infty) = 1.833$ cm, $h(o) - h(s,\infty) = 3.631$ cm, $z = 6.3 \times 10^{-5}$, $n = 2.12$, $\frac{a}{2(M - \chi_\infty)} = 1.05\ \text{cm}^{-1}$, $\tau = 4{,}200$ mins, giving $\sigma = 1.17\%$ (difference plot Fig.3.11A). This fit, apparently excellent, is not considered valid, but arises from a compensation of errors; the calculated value (1.833 cm) of the total contraction in the Avrami stage of the combined process is much

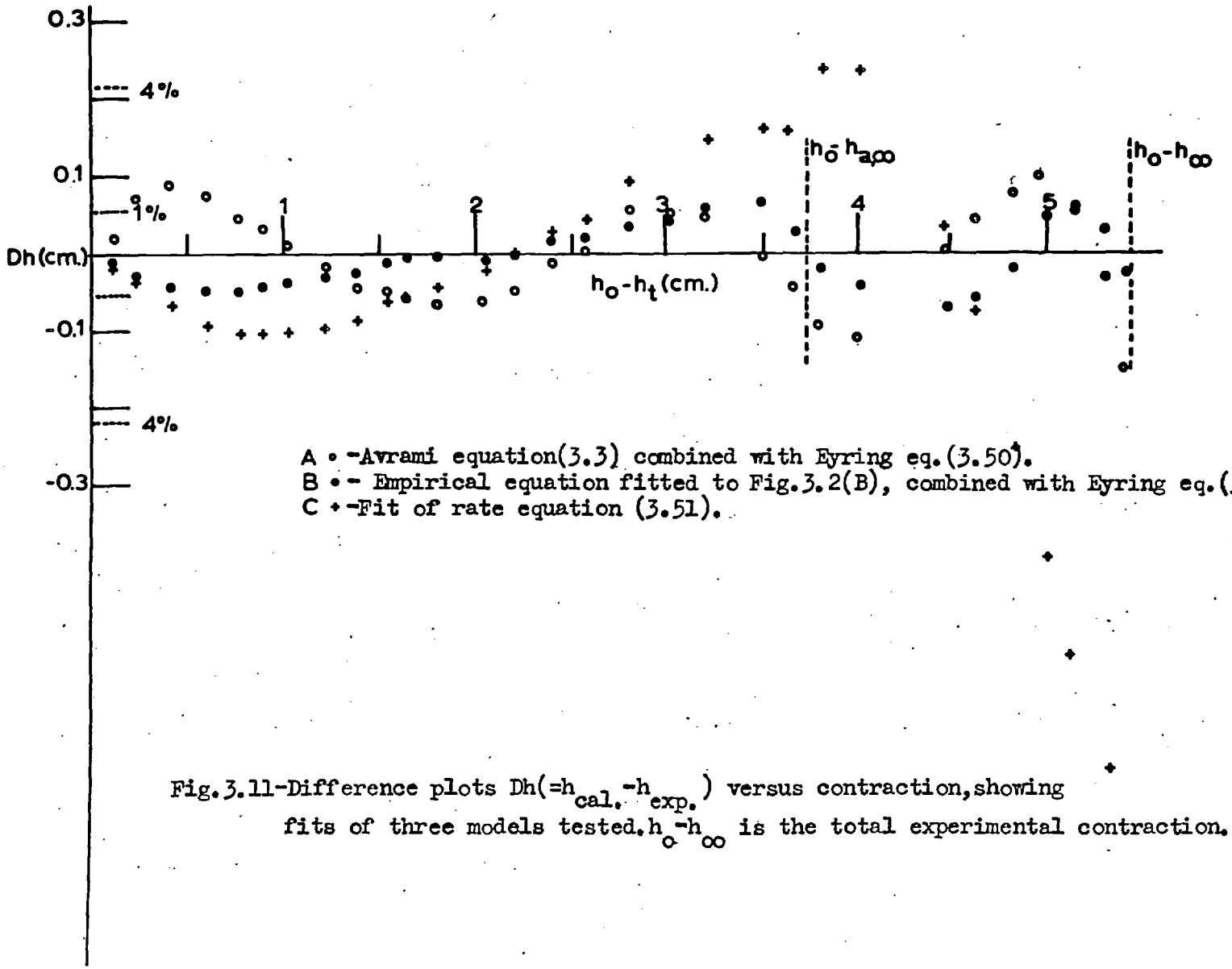


Fig.3.11-Difference plots $Dh(=h_{cal.}-h_{exp.})$ versus contraction, showing fits of three models tested. h_o-h_∞ is the total experimental contraction.

smaller than that measured (3.737 cm) on the isolated Avrami process. The best analytical fit for the primary crystallization process alone was still greater than 1% (folded chain model + first-order birth, section 3.3, Table 3.2).

(2) To provide a sensitive test of the post-Avrami rate equations, an empirical equation was fitted to the limit of the experimental accuracy to $\chi_{a,t}$ measured in the absence of the secondary process (Fig.3.2B). Thus, a least squares fit of a Chebychev polynomial of order 15 gave a standard deviation of approximately 0.2% (eq.2.59). This empirical expression was then substituted into eq.3.47 which was modified to take account of the slight lateral displacement of Fig.3.2A with respect to Fig.3.2B. This displacement may be due to a slight lowering of T_m because of a change in the molecular weight after the prolonged thermal treatment, or to uncertainty in the temperature setting. The displacement in the rate curve corresponds to a change in $(T_m - T)$ of only 0.06 ^{o}C. It is allowed for by an additional parameter, k, i.e. by replacing t by kt. A least squares fit (σ = 0.67%, difference plot Fig.3.11B) gave the two parameters

$$k = 1.17 \quad ; \quad \frac{a}{2(M - \chi_{\infty})} = 1.19 \text{ cm}^{-1}$$

This gives a value of the dimensionless parameter a = 136. The value of τ was kept constant, at 4,200 mins as only the final points are at all sensitive to its value.

(3) The secondary crystallization process is frequently taken to be linear with log(t), and this is seen to be approximately true (Fig.3.2A) for a substantial part of this process. With the primary process described by the empirical expression [c.f.(2)] and the secondary one by this log(t) relationship, the overall rate equation becomes:

$$\chi_{c,t} = \chi_{a,t} + \beta \int_0^t \frac{\chi_{a,\theta}}{\chi_{a,\infty}} \quad \frac{1}{t + 1 - \theta} \; d\theta \qquad 3.51$$

Here, we have assumed that the secondary crystallization is given by the expression

$$\chi_{s,(t-\theta)} = \beta \ln(1 + t - \theta) + \chi_{a,\infty} \qquad 3.52$$

The unit added to $(t - \theta)$ on the right serves to give the proper boundary condition at zero time. The least squares fit to this equation gave the parameters

$$\beta = 0.118 \; ; \qquad k = 1.16$$

with $\sigma = 2.5\%$ (difference plot Fig.3.11C).

Discussion of fit of dilatometric data

The difference plot (Fig.3.11) showing the fit of the various special cases of the general rate equation 3.42 demonstrates that the most satisfactory equation is the one combining the empirical equation fitted to the kinetically isolated primary process, with the secondary process described by the Hirai-Eyring equation. This result supports the basic concept underlying all of the rate equations tested: that there are

two consecutive rate processes occurring in the crystallization of polyethylene, viz., the primary one which occurs instantaneously at any point in space, and immediately triggers off the slow secondary one. The contention that the specific thermal treatment has resulted in the complete suppression of the secondary crystallization is also supported. These plots also show that the Hirai-Eyring equation successfully describes the secondary crystallization, the superiority over the usual χ vs. log(t) relationship being especially evident in the transition region between the two processes, and at the end of the secondary process.

Chain folding and the post-Avrami crystallization

It has been shown that a model incorporating the growth of single crystals by a chain-folding mechanism can be satisfactorily fitted to the kinetics of the isolated primary crystallization process (section 3.3). The substantial amorphous fraction (approximately 60 - 70%) remaining after completion of the primary crystallization is accounted for on this model by a disordered region between the crystals containing chain segments emanating from the crystal face. These segments may form loops projecting from one crystal or connect two crystals. Fischer and Schmidt (1962) have shown by X-ray measurements that in polyethylene crystallized both from the bulk, and from dilute solution, the long spacing varies linearly with log (t) and is here equated with the secondary crystallization observed dila-

tometrically which varies nearly linearly with log (t) (Fig.3.2A). Fischer (1962), deduced that this increase in the long period (which may double in 24 hours) cannot be due to the growth of crystallites at the expense of the interstitial amorphous regions. He postulated that the micro-structure breaks down when the long period increases which will require a complete refolding of the chains on the single crystal mechanism. Fitting dilatometric data alone to the Hirai-Eyring eq.3.45, cannot give detailed mechanistic information, because of its great generality, apart from the size of the relaxing unit (see below). Many investigators (Fisher and Schmidt 1962; Stratton and Geil 1960; Ranby, Moorhead and Walter 1960) have found that when single crystals grown at a low temperature are annealed at a higher one, an increase in the long period is also found. Fischer et al.(1962) and Stratton et al.(1962) have noted a similar result for bulk crystallized polyethylene. Geil (1962) has further shown that the low angle spacings correspond to the actual lamellar thickness as measured by electron microscopy. These results suggested that the analogy between solution and bulk crystallized polyethylene could be further investigated dilatometrically by bulk crystallization at a low temperature at which the primary process is completed within a few minutes, followed by annealing at a higher temperature. A sample of the polymethylene in which the secondary process was still present was crystallized from the melt at 58.23 ^{o}C until all crystallization had finished. The temperature was then raised to 127.60 ^{o}C when further

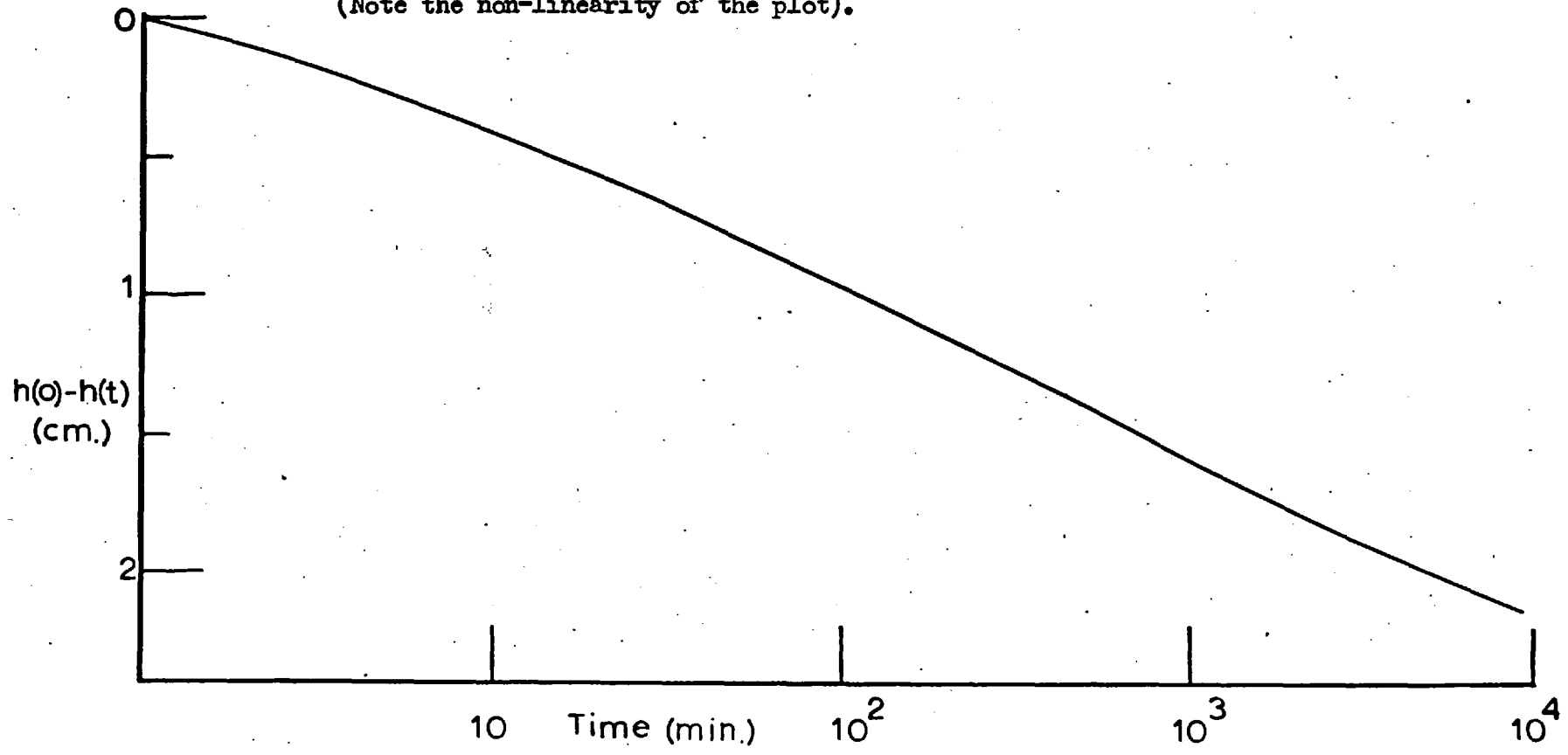
crystallization was observed (Fig.3.12. Note departure from linearity). The least squares fit to the Eyring equation was extremely close (σ = 0.33% with the two parameters

$$\frac{a}{2(M - \chi_\infty)} = 1.88 \text{ cm}^{-1} \; ; \quad h(o) - h(s,\infty) = 2.366 \text{ cm}$$

giving a = 275.

The very low standard deviation indicates that this fit is approaching the limit of the experimental error. The good agreement to the Eyring equation, and the similarities of the degree of crystallinity added during the secondary crystallization (0.166, 0.181) support the contention that this process, and the one occurring concurrently with the primary process when polymethylene is crystallized at a high temperature are the same. The value of the parameter a, is related to the number of units involved in the relaxation (eq.3.33). For the sample rapidly quenched, and then annealed, it is approximately twice that found for the sample isothermally crystallized at 127.18 ^{o}C. This behaviour is expected since the crystallites formed at the low temperature will be less perfect than those formed at the high temperature, and hence the subsequent relaxation will involve a greater number of repeat units. The value of the parameter a, calculated from eq.3.33 for a single ethylene repeat unit $-CH_2-CH_2-$ is found to be about 4. (The value of $\Delta\beta$ used was that for polystyrene 4×10^{-11} cm^2 dyne^{-1}, due to the scanty information

Fig.3.12.-Experimental plot of secondary crystallization rate curve after a sudden increment in temperature from 58.23°C to 127.6°C.
(Note the non-linearity of the plot).



available on polyethylene.) Agreement with Eyring's scheme therefore demands a relaxing unit of approximately 70 repeat units in the case of the quenched sample, and 35 for the isothermally crystallized one. The thickness of the lamellae was found to be of the order 100 - 200 Å which corresponds to about 50 ethylene repeat units (see section 3.1).

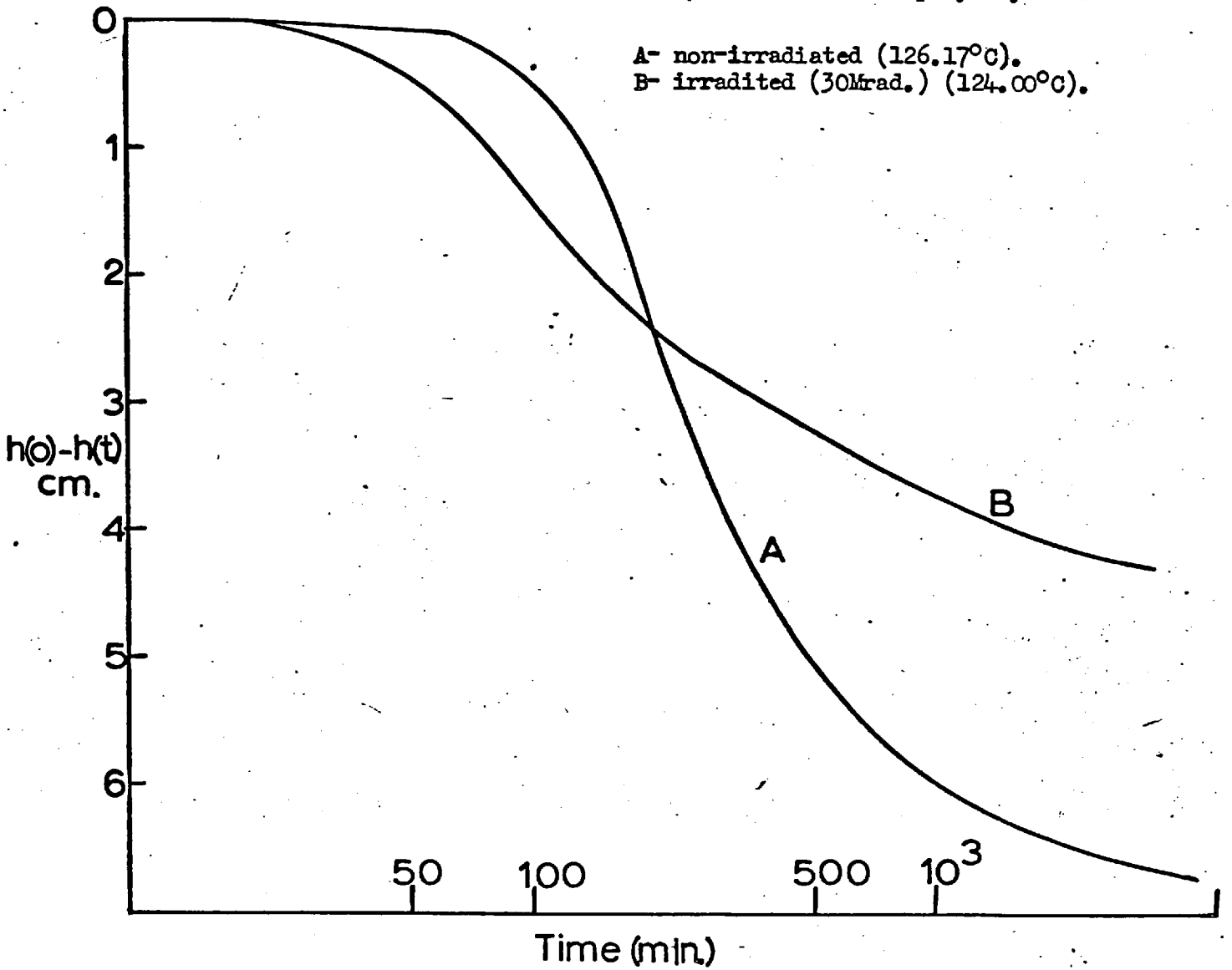
The two techniques of thermal pretreatment and changing the crystallization temperature allow the kinetic isolation of the two consecutive crystallization processes which occur in polyethylene. (High pressures also allow some separation of the two processes - Matsuoka 1960). The mechanism whereby the thermal pretreatment suppresses the occurrence of secondary crystallization in subsequent runs is not known. It may result from a small degree of cross-linking which decreases the chain mobility in the amorphous layer to such an extent that the rearrangement necessary for the further increase in the lamellar thickness may be unable to take place.

The Effect of Radiation on the Secondary Crystallization

To determine if the secondary crystallization can be suppressed by cross-linking, crystalline samples have been irradiated with γ-radiation from a Co^{60} source. Irradiation was carried out with the sample in the dilatometer, a measure of the degree of cross-linking being obtained by measuring the mercury displacement in the dilatometer stem due to the evolved

hydrogen. Any estimate of dose, derived from the distance of the dilatometer from the source must be approximate due to the shielding of the sample by the glass and mercury. The effect of radiation on the crystallization of a fraction of Philips polyethylene (M_w = 6 800) is shown in Fig.3.13. The sample was crystallized (Curve A) to give 67% crystallinity, and then irradiated (approximately 30 megarads) the volume of hydrogen evolved corresponding to approximately 1 cross-link per polymer chain. On subsequent crystallization (Curve B), the final degree of crystallinity was reduced to 44% but there is no evidence for the suppression of the secondary crystallization. When a sample of crystallized polymethylene was irradiated with approximately the same dose, the subsequent crystallization after melting was initially too fast to be measured, even at 130 ^{o}C, when the rate would be expected to be very slow. After this initial rapid crystallization, the slow secondary crystallization was still present. This initially rapid crystallization may be due to parallel chain segments in a primary or secondary nucleus being cross-linked so that on melting, the nuclei cannot be destroyed without chemical degradation, the subsequent crystallization resembling the 'seeded' experiments. In the low molecular weight sample, a critical nucleus may consist of more than one polymer chain, and hence on melting, the critical nucleus can be destroyed. This explanation receives support

Fig.3.13.- Effect of radiation on the crystallization of polyethylene.



from the observation of a number of workers (Koncally, Gard and Alder 1964; Mandelkern, Roberts and Halpin 1960; Hammer, Brandt and Peticolas 1957) that the birefringence of polyethylene which has been irradiated in the crystalline state can persist above the melting point.

Keller (1964) has shown that the long spacing of single polyethylene crystals, crystallized from solution, is still increased by annealing, even after being cross-linked by irradiation. He interprets this as being due to the cross-linking occurring preferentially near the fold.

3.5 Crystallization after Partial Melting ('Seeding')

Fig.3.14 shows plots of the volume of an isolated entity against time, for the sample of polymethylene deprived of its post-Avrami crystallization, crystallized from various degrees of seed crystallinity (χ_s/χ_∞ = 0.2% → 33.3%) the unseeded run D also being shown. The seeded runs A, B and C when conventionally analysed in terms of the Avrami equation correspond to values of n near unity. Its value will vary from below unity for A, to above unity for C. The unseeded run (D) corresponds to an Avrami exponent of 2.28 (Table 3.2).

Seeding and reversibility

Fig.3.14 shows that, between 0 and 30% seed crystallinity the final linear growth rate is practically independent of the

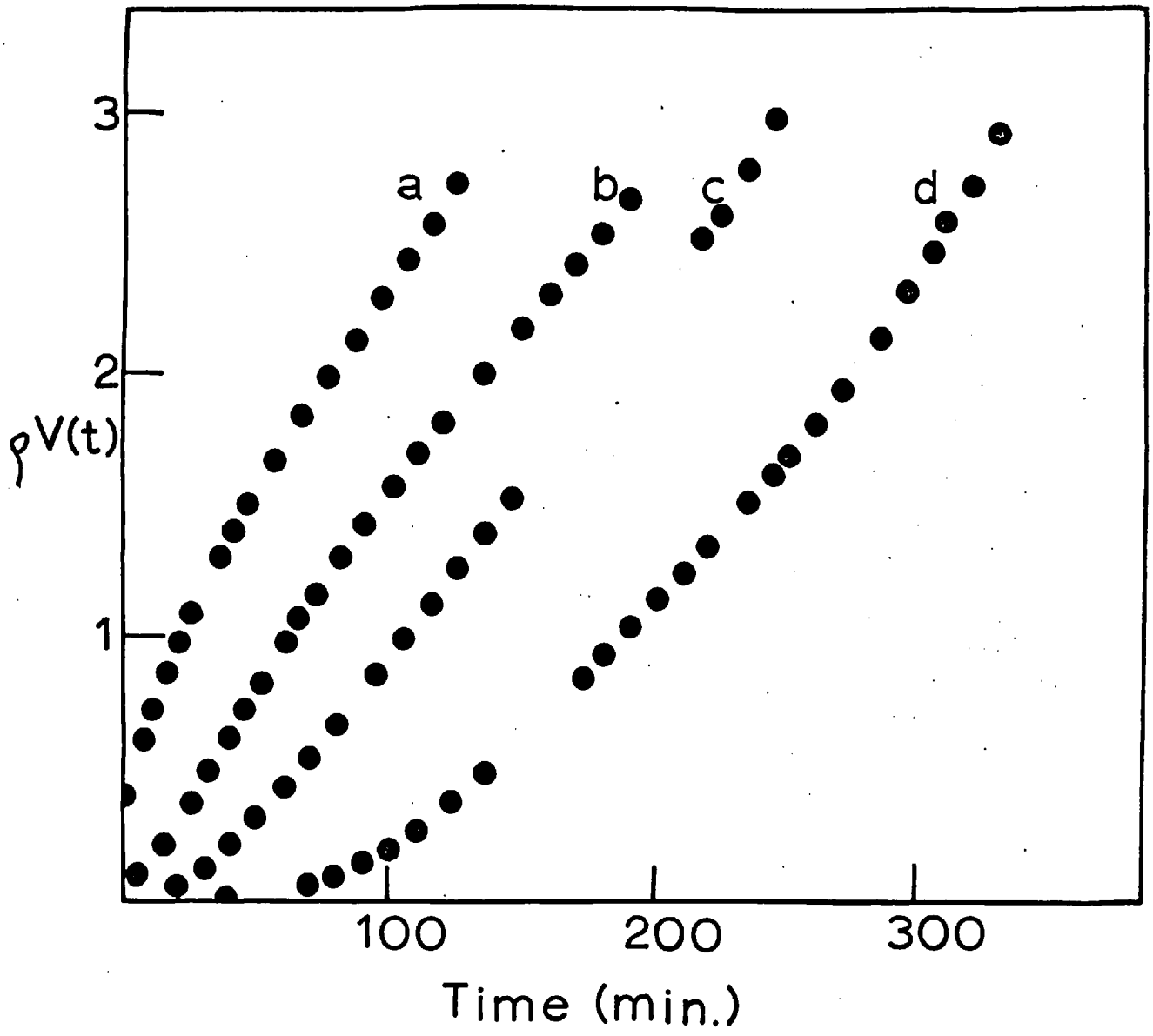


Fig.3.14-Effect of varying 'seed' concentration on the growth of entities. (127.61°C).

a,33.3%; b,6.9%; c,0.2%; d,0%;

amount of seed crystallinity. This could be achieved by cancellation of changes in ρ and dV/dt with varying seed crystallinity, but it is more reasonable to assume that both quantities are constant at high times. The constancy of the final slopes of the plots A to D in Fig.3.14 suggests that there is an element of reversibility in the cycle of partial melting and subsequent crystal growth, and the constancy of ρ would show that the partial melting process does not lead to the total loss of any crystal entities (by shrinking them below their critical size). The initial increase in growth rate of plot A, when compared to D, suggests the following picture of partial melting. Ordered chain segments are lost by disordering at the surface of a partially melted crystal, which thus shrinks (but not below its critical size). However, the disordered chain segments which lie near the surface retain some memory of their state of order, leading to rapid initial crystal growth on subsequent isothermal crystallization at a lower temperature.

CHAPTER IV

The Crystallization of Polypropylene, Polybutene, Poly-(ethylene oxide) and Polystyrene

Introduction

In this chapter, the results of studies of the kinetics of crystallization of four further polymers will be described. The secondary crystallization which complicates the interpretation of the crystallization of polyethylene is absent, or only present to a slight extent in these four polymers. In addition, these polymers with the exception of polystyrene readily show spherulites under the polarizing microscope. Polypropylene, polybutene and poly-(ethylene oxide) are thus good systems for investigating the validity of the Avrami equation, as all three polymers would be expected to give values of the Avrami exponent of 3 or 4 (eqs. 2.16, 2.19, 2.25) corresponding to the constant radial growth of instantaneously or sporadically nucleated spheres (section 2.2).

4.1 Morphology

Unlike polyethylene, the morphology of these polymers, both when crystallized from dilute solution and from the bulk, has not been intensively studied. However, single crystals of polypropylene (Ranby, Morehead and Walter 1960), polystyrene (Kargin, Bakeer, Li and Ochapovskaya 1960) and poly-(ethylene oxide) (Keller 1962) have been detected when crystallization occurs from dilute solution.

The bulk morphology of polypropylene has been investigated using Palmer's etching technique (section 3.1). Treatment of a film of polypropylene with ozone for three days rendered it brittle. Fig.4.1a and b show such a film of polypropylene under the polarizing microscope before and after treatment with ozone. Fig.4.1b shows that after slight scratching, radial cracks have developed in the film. When the film was dispersed in water using ultrasonics, and the resulting suspension examined by the electron microscope, rhomb-like structures were seen. Fig.4.1c shows such an object after shadowing with gold and palladium, which has apparently split down the middle. Terraces can also be seen on the face of this object which may indicate a lamellar structure. Similar treatment of a film of poly-(ethylene oxide) with ozone was fruitless since it rendered the material soluble in water, owing to excessive degradation.

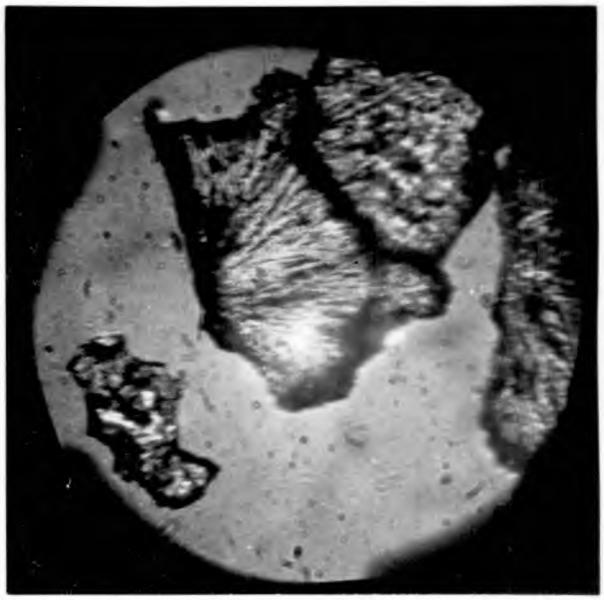
4.2 The Crystallization of Polypropylene

Previous workers studying the crystallization of this polymer (Griffith and Ranby 1959; Marker, Hay, Tilley, Early and Sweeting 1959) quote the best integral value of the Avrami exponent as 3, although the data of Griffith and Ranby show deviations from the theoretical curve towards the end of the crystallization (see their Fig.2). Parrini and Corrieri (1963) found that the value of n depends upon molecular weight and

Fig.4.1



a)Polypropylene spherulites (x100).



b)Polypropylene spherulites after degradation by ozone. (x100).



c)Electron micrograph of degraded specimen (b). (original negative x5,500)

crystallization temperature, varying from 2.8 to 4.1. These values were obtained by the conventional double logarithmic plot (section 2.7) and so little measure of the goodness of the fit is available. The polypropylene ($P_v = 9.8 \times 10^3$) used in the present investigation was obtained from Shell Research Ltd. Fig.4.2 shows seven crystallization isotherms covering a temperature range of 15 °C. The almost total absence of any secondary crystallization facilitates the analysis of these runs. However, owing to the slight degree of secondary crystallization, the value of $[h(o) - h(\infty)]$ was made a further adjustable parameter when fitting the Avrami equation (2.25) to the data. Table 4.1 shows the result of the least-squares fits. In only one run is the difference between the final experimental measurement taken, and the optimum value of $[h(o) - h(\infty)]$ greater than 3% of $[h(o) - h(\infty)]$. The remarkably low standard deviations (0.34 - 1.26%) show that the crystallization is well fitted by the Avrami equation. The difference plot of a representative run (Fig.4.3a) shows that the deviations are still highly systematic, although it is found that the pattern varies in different runs. This indicates that the residual deviations may in some part be due to experimental scatter. In all the runs, the value of the Avrami exponent is 2.5 ± 0.1 (Table 4.1) and is constant over a temperature range which varies the Avrami rate constant (z) by a factor of 2×10^4.

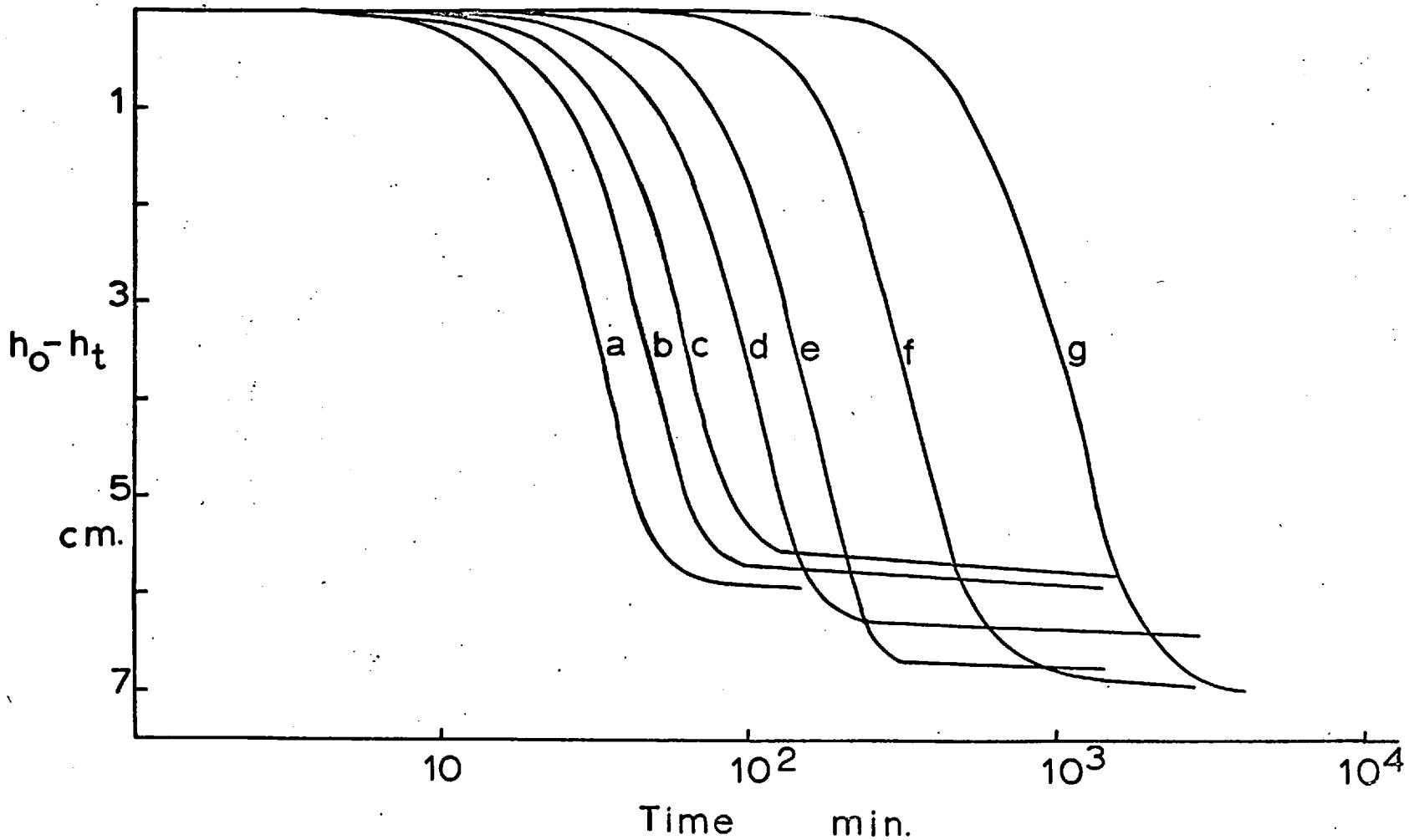


Fig.4.2 Crystallization of Polypropylene.
(a) 134.08°C, (b) 135.50°C, (c) 137.04°C, (d) 138.98°C, (e) 140.20°C, (f) 143.54°C, (g) 149.30°C.

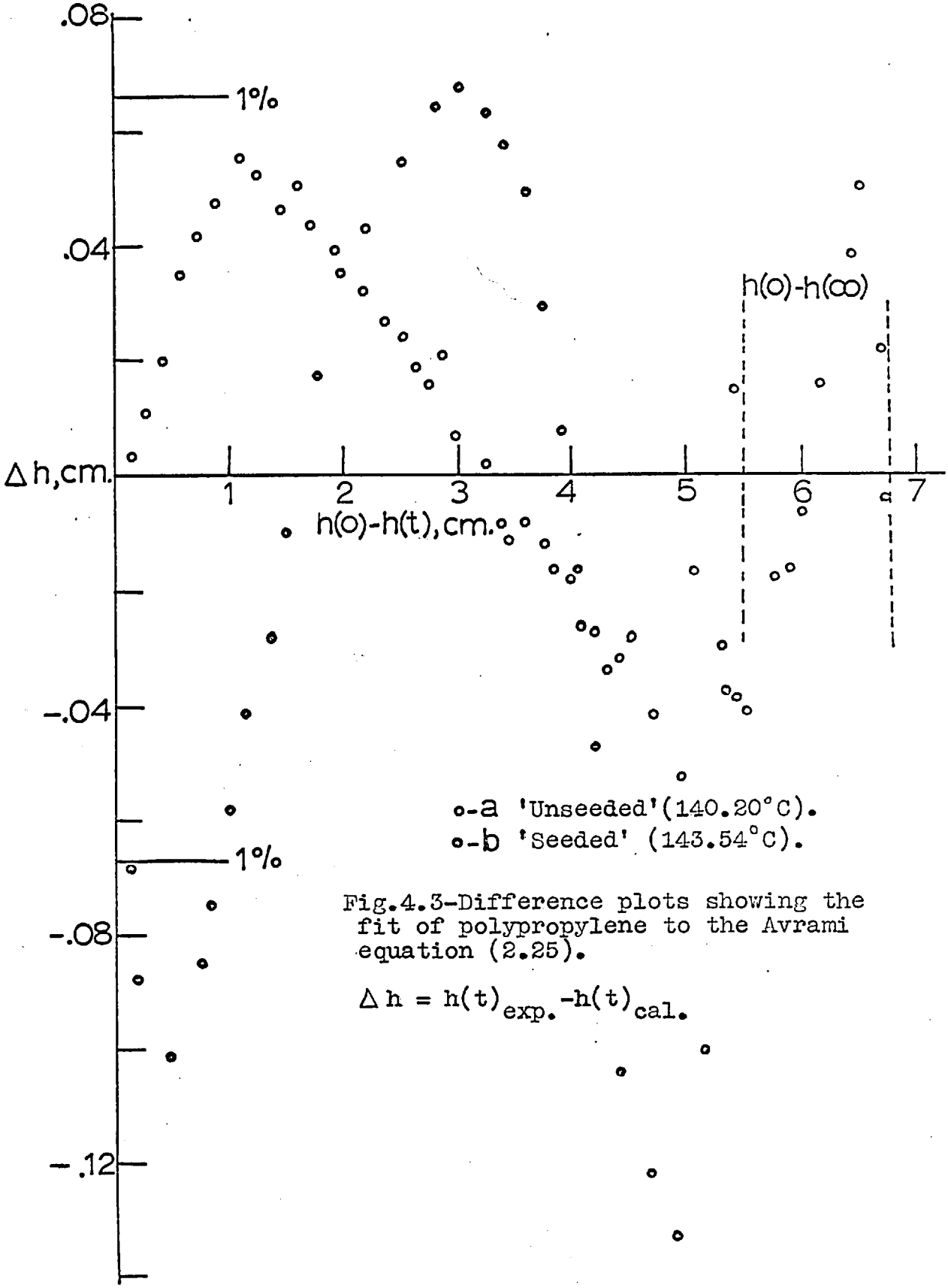


Fig.4.3-Difference plots showing the fit of polypropylene to the Avrami equation (2.25).

$\Delta h = h(t)_{exp.} - h(t)_{cal.}$

Table 4.1

Fit of Avrami equation (2.25) to Polypropylene

Temp. (°C)	No. of points	n	z (time in mins.)	[h(o) - h(∞)] (cm) expt. value	[h(o) - h(∞)] (cm) optimum value	σ(%)
134.08	44	2.48	1.44, -4	5.88	6.12	1.00
135.50	62	2.52	5.44, -5	5.77	5.86	0.81
137.04	77	2.54	2.52, -5	5.77	5.60	0.34
138.98	71	2.60	5.64, -6	6.23	6.24	1.26
140.20	71	2.48	3.38, -6	6.71	6.73	0.47
143.54	33	2.46	5.07, -7	6.94	6.88	0.45
149.30	20	2.40	3.74, -8	6.97	6.88	1.15

Analysis of 'seeded' runs

χ_s/χ_∞							
0.14	147.94	61	3.00	8.03, -7	5.60	-	4.01
0.09	143.54	55	2.95	4.00, -6	5.59	-	1.82

In other polymers, the temperature dependence of n has made interpretation difficult (Sharples and Swinton 1963; Banks et al.1963a). Although n is non-integral, the Avrami equation does allow it to be a multiple of 1/2 (section 2.2). The value of 2.5, corresponds to sporadically nucleated spheres, whose radii varies as $t^{1/2}$ (i.e. diffusion controlled growth). Microscopically, in thin films of the polymer, spherulites growing with constant radial rate are observed (Marker et al.1959). This was also found to be the case for the sample of polypropylene investigated in this work. However, there need be no correlation between the growth rate observed in a thin film and in the bulk state. The total contraction observed increases (Table 4.1) by about 20% when the temperature of crystallization is greater than 140 °C but the constancy of the value of n indicates that there is no change in mechanism when this change in contraction occurs. (This effect cannot be due to any irreversible systematic degradation of the polymer since the results remained reproducible throughout the investigation.) Although this effect has been observed in the case of poly-(decamethylene terephthalate) (Sharples and Swinton 1963) no complete explanation of it has been given. It is probably due to a change in crystal modification at 140 °C. It has been reported (Padden and Keith 1959) that polypropylene spherulites exhibit positive birefringence below 134 °C, and negative birefringence

above 138 °C, the form observed between these two temperatures being a fibrilar mixture. The transition observed dilatometrically at approximately 140 °C may be due to this change from the fibrilar mixture to negatively birefringent spherulites.

The results of two 'seeded' runs, analysed according to the Avrami equation, the value of $[h(o) - h(\infty)]$ corresponding to the final experimental point, is shown in Table 4.1. The close proximity of the Avrami exponent to 3 indicates that instantaneously nucleated spheres ('seeds') are growing with constant radial velocity. This change in the radial growth rate, from a dependence upon $^{1}/_{t}{}^{1/2}$, to a constant value on 'seeding' may originate from some order (or 'memory') remaining in the amorphous regions after partial melting, so that subsequent growth is no longer diffusion controlled. A similar acceleration of growth has been observed when polymethylene is crystallized from 'seeds' (section 3.5, Fig.3.14). It is noteworthy that polypropylene is the only polymer studied to date which shows an increase in the Avrami exponent when crystallization occurs from 'seeds'. The difference plot (Fig.4.3b) shows that the greatest deviations occur towards the end of the crystallization where the experimental contraction lags far behind the calculated value. This is to be expected as the 'memory' effect will be smaller, the greater the distance from the 'seed' nucleus.

Temperature dependence of rate constants

The temperature dependence of the Avrami rate constants is shown in Fig.4.4 where log(z) is plotted against $1/(T_m - T)^2$, corresponding to three dimensional secondary nucleation. [The value of T_m was found to be 173.0 °C (Fig.4.5).] although there are only two points on one portion, This plot probably indicates two straight portions; and although the discontinuity cannot be exactly located, it occurs in the region where the contraction changes sharply. (Also shown on Fig.4.4.) It has been shown (eq.2.48) that the slope of this plot depends upon the free surface energies of the critical secondary nucleus. The change in slope observed here probably represents a difference in the surface free energies involved in forming the critical secondary nucleus of the two different crystal modifications. The sign of the effect agrees with this interpretation, since the modification of higher surface energy should always be formed at high degrees of supercooling.

4.3 The Crystallization of Polybutene

Previous workers (Boor and Mitchell 1963) report that the crystallization kinetics of polybutene is described by the Avrami equation with the best integral value of n of 4. The fit (their Fig.5) is not good after 50% of the process has been completed, and no standard deviations indicating the goodness of the fit are given. The sample investigated here was obtained from Cabot Corporation, in the form of pellets.

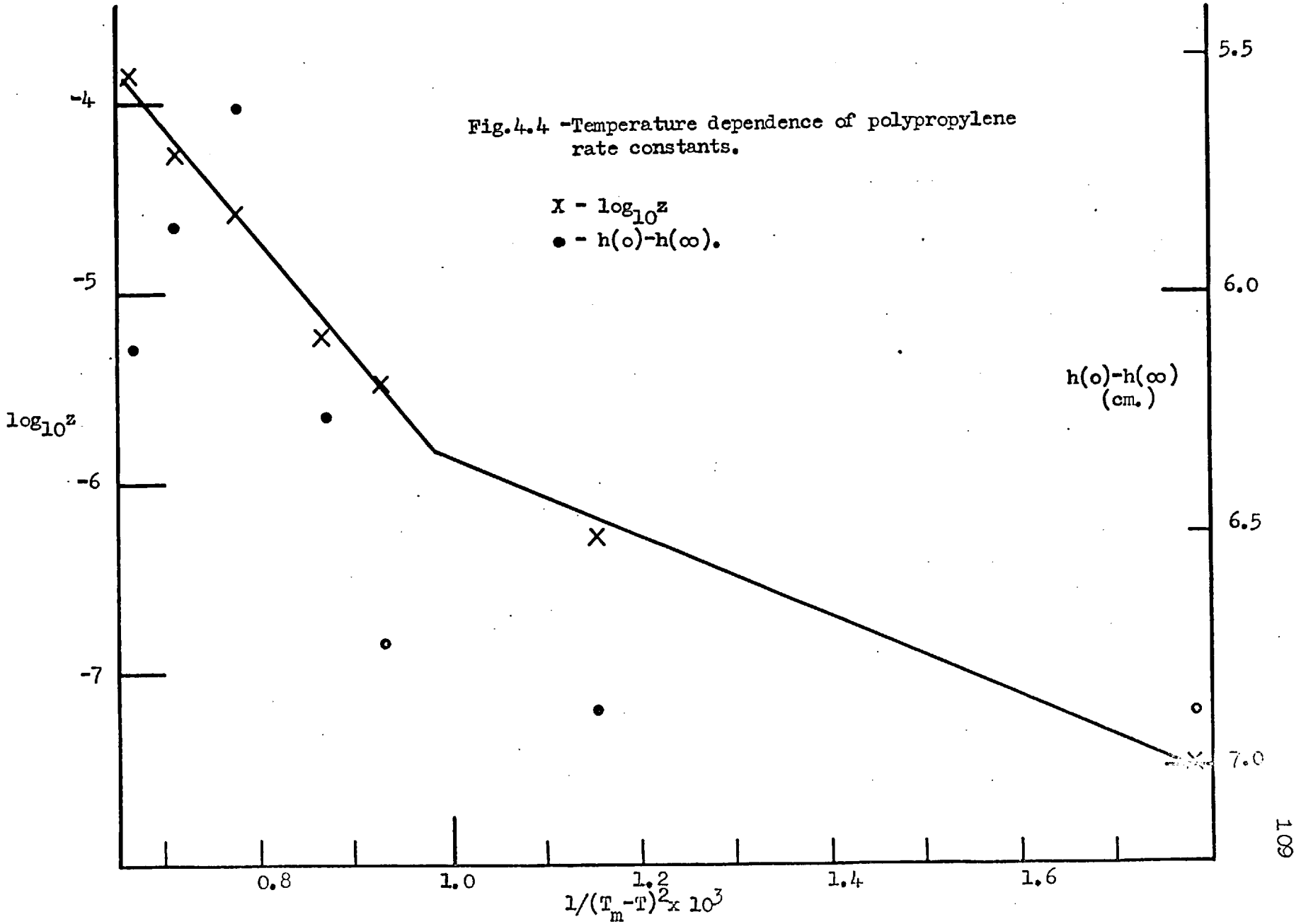


Fig.4.4 -Temperature dependence of polypropylene rate constants.

X - $\log_{10}z$

● - h(o)-h(∞).

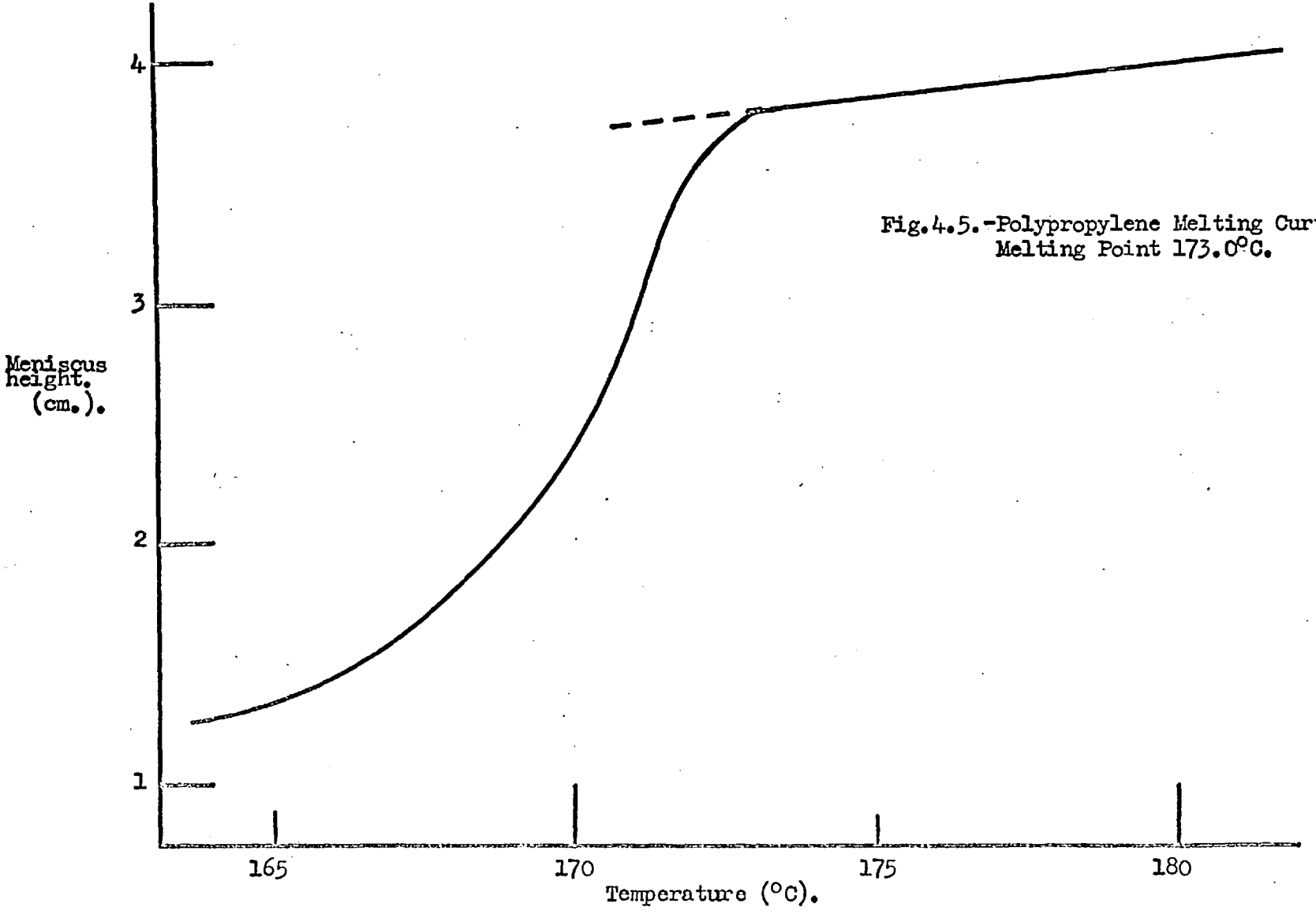


Fig.4.5.-Polypropylene Melting Curve.
Melting Point 173.0°C.

Table 4.2 shows the fit of eight runs to the Avrami equation (2.25). Again $[h(o) - h(\infty)]$ was made an adjustable parameter owing to the slight degree of secondary crystallization present. In two runs only did the final experimental point taken differ from the adjusted value of $[h(o) - h(\infty)]$ by more than 3%. The very low standard deviation (0.83 - 1.42%) show the good fit of the data to the Avrami equation. The residual deviations are again systematic, but do not follow the same pattern in all the runs. The value of n in all the runs is very close to 3 (Table 4.2) corresponding on the simple Avrami picture to linear radial growth of spontaneously nucleated spheres. There is however a definite tendency for n to be slightly greater than 3, which is possibly due to some degree of sporadic nucleation. As for polypropylene, the total contraction observed changes sharply as the crystallization temperature is varied. (In this case at approximately 100 ^{o}C.) Again, this has no effect on the value of the Avrami exponent, indicating that no change in the crystallization mechanism occurs.

Temperature dependence of rate constants

The temperature dependence of the Avrami rate constants (Table 4.2) is shown in Fig.4.6. The plot of log(z) vs $1/(T_m - T)^2$ (T_m = 117.7 ^{o}C, melting curve Fig.4.7) corresponding to three dimensional secondary nucleation shows two distinct straight portions. Although the discontinuity cannot be

Table 4.2

Fit of Avrami equation (2.25) to Polybutene

Temp. (°C)	No. of points	n	z (time in mins.)	[h(o) - h(∞)] (cm)		σ (%)
				expt. value	optimum value	
97.31	33	3.06	3.47, -6	1.95	1.96	0.94
98.47	47	3.09	9.84, -7	1.82	1.86	0.83
98.88	47	3.19	3.93, -7	1.94	1.93	0.95
100.62	32	3.00	1.38, -7	2.36	2.27	1.42
101.54	35	3.00	6.27, -8	2.48	2.46	0.64
103.10	32	3.23	2.15, -8	2.07	1.95	1.10
105.81	34	3.15	5.97,-10	2.53	2.49	0.96
107.08	17	3.13	5.31,-11	2.69	2.63	0.91

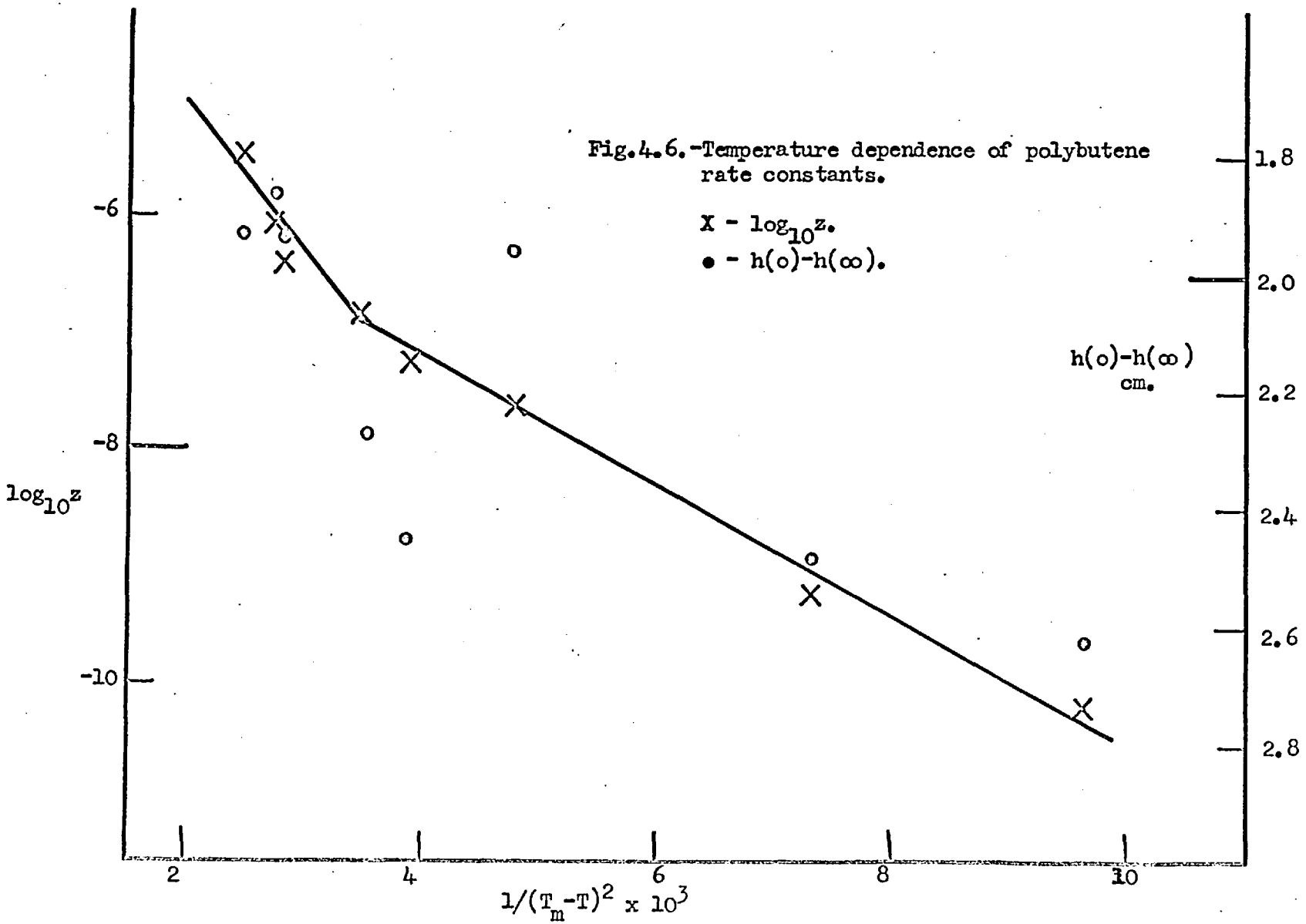
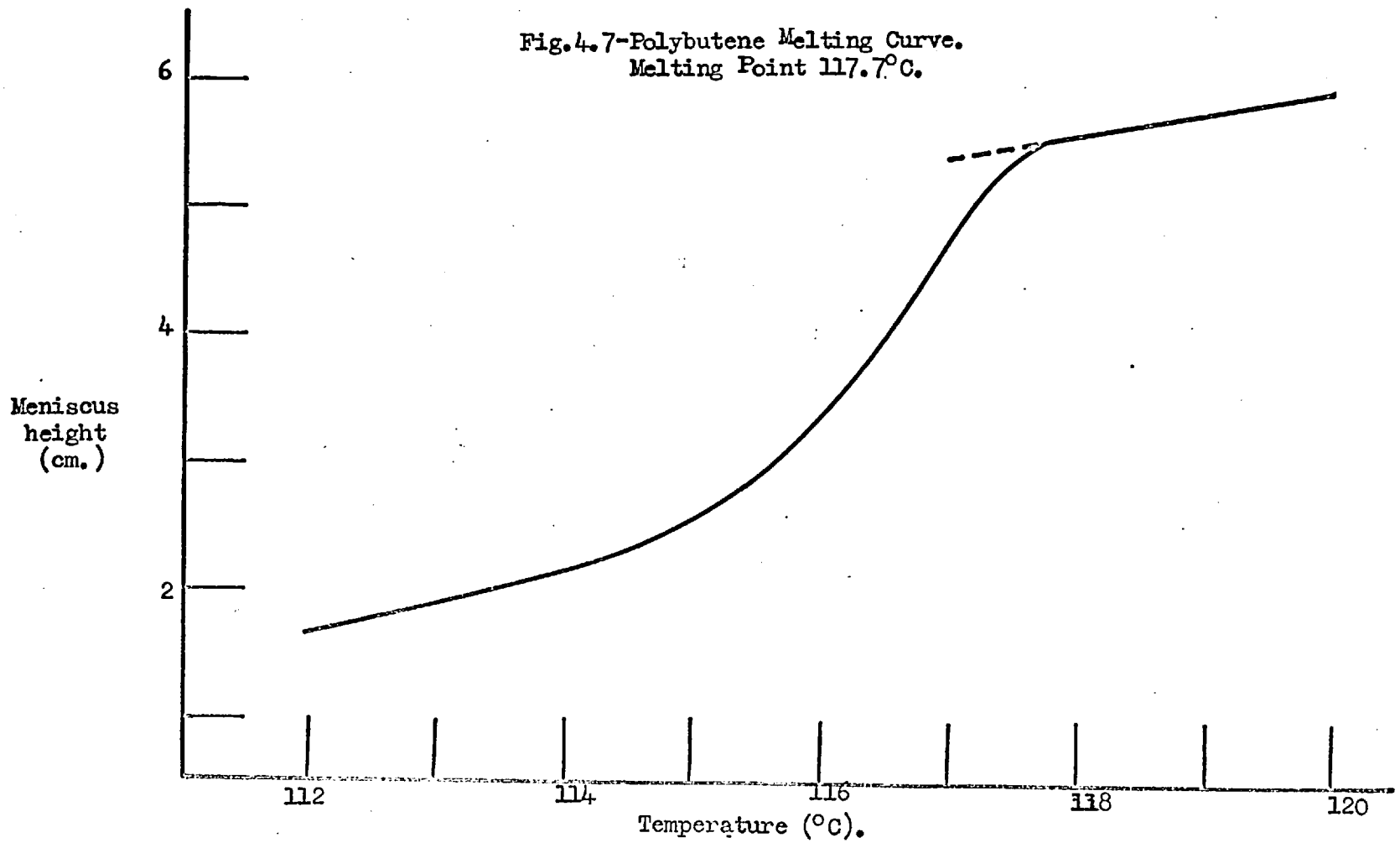


Fig.4.6.-Temperature dependence of polybutene rate constants.

X - $\log_{10} z$.

• - h(o)-h(∞).

Fig.4.7-Polybutene Melting Curve.
Melting Point 117.7°C.



exactly located, it again occurs in the region where the sharp change in the total contraction (also shown in Fig.4.6) is found. This change in slope occurs in the same direction as was found for polypropylene (section 4.2) where it has been discussed.

4.4 The Crystallization of Poly-(ethylene oxide)

Poly-(ethylene oxide) readily crystallizes in the form of large (up to 1 mm dia.) spherulites both in thin films and in bulk (Banks and Sharples 1963). When the crystallization kinetics are analysed according to the Avrami equation, the value of n is found to be 2 (Banks and Sharples 1963; Barnes, Luetzel and Price 1961) or 3 or 4 (Barnes et al.1961) depending on molecular weight. The value n = 2 is incompatible with the simple Avrami picture of spherulites growing with a constant radial velocity (Barnes et al.1961).

For the investigations reported here, a sample of poly-(ethylene oxide) (Polyox WSR35) obtained from Union Carbide Ltd. was used. Table 4.3 shows the data fitted to the Avrami equation, the value of $[h(o) - h(\infty)]$ used corresponded to the final experimental point taken. The optimum values of the Avrami exponent are very close to 2, and the low standard deviations show that the Avrami equation well represents the data. The value of the exponent is decreased on seeding (Table 4.3) to approximately 1.4. These values of n are seen

Table 4.3

Analysis of Poly-(ethylene oxide) kinetics

Fit of Avrami equation (2.25)

Temp. (°C)	No. of points	n	z(time in mins.)	h(o)-h(∞) (cm)	σ(%)
51.14	95	1.91	9.82,-4	7.05	1.13
53.77	66	1.99	1.39,-4	6.96	1.51
'Seeded' (χ_s/χ_∞ = 0.14)					
58.23	46	1.39	1.70,-4	6.03	1.38

Fit of Single Crystal Model (eq.4.1)

Temp. (°C)	k_1 (min^{-1})	k_2	h(o) - h(∞) (cm)	σ (%)
51.14	3.98,-3	190	7.05	1.05
53.77	2.03,-3	142	6.96	1.71

Fit of Superposed Avrami processes (eq.4.5)

Temp. (°C)	k_o	k_1	k_2	k_3	σ (%)
51.14	3.16,-2	-7.99, -3	1.15,-3	-6.52,-6	0.73
53.77	5.64,-3	-3.25, -3	2.21,-4	-5.20,-7	0.37

to be very similar to those found for polymethylene (section 3.3, table 3.2). The added similarity of the difference plot (Fig.4.8a) for the run at 51.14 °C (the deviations follow the same pattern for the run at 53.77 °C) when compared to that for polymethylene (Fig.3.3C) further shows the similar dilatometric behaviour of these two polymers.

The lack of correlation between the dilatometric results, and the microscopic observations suggest that the spherulite is composed of some sub-unit of structure whose growth law leads to the observed kinetic behaviour. The dilatometric results are very similar to those found for polymethylene, which have been fitted to a single crystal model (Chapter 3). Poly-(ethylene oxide) is known to crystallize from dilute solution in the form of single crystals (Keller 1962) and it is suggested that the anomalous kinetics may be explained by extending this observation to the bulk.

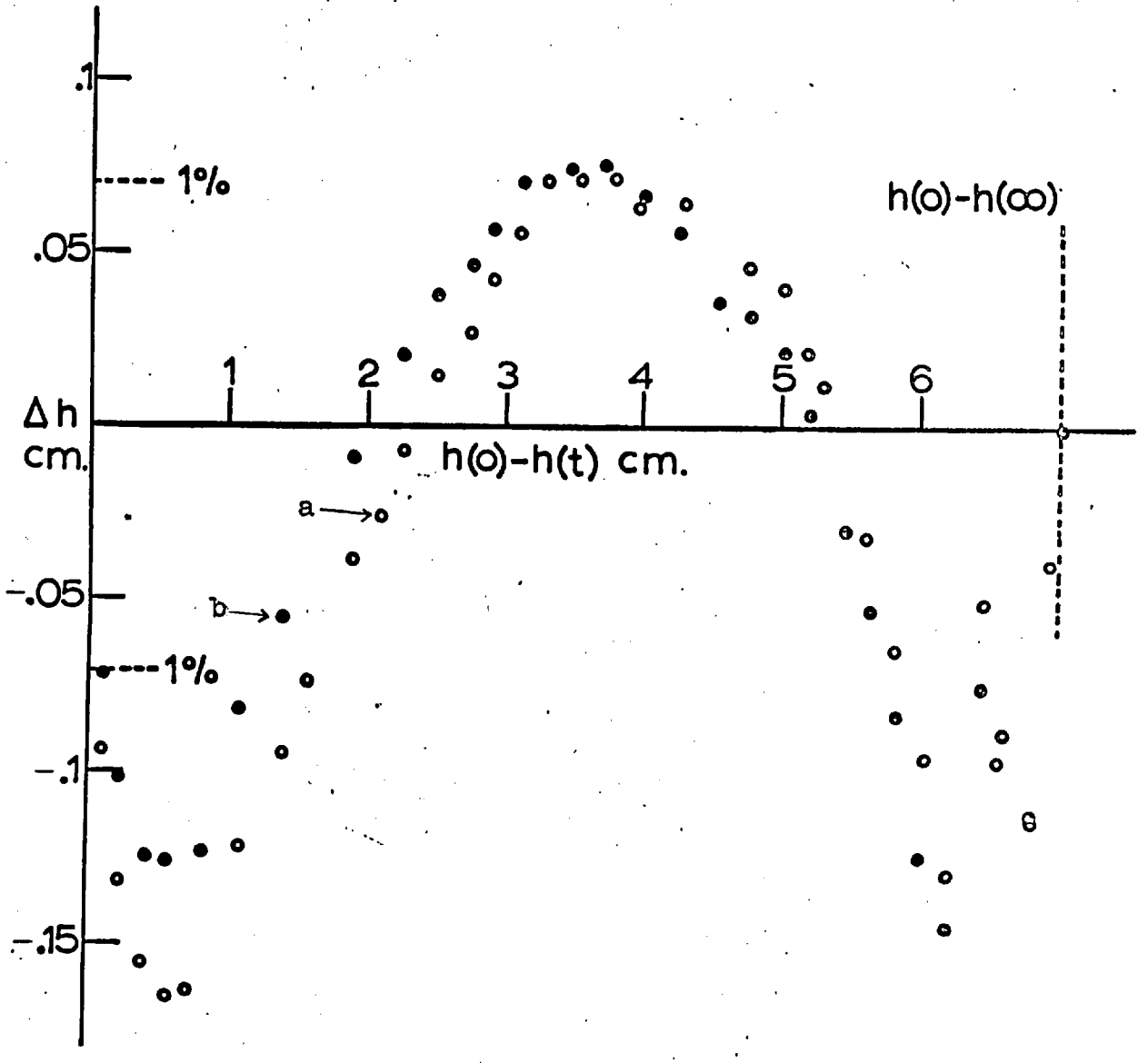
In Chapter 3, a model which postulates the growth of randomly placed single crystal platelets by a chain folding mechanism was described, and led to the rate equation (eq.3.16) in terms of the measured dilatometric heights [h(t)].

$$\frac{h(o) - h(t)}{h(o) - h(\infty)} = 1 - \exp\ -k_2[2 + k_1 t - 2(1 + k_1 t)^{1/2}] \qquad 4.1$$

where k_1 and k_2 are related to the waiting times τ_f and τ_c for renucleation at the face and corner sites of the growing platelet (eqs.3.17, 3.18). This rate equation, which is

Fig.4.8.- Difference plots showing the fit of two models to poly-(ethylene oxide) at 51.14°C. (Only a representative number of the 95 points are plotted).
$\Delta h = h(t)_{exp.} - h(t)_{cal.}$

a- o Avrami equation (2.25)
b- ● Folded chain model (eq. 4.1).



applicable to the growth of individual lamellae has to be reconciled in the case of poly-(ethylene oxide), with the observation of macroscopic spherulites. Keller and Sawada (1964) have shown that spherulitic polyethylene is composed of lamellae. The actual space-filling problem is unresolved at present, although it has been suggested that the lamellae are arranged in a 'splaying book' fashion (Hoffman and Lauritzen 1961). This splaying geometry ensures that any two lamellae within one 'book' do not collide during their growth. The rate of growth of a book of N lamellae is then N times the rate for one lamella. Provided the centres of the 'books' are randomly placed, the formal rate law is thus unchanged by grouping the lamellar entities of the single crystal model into 'splaying books'. This grouping together may increase the degree of fragmentation (section 3.3) and thus the amorphous content of the crystallized specimen, because the space between the leaves of each book are rather well screened from direct access by lamellae belonging to other 'books'. This is merely re-stating the 'space-filling problem' confronting the authors of morphological studies (Keller and Sawada 1964).

Table 4.3 shows the fit of this single crystal rate equation (4.1) to the two poly-ethylene oxide runs. The low standard deviations are comparable with those obtained for the fit of the Avrami equation. However, since the Avrami equation

leads to anomalous values of the exponent n, the fit to the rate equation (4.1) based on a definite model is considered to be of greater validity. The difference plot (Fig.4.8b) showing the fit of the single crystal rate equation to the run at 51.14 °C shows that the deviations are still highly systematic, and follow the same pattern found when the crystallization of polymethylene is similarly analysed (Fig.3.3A). Furthermore, the rate constants $k_1k_2(\propto \frac{1}{\tau_f})$ and $k_1k_2^{1/2}(\propto \frac{1}{\tau_c})$ vary with temperature similarly to those of polymethylene. For the two runs which were performed, the ratio

$$\frac{d(\ln k_1k_2)}{d(1/\Delta T)} \quad : \quad \frac{d(\ln k_1k_2^{1/2})}{d(1/\Delta T)} \quad = \quad 1.18$$

compares with the corresponding value of 1.36 for polymethylene (Fig.3.8). The possibility that the anomalous value of the Avrami exponent found in the case of poly-(ethylene oxide) may arise through the simultaneous occurrence of a number of Avrami processes has also been investigated. If the number of such processes is N, each described by the number of bodies (ρ_i) growing with growth law $V_i(t)$ then

$$\rho\bar{V}(t) \quad = \sum_{i=1}^{N} \rho_i V_i(t) \qquad 4.2$$

If each growth law can be written (section 2.2)

$$\rho_i V_i(t) \quad = \quad k_i t^i \qquad 4.3$$

where i is the Avrami exponent, then substituting eq.4.3 into eq.4.2 and using the result in eq.2.7, the rate equation in

terms of dilatometric measurements becomes

$$\frac{h(o) - h(t)}{h(o) - h(\infty)} = 1 - \exp - \left(\sum_{i=1}^{N} k_i t^i \right) \qquad 4.4$$

or,

$$-\ln\left[\frac{h(t) - h(\infty)}{h(o) - h(\infty)}\right] = \sum_{i=1}^{N} k_i t^i \qquad 4.5$$

Eq.4.5 was tested by fitting $-\ln\left[\frac{h(t) - h(\infty)}{h(o) - h(\infty)}\right]$ to a polynomial in t, up to i = 3, the results being given in Table 4.3. The negative values of some of the coefficients, and the small improvement in standard deviations over the single Avrami process considering the increased number of parameters, shows that this is not a possible explanation of the anomalous kinetic results.

4.5 The Crystallization of Polystyrene

No dilatometric measurements on the crystallization of this polymer have been reported in the literature. The kinetics of spherulite growth has been measured microscopically (Kenyon, Gross and Wurstner 1959), the linear growth rate showing a maximum at approximately 175 °C. This is because the rate of secondary nucleation ($\dot{N}$) is controlled at low temperatures by the energy of activation for viscous flow (ΔH^*) and at high temperatures by the free energy of formation of a critical nucleus ($\Delta\phi^*$) (section 2.5). This leads to eq.2.37

$$\ln\left(\frac{\dot{N}}{T}\right) = \log C - \Delta H^*/RT - \Delta\phi^*/RT \qquad 4.6$$

The sample of polystyrene used in this investigation was kindly given by Professor Burnett. The polymer was refluxed with methyl-ethyl ketone to remove atactic polymer. The analysis of the runs was complicated by the observation that towards the end of the run, an increase in volume of the sample occurred. Table 4.4 shows the data fitted to the Avrami equation. The least squares fit was carried out with the total contraction $[h(o) - h(\infty)]$ made an adjustable parameter. Only those experimental measurements which were taken before any expansion occurred were fitted. The value of the maximum contraction which was observed before any contraction occurred is also given in Table 4.4. The optimum value of $[h(o) - h(\infty)]$ is larger than the maximum contraction observed in all the runs, the difference being most pronounced at the lower temperatures. That this expansion is not due to any irreversible degradation of the polymer is indicated by the fact that although the runs were performed in random order, the total observed contraction increases fairly regularly with temperature. (Only one run does not follow this trend.) The low standard deviations (0.52% - 2.30%) given in Table 4.4 show that the Avrami equation is a good fit to the data. The value of the exponent n is however non-integral, and also varies with crystallization temperature, from about 2.5 at 150 ^{o}C to 1.6 at 210 ^{o}C. This behaviour cannot be accounted for by any of the simple variants of the Avrami model, but may be accommodated by the

Table 4.4

Fit of Avrami equation (2.25) to Polystyrene

Temp. (°C)	n	z (time in mins.)	[h(o) - h(∞)] (cm)		σ (%)
			expt. value	optimum value	
149.06	2.36	3.51,-6	1.53	1.52	2.30
159.30	2.50	4.04,-6	1.58	1.61	0.88
171.18	1.74	2.44,-4	1.73	1.94	1.23
175.0	2.08	6.50,-5	1.63	1.73	0.52
180.0	2.28	2.23,-5	1.67	1.67	0.86
186.8	2.50	6.65,-6	1.66	1.67	1.28
200.4	2.19	3.00,-6	1.85	1.85	1.25
203.4	1.70	1.80,-5	2.06	2.07	1.10
209.7	1.64	6.83,-4	2.32	2.46	0.88

single crystal platelet model described previously (section 3.3). Single crystals have been observed when polystyrene is crystallized from dilute solution (Kargin et al.1960), and Natta (1957) has observed sheaves when it is crystallized from the melt. The sample used does not show resolvable spherulites under the polarizing microscope. Even if spherulites are present, the single crystal model may be fitted to the data, but as with poly-(ethylene oxide), the error in the theory due to fragmentation may be increased. Table 4.5 shows the fit of the nine runs to the single crystal model rate equation (eq.4.1). The value of $[h(o) - h(\infty)]$ was again treated as an adjustable parameter, the optimum values being larger than the maximum total contraction observed (Table 4.5). However, even in the run in which there is the greatest difference between the optimum value of $[h(o) - h(\infty)]$ and the experimental value, the values of the two parameters k_1 and k_2 are not changed appreciably by making $[h(o) - h(\infty)]$ an adjustable parameter. Thus, in the run at 159.30 ^{o}C, where the optimum value of $[h(o) - h(\infty)]$ is 1.83 cm compared with the experimental value of 1.58 cm the parameters k_1 and k_2 are only changed from 4.25, - 4 and 1116, to 3.95, - 4 and 985.6 when the total contraction is allowed to vary. The standard deviations (0.96% - 2.74%) are generally slightly larger than those obtained for the fit of the Avrami equation. The residual

Table 4.5

Fit of Single Crystal Model (eq.4.1) to Polystyrene

Temp. (°C)	k_1 (min^{-1})	k_2	k_1k_2	$(k_1k_2)^{1/2}$	$[h(o) - h(\infty)]$ (cm) expt. value	$[h(o) - h(\infty)]$ (cm) optimum value	σ (%)
149.06	2.87,-4	105 9	0.304	9.34,-3	1.53	1.62	1.75
159.30	3.95,-4	985.6	0.390	1.24,-2	1.58	1.83	1.86
171.18	5.67,-4	101 2	0.574	1.80,-2	1.73	1.81	1.16
175.0	1.77,-3	116.6	0.264	1.91,-2	1.63	1.82	0.96
180.0	1.58,-3	132.2	0.210	1.82,-2	1.67	1.79	2.40
186.8	1.41,-3	134.2	0.189	1.63,-2	1.66	1.78	2.74
200.4	8.79,-4	48.3	0.0424	6.11,-3	1.85	1.93	2.38
203.4	5.58,-4	43.2	0.0241	3.67,-3	2.06	2.07	2.06
209.7	3.79,-4	18.8	0.00713	1.64,-3	2.32	2.39	1.35

deviations were highly systematic, but their pattern varied in different runs.

Temperature Dependence of Rate Constants

Table 4.5 giving k_1, k_2 and the related quantities

$$k_1k_2 = 2\rho a^2 l/\tau_f \quad \text{(eq.3.17)} \qquad 4.7$$

$$k_1k_2^{1/2} = a\sqrt{2\rho l}/\tau_c \quad \text{(eq.3.18)} \qquad 4.8$$

shows that both k_1k_2 and $k_1k_2^{1/2}$ pass through a maximum in the temperature range 170° - $175\ ^\circ C$. Although the values of τ_c and τ_f cannot be isolated, the maxima in the values of k_1k_2 and $k_1k_2^{1/2}$ demonstrate that both these characteristic waiting times exhibit a maximum, as the fold length l and the number of nuclei ρ are expected to vary monotonically with temperature. The detailed temperature dependence of k_1k_2 and $k_1k_2^{1/2}$ is now analysed in terms of eq.4.6. The melting point of the polystyrene was taken to be $230\ ^\circ C$ (Kenyon et al.1959). Since kinetic measurements were performed over a wide temperature range, the subsequent analysis of the temperature dependence of the rate constants will be relatively insensitive to the value of T_m. For computational purposes, eq.4.6 becomes

$$\log_{10}\left(\frac{k_1k_2}{T}\right) = A_1 - B_1/T - C_1/(T\Delta T) \qquad 4.9$$

and

$$\log_{10}\left(\frac{k_1k_2}{T}\right)^{1/2} = A_2 - B_2/T - C_2/(T\Delta T) \qquad 4.10$$

The least squares fit of k_1 and k_2 to eqs.4.9 and 4.10 give the parameters

$$A_1 = 2.14; \quad B_1 = 1.79 \times 10^3; \quad C_1 = 3.29 \times 10^4 \quad \text{with} \quad \sigma = 1.9\%$$

and

$$A_2 = 0.39; \quad B_2 = 1.80 \times 10^3; \quad C_2 = 2.07 \times 10^4 \quad \text{with} \quad \sigma = 3.3\%$$

The good fit supports the picture underlying eq.4.6 namely that at low temperatures, the rate of secondary nucleation is governed by the energy of activation for viscous flow, and at high temperatures by the free energy of formation of the critical nucleus. The parameters B_1 and B_2 lead to values of 8.2kcal./mole. and 8.3 kcal./mole. respectively for the energy of activation for viscous flow. The equality of these values is supported by the model since the energy of activation should not depend on the secondary nucleus being at a face or corner site on the growing platelet. This interpretation assumes that any variation with temperature of ρ and l is contained in the parameters C_1 and C_2. The behaviour of the values of C_1 and C_2, which depend upon the free energy of formation of the critical nucleus, bears a striking resemblance to that found in the case of polymethylene. It is again found that $k_1 k_2 (\propto \frac{1}{\tau_f})$ is more temperature dependent than $k_1 k_2^{1/2}$ $(\propto \frac{1}{\tau_c})$. This does not imply that $\frac{1}{\tau_f}$ varies more strongly with temperature than $\frac{1}{\tau_c}$ owing to the temperature dependence of ρ and l also contained in C_1 and C_2. This similarity further

extends to the ratio C_1/C_2. It is 1.59 for polystyrene and 1.36 for polymethylene (Fig.3.8).

This temperature dependence shows qualitatively why the apparent Avrami exponent decreases with increasing temperature (Table 4.4). It will be recalled (section 3.3) that an Avrami exponent near 2 corresponds to the situation where the rate is dominated by nucleation at a corner site, whilst a lower value (decreasing to unity) arises when the rate is determined by nucleation at face sites on the growing platelet. This can occur when geometric factors determine which nucleation step dominates. In addition, if the temperature dependence of k_1k_2 and $k_1k_2^{1/2}$ changes, then the overall best value of the Avrami exponent may also change. At low temperatures, where both $k_1k_2(\propto\frac{1}{\tau_f})$ and $k_1k_2^{1/2}$ $(\propto\frac{1}{\tau_c})$ have the same temperature dependence, and where an Avrami exponent near 2 is found (Table 4.4), it is inferred that the overall rate is determined by nucleation at the corner sites. At high temperatures, k_1k_2 becomes more temperature dependent than $k_1k_2^{1/2}$ so that for the same platelet size, the face sites will have a greater effect on the overall rate, giving a lower value of n.

Eqs.4.9 and 4.10 assume that the activation energy of viscous flow ($\propto$ B) is temperature independent. However, this is not compatible with viscosity data on simple liquids, and also fails for supercooled liquids and polymers as the glass

transition temperature (T_g) is approached (approximately 100 °C for polystyrene). The relationship (Ferry 1961)

$$\Delta H_a = 2.303\ R c_1^g c_2^g T^2/(c_2^g + T - T_g)^2 \qquad 4.11$$

where c_1^g and c_2^g are characteristic of the material, gives the sharp increase in the activation energy of viscous flow (ΔH_a) with decreasing temperature. This arises from the severe decrease in free volume as the glass transition temperature is approached. To fit the temperature dependence of the rate constants (k_1k_2, $k_1k_2^{1/2}$) taking this variation of ΔH_a into account, it was assumed

$$T_g = 100\ ^\circ C \qquad 4.12$$

$$c_2^g = 50^\circ \qquad 4.13$$

when eq.4.9 becomes, using 4.11, 4.12, 4.13

$$\log_{10}\left(\frac{k_1k_2}{T}\right) = A_1 - D_1T/(50 + T - 100)^2 - C_1/(T\Delta T) \qquad 4.14$$

where $D_1 = c_1^g c_2^g$. The corresponding equation for $\log_{10}(k_1k_2^{1/2}/T)$ follows similarly. The least-squares fit of these equations gave

$$A_1 = -1.38,\quad D_1 = 18.2,\quad C_1 = 3.12 \times 10^4 \text{ with } \sigma = 1.8\% \qquad 4.15$$

and

$$A_2 = -2.34,\quad D_2 = 37.7,\quad C_2 = 2.43 \times 10^4 \text{ with } \sigma = 1.7\% \qquad 4.16$$

This leads to values of $c_1^g c_2^g$ which are too small [values in the region of 1000 are quoted by Ferry (1961) for a range of materials]. Moreover, the calculated values of $c_1^g c_2^g$ differ

for face and corner nucleation. Nevertheless, the decrease in standard deviation with no further adjustable parameters does indicate the expected decrease of ΔH_a with temperature. The data are not sufficiently accurate to determine the magnitude of this change reliably. Figs.4.9 and 4.10 show these least-squares fits of the values of $k_1 k_2$ and $k_1 k_2^{1/2}$ (Table 4.5).

Discussion of Kinetic Results

The rate equation (eq.3.16) derived for the growth of single crystal lamellae has been shown to satisfactorily describe the crystallization kinetics of polymethylene, polystyrene and poly-(ethylene oxide). Although both the Avrami equation and the single crystal equation fit the data equally well, the anomalous values of the Avrami exponent render the latter model more valid. In the case of polymethylene, the suppression of the secondary crystallization has allowed both the primary and the secondary crystallization processes to be more extensively analysed than has previously been possible. When the crystallization kinetics of these three polymers are analysed according to this model, a number of similarities in their behaviour become apparent. Both polymethylene and poly-(ethylene oxide) which give Avrami exponents near 2 (Tables 3.2, 4.3) fit the single crystal model with standard deviations of about 2%. The residual deviations in both cases follow the same pattern remarkably

Fig.4.9- Temperature dependence of growth and nucleation parameters ($k_1 k_2^{1/2}$) for polystyrene.

o-experimental values (table 4.5).

full line- best fit of rate parameters to eq.4.14.

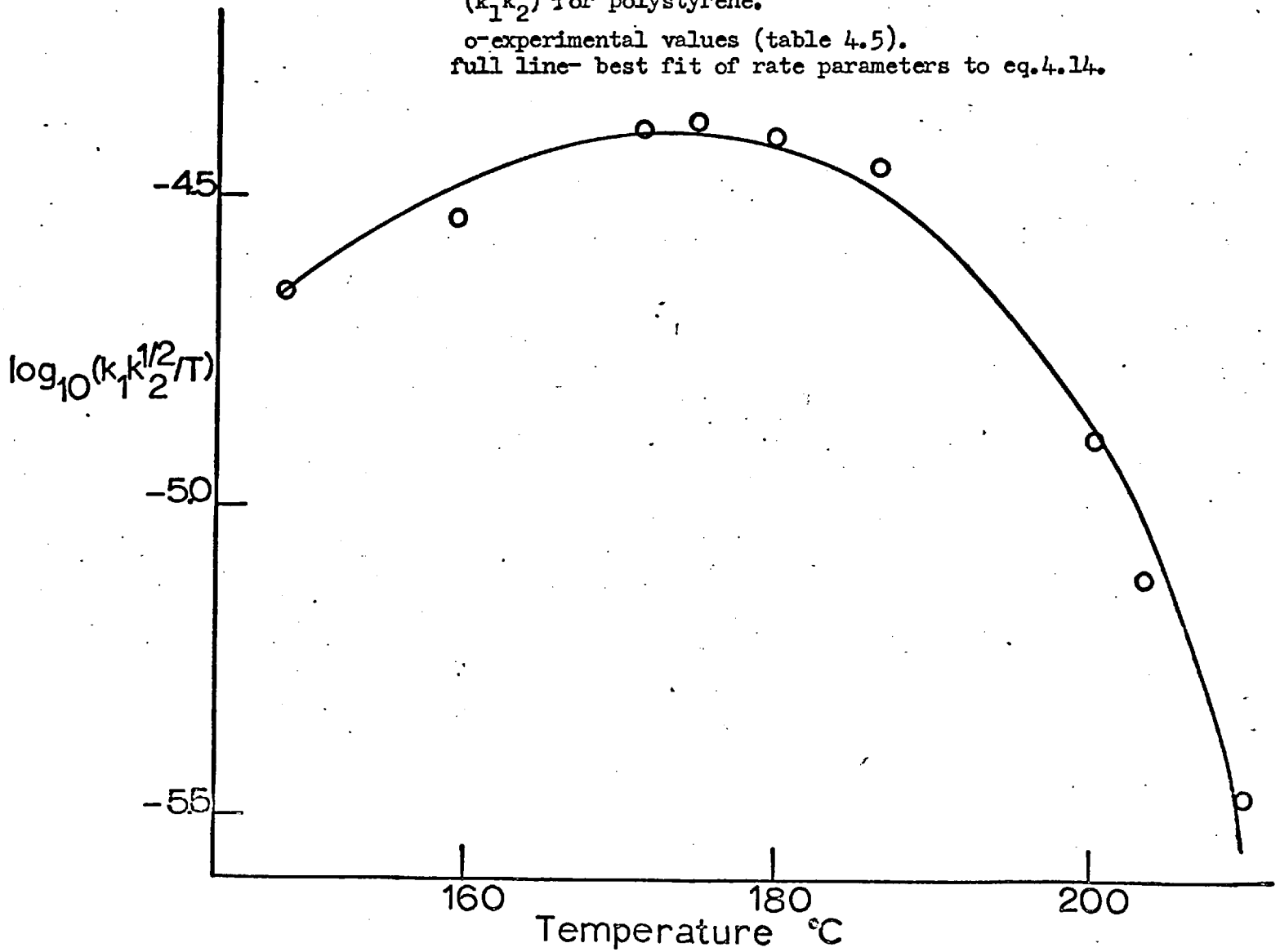
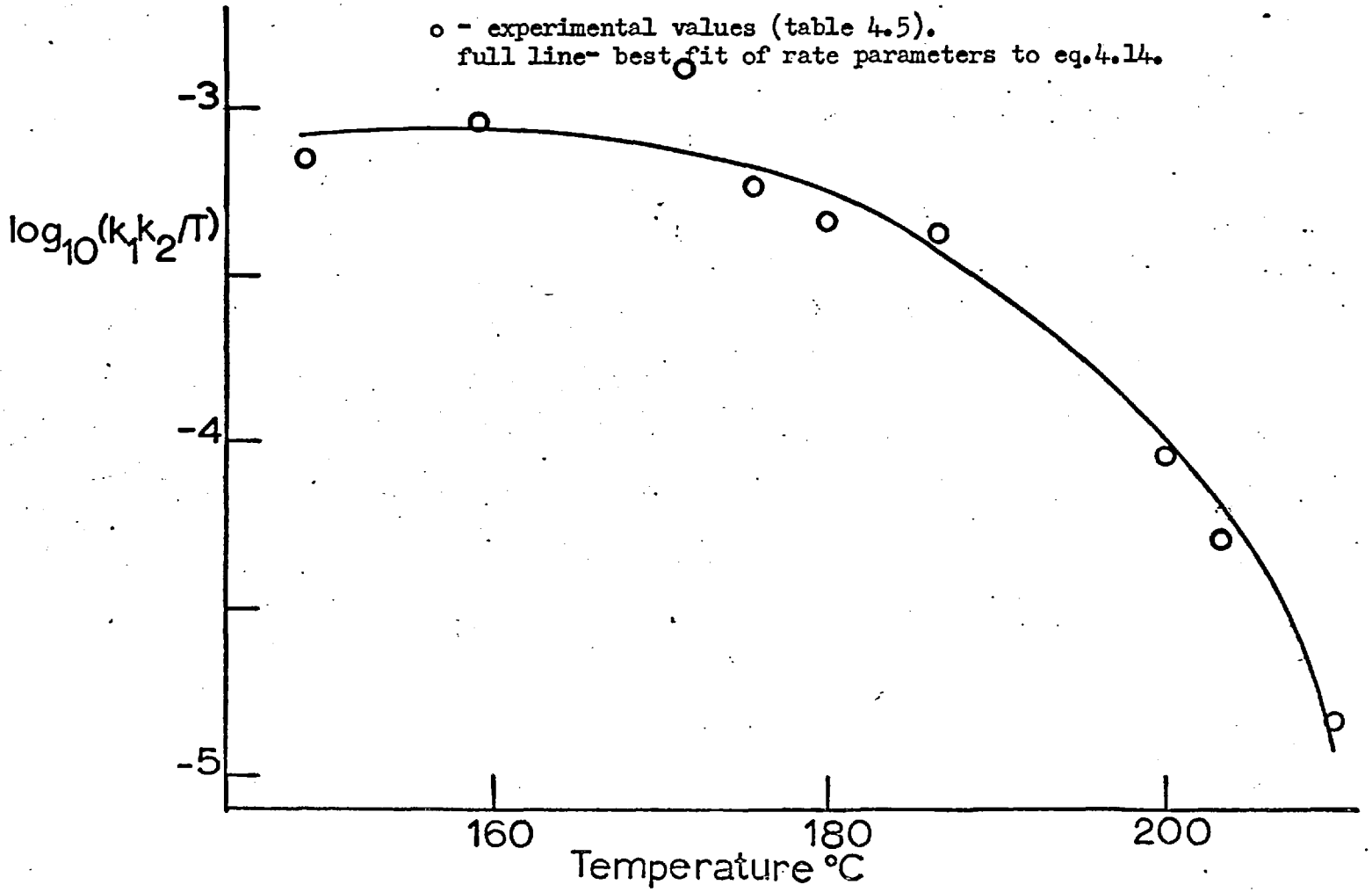


Fig.4.10-Temperature dependence of growth and nucleation parameters ($k_1 k_2$) for polystyrene.

o - experimental values (table 4.5).
full line- best fit of rate parameters to eq.4.14.



closely (Figs.3.3, 4.8). This implies that the experimental results on the two polymers can be empirically superposed to a much higher degree of concordance than can be achieved by fitting either of them to a two-parameter model. The pattern of the residual deviations is not the same in all the polystyrene runs, and may in some measure be due to the uncertainty in the value of the total contraction. The temperature variation of the rate constants which depend on the two secondary nucleation steps postulated in the model, is also very similar for all three polymers. The two characteristic waiting times τ_c and τ_f, cannot be absolutely determined owing to the inclusion of the number of nuclei (ρ) and the fold length (l) in the rate constants k_1 and k_2 (eqs.3.17, 3.18) evaluated from the dilatometric data. However, in all three polymers $k_1 k_2 (\propto \frac{1}{\tau_f})$ varies more strongly with temperature than $k_1 k_2^{1/2} (\propto \frac{1}{\tau_c})$, this similarity also extending to the magnitude of this difference.

As it is well established that polyethylene crystallizes from the bulk in the form of lamellae, the similarities in the behaviour of these polymers (summarized in table 4.6) lends support to the contention that this is the crystallization habit of polystyrene and poly-(ethylene oxide). This similarity is not immediately expected as these three polymers crystallize with different structures. Polyethylene being a planar zigzag,

Table 4.6

Comparison of Kinetic Behaviour of Polymethylene, Poly-(ethylene oxide) and Polystyrene

	Polymethylene	Polyethylene oxide	Polystyrene
Value of Avrami exponent found by fit of eq.2.25	1.81 - 2.55 (σ = 1.72 - 3.48%)	1.91 - 1.99 (σ = 1.13 - 1.51%)	1.64 - 2.50 (σ = 0.52 - 2.30%)
Fit of single crystal model (eq.3.16)	σ = 1.38 - 3.43%	σ = 1.05 - 1.71%	σ = 0.96 - 2.74%
Residual deviations after fit of single crystal model (eq.3.16)	Very similar (Figs.3.3, 4.8); the same pattern is followed in all the runs		Pattern varies in different runs
Temperature dependence of single crystal model rate constants (eq.3.16) $\frac{d(\ln k_1 k_2)}{d(1/\Delta T)}$: $\frac{d(\ln k_1 k_2^{1/2})}{d(1/\Delta T)}$	1.36	1.18	1.59 (energy of activation of viscous flow assumed constant eqs. 4.9, 4.10.) 1.28 (activation energy taken to be temperature dependent eqs.4.11, 4.14.)

whilst polystyrene and polyethylene oxide have helical structures (Bunn and Holmes 1958). The relationship of the single crystal lamellae to the spherulites observed microscopically is unresolved at present. The inaccuracy introduced into eq.3.16 owing to fragmentation of the growing lamellae (section 3.3) may be larger when the lamellae are grouped together in a splaying book fashion to form spherulites. However, the systematic residual deviations (Difference plots 3.3, 4.8) especially those at low values of the total crystallinity, are not expected to be solely due to fragmentation. They do, however, indicate a departure from some assumption of the single crystal model, or the basic Avrami picture (section 2.1, eq.2.7).

The remaining polymers studied, polybutene, and polypropylene give good fits to the conventional Avrami equation (eq.2.25). The fractional values of the exponent n, which are found for many other polymers, and which are not allowed by the simple Avrami model, are not encountered here. The values of n, which are close to 3 for polybutene, and 2.5 for polypropylene can be simply explained in terms of the growth of spherical crystalline bodies.

CHAPTER V

Statistics of Random Placement, Subject to Restrictions, on a Linear Lattice

In the discussion which follows, the 'fringed micelle' picture for a polymer crystallite is considered, in which a single polymer molecule occurs in a number of separate crystalline and amorphous regions (Flory 1953). It follows that the condition of the amorphous phase will vary as the degree of crystallinity increases. This variation may arise from restrictions on the mobility of chain segments attached to crystallites, and the formation of irresolvable chain entanglements (Roe, Smith and Krigbaum 1961). Only one aspect of this problem will be treated here, namely the amorphous fraction which may arise by the isolation of sequences whose length is less than a desired minimum. Without considering the precise mechanism of nucleation and growth, it is assumed that crystallization occurs by the random selection of a sequence of repeat units, such that the probability that any segment is selected depends solely on the length of the uncrystallized sequence to which it is attached. This consideration precludes crystallization mechanisms entailing chain folding (Chapter 3). It is further assumed that crystallization consists of the selection of a definite number of chain segments, that number being the minimum required for

thermodynamic stability. The crystallization process is pictured to occur by the random occupation of a number of adjacent sites on a linear lattice (Fig.5.1a), (a site corresponding to a repeat unit of the polymer molecule). This results in an increasing subdivision of the uncrystallized length into progressively shorter sequences, some of which may be shorter than the minimum length required for crystallization. When no sequences of the minimum length are left, a degree of 'wasted space' remains which corresponds to the amorphous fraction of the polymer. This problem is mathematically similar to that of parking cars of the same length along a road. If the distance between two adjacent cars is less than the car length then the space is not available for further occupation.

The amorphous fraction of a crystallized polymer is calculated using this model, and then further problems of occupation of sites on a linear lattice at random, subject to specified restrictions are examined and applied to sorption on graphite, and the close packing of spheres in one dimension.

These statistical problems arise in connection with linear lattices with sites which may be in one of two states (empty or occupied), and when occupation of sites is arranged to occur at random subject to specified restrictions. The following are typical:

Problem I

A linear lattice (Fig.5.1a) of i sites is progressively covered by treating it to successive occupation of blocks of n adjacent sites at a time, each block being placed at a random position on the lattice subject to avoidance of overlap with all previously placed blocks. This process necessarily reaches completion when no further blocks of n adjacent vacant sites remain available for occupation.

Problem Ia

Find the statistical mean number of sites $S_{i,\,n}$ remaining unoccupied at this stage of completion, and especially

$$\lim_{i} S_{i,\,n}/i \equiv T_{\infty,\,n} \qquad 5.1$$

(Clearly $1 - T_{\infty,\,n}$ is the average final density of occupation while $T_{\infty,\,n}$ may be called the statistical wastage of sites.)

Problem Ib

Find the distribution of the lengths n' of blocks of unoccupied sites at the stage of completion (Fig.5.1b). This distribution ranges over

$$0 \leqslant n' \leqslant n - 1 \qquad 5.2$$

where the case n' = 0 refers to the absence of a gap between two continuous blocks of occupied sites. The mean of this distribution is clearly given by:

$$\bar{n}' = nT_{\infty,\,n}/(1 - T_{\infty,\,n}) \qquad 5.3$$

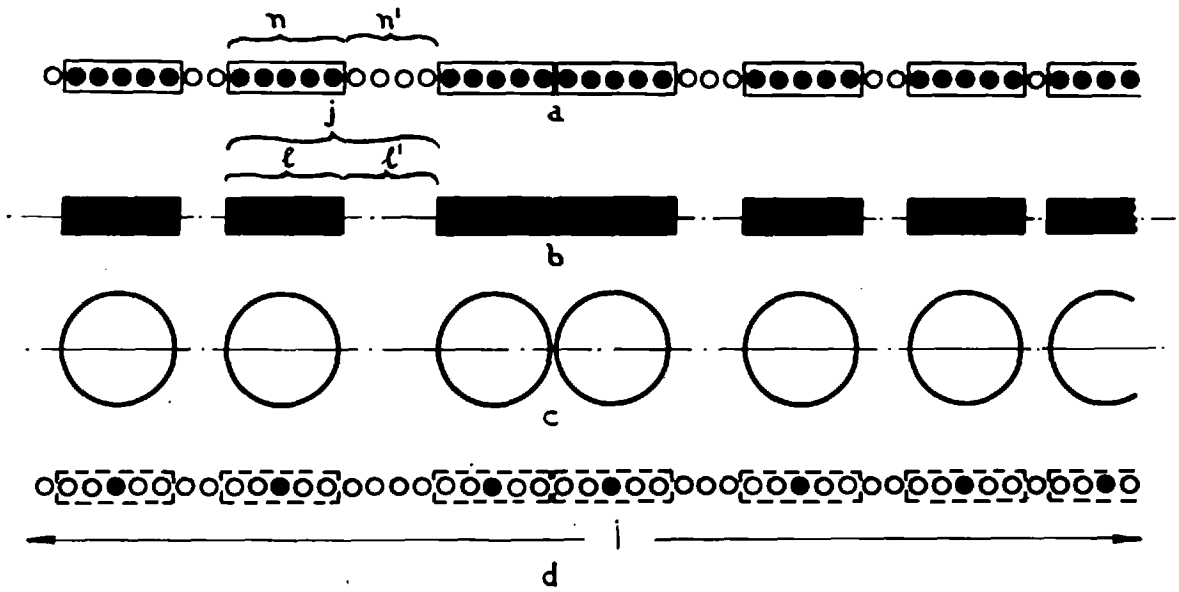


Fig.5.1. Schematic representation of occupation of linear lattice subject to avoidance of overlap.

(a) Occupation of blocks of n adjacent sites subject to avoidance of overlap.

(b) Occupation by line segments of length ℓ, subject to avoidance of overlap.

(c) Occupation by spheres, subject to avoidance of overlap.

(d) Occupation of individual sites, subject to minimum number of intervening sites.

Problem II

To find the quantities corresponding to those in Ia and Ib for the case that $i \to \infty$, and (thereafter) $n \to \infty$. This is the important case when the lattice goes over to a continuous line of infinite length, and the covering process goes over into placing line segments of constant length 1 on the line successively in random positions subject to the avoidance of overlap until no further vacant line segments of length 1 remain available.

Problem IIa

To find

$$\lim_{n \to \infty} T_{\infty, n} = T_{\infty, \infty} \qquad 5.4$$

i.e., the statistical wastage of the line segment at completion.

Problem IIb

To find the distribution of vacant line segments (Fig.5.1b) of lengths

$$0 < l' < 1 \qquad 5.5$$

about their mean

$$l' = lT_{\infty, \infty} / (1 - T_{\infty, \infty}) \qquad 5.6$$

Note the correspondence between equations 5.1 - 5.3 and 5.4 - 5.6.

Problem III

A problem which turns out to be closely related mathematically to the preceding ones arises as follows. A linear lattice of i sites is treated to the occupation of single sites one after another, each chosen at random except for the restriction that no site may be occupied within a distance of n sites of one previously occupied (Fig.5.1d).

Problem IIIa

For $i = \infty$, find the statistical proportion $t_{\infty, n}$ of sites remaining vacant at the end of the process, and also the statistical wastage $w_{\infty, n}$ of sites which here requires special definition (see below).

Problem IV

Find

$$\lim_{n \to \infty} t_{\infty, n} \quad \text{and} \quad \lim_{n \to \infty} w_{\infty, n}$$

Solution of Problem Ia

The simplest case concerns blocks of n = 2 sites, and arises, for instance, when couples fill up a row of i seats in a cinema by sitting down successively in randomly chosen pairs of adjacent vacant seats. Here the final number of 'stranded' (vacant) seats is given by:

$$S_i = \sum_{j=1}^{i} \sum_{k=0}^{j-1} 2^k/k! \qquad 5.7$$

which for increasing i rapidly converges to yield

$$\lim_{i \to \infty} S_i/i = 1/e^2 \qquad 5.8$$

for the fraction of stranded seats.

Application

These results were found by Flory (1939) in connection with the statistical situation in certain cyclization reactions of polymers, and were used by Gordon (1951) to verify the mechanism of cyclization of rubber.

By generalizing Flory's treatment to the case where $n > 2$ one obtains the difference equation:

$$(i - n + 1)S_{i,\,n} - (i - n)S_{i-1,\,n} = 2S_{i-n,\,n} \qquad 5.9$$

with the following boundary conditions for small i values:

$$S_{i,\,n} = i \quad (1 \leqslant i \leqslant n - 1) \qquad 5.10$$

$$S_{n,\,n} = 0 \qquad 5.11$$

More generally one can show that for all i, n and k

$$[(i + k)E_i^{\,n} - iE_i^{\,n-1} - 2]\,\Delta_i^{\,k-1}S_{i,\,n} = 0 \qquad 5.12$$

The operators are defined as follows (Levy and Lessman 1959):

$$E_i f(i) \equiv f(i + 1) \qquad 5.13$$

$$\Delta_i f(i) \equiv f(i + 1) - f(i) \qquad 5.14$$

and raising an operator to the power k denotes k successive applications of the operator. It is consistent (see below)

with our notation to denote $\Delta_i S_{i,\,n}$ (i.e. $S_{i+1,\,n} - S_{i,\,n}$) by $T_{i,\,n}$. It thus follows from 5.12 for k = 2:

$$T_{i,\,n} = [(i-n)T_{i-1,\,n} + 2T_{i-n,\,n}]/(i-n+2) \qquad 5.15$$

and the initial conditions are

$$T_{i,\,n} = 1 \quad (1 \leqslant i \leqslant n-2) \qquad 5.16$$

$$T_{n-1,\,n} = 1-n \qquad 5.17$$

$$T_{n,\,n} = 1 \qquad 5.18$$

It can be shown from eq.5.9 that

$$\lim_{i\to\infty} S_{i,\,n} = \lim_{i\to\infty} (i+n)T_{i,\,n} \qquad 5.19$$

which justifies the notation defined in eq.5.1. In particular (cf. above):

$$T_{\infty,\,2} \left(\equiv \lim_{i\to\infty} T_{i,\,2} \right) = 1/e^2 \qquad 5.20$$

It has not been possible to find analytical solutions for $T_{\infty,\,n}$ with $n > 2$, but those shown in Table 5.1 have been calculated to a satisfactory approximation, using iteration with respect to i upon equations 5.15 - 5.18. The approximation consisted in identifying $T_{\infty,\,n}$ with $T_{j,\,n}$, where j was the lowest integer for which $T_{j,\,n}$ and $T_{j+1,\,n}$ agreed to five significant figures. In this way, column 2 of Table 5.1 was produced on the Mercury Computer in a few minutes. The speed of convergence is such that $j \approx 6n$.

Table 5.1

Statistical Wastage $T_{\infty, n}$ (eq.5.1)

n	$T_{\infty, n}$	$T'_{\infty, \infty}$	$T''_{\infty, \infty}$
2	$1/e^2 = 0.135335$		
3	0.17634		
4	0.19610		
5	0.20772		
6	0.21537		
20	0.24150		
40	0.24697	0.24969	
60	0.24878	0.25059	0.25150
80	0.24970	0.25104	0.25176
100	0.25025	0.25132	0.25185
120	0.25060	0.25150	0.25193
140	0.25086	0.25163	0.25202
160	0.25105	0.25173	0.25206
180	0.25120	0.25180	
100	0.25025		
200	0.25132	0.25186	
300	0.25168	0.25204	
400	0.25186		

Solution of Problem II

The limit of $T_{\infty, n}$ as n tends to infinity can be estimated by extrapolation from Table 5.1. As convergence is slow, the following formal procedures of extrapolation were used. Aitken's δ^2-process, based on the formula

$$T'_{\infty,\infty} = T_{\infty, n+h} - (T_{\infty, n+h} - T_{\infty, n})^2/(T_{\infty, n+h} - 2T_{\infty, n} + T_{\infty, n+h}) \qquad 5.21$$

led to the estimates of $T_{\infty,\infty}$ in column 3 of Table 5.1. Here h is the interval of tabulation in n-values, i.e. 20 or 100.

Solution of Problem IIa

Extrapolation of the values in this column to $n = \infty$ was carried out by applying the δ^2-process to them also, leading to the more rapidly converging values (denoted by $T''_{\infty,\infty}$) in column 4. Further repetition of this process is foiled by rounding-off errors. There is close agreement between the apparent limit of convergence of column 4 and the independent calculation of $T_{\infty, 200}$, $T_{\infty, 300}$ and $T_{\infty, 400}$ at the bottom of column 2 which refer to n values much higher than those used in column 4. The three directly calculated values just mentioned furnish, of course, lower bounds for $T_{\infty,\infty}$ and employing the δ^2-process to them leads to the final figure in column 3 which agrees to better than 0.01% with the final figure in column 4. It is thought safe to conclude that the correct value of the limit is

$$T_{\infty,\infty} = 0.25216 \pm 0.0003 \qquad 5.22$$

The density of coverage of an infinite line with line segments of constant length, placed at random subject to avoidance of overlap is given by,

$$1 - T_{\infty,\infty} = 0.74784 \pm 0.0003 \qquad 5.23$$

and the mean length of the unoccupied segments (eq.5.6) by

$$\mathbf{1}' = (0.33719 \pm 0.00054)\mathbf{1} \qquad 5.24$$

After this work had been completed it was found that this result had previously been derived by Renyi (1958), who obtained an analytical solution in the form:

$$1 - T_{\infty,\infty} = \int_0^{\infty} \exp - \left[2 \int_0^{t} \left(\frac{1 - e^{-u}}{u}\right) du\right] dt \approx 0.748$$

Application

Equation 5.23 furnishes a maximum estimate for the degree of crystallinity attainable according to the 'fringed micelle' model used for the crystallization in bulk of high polymers. Here the individual polymer chain constitutes the individual linear 'lattice' approximating to a continuous line of infinite length. The covering of the line with segments of constant length here corresponds to the inclusion of randomly chosen stretches of the polymer chain in three-dimensional crystallites, while the amorphous regions of the bulk polymer contain the 'unoccupied' segments of the line. The underlying assumption that all the crystallites have the same length (n or 1) in the chain direction is probably approximately true.

It must, however, be recognised that the 'fringed micelle' models oversimplify the situation in a number of respects, e.g., by neglecting chain folding, etc. Experimental measurements of the final degree of crystallinity attained by bulk polymers after primary and secondary crystallization processes have come to an end, often approach 0.75 (eq.523) (Banks et al.1963a) and rarely exceed this figure. This suggests that statistical wastage due to the random placing of crystallites along a chain may be an important contributory factor.

Solution of Problems Ib and IIb

Having found the mean length $\bar{n}'$ or $\bar{l}'$ of the unoccupied parts of the lattice or line, the distribution of these lengths about the mean can be found by standard variational methods, i.e., by maximizing the entropy of the assembly subject to this mean value, and to the alternation of occupied and unoccupied sequences. (This rule of alternation is locally infringed only in the particular case $n' = 0$, eq.5.2, and is automatically allowed for in what follows). Thus each unoccupied sequence of length n' $(0 \leqslant n' \leqslant n - 1)$ is imagined to be coupled (Fig.5.1b) to its left-hand neighbouring occupied sequence of length n, to produce a composite sequence of length

$$m = n + n' \quad (n \leqslant m \leqslant 2n - 1) \qquad 5.25$$

The mean length of the coupled sequences is

$$\bar{m} = n + \bar{n}' = n/(1 - T_{\infty,\, n}) \qquad 5.26$$

Let p_m be the probability of finding a composite sequence of length m. Then the following three equations ensure (Tribus 1962) that the entropy of the system is maximised (eq.5.27), subject to normalization of the p_m (eq.5.28) and the constancy of the mean length $\bar{m}$ (eq.5.29):

$$\sum_{m=n}^{2n-1} \ln p_m dp_m = 0 \qquad 5.27$$

$$\lambda_o \sum_{m=n}^{2n-1} dp_m = 0 \qquad 5.28$$

$$\lambda_1 \sum_{m=n}^{2n-1} m dp_m = 0 \qquad 5.29$$

From these equations the probability distribution is found to be

$$p_m = \exp(-\lambda_o - \lambda_1 m) \qquad n \leqslant m \leqslant 2n-1 \qquad 5.30$$

The two Lagrangian multipliers λ_o and λ_1 are found respectively from the normalization condition:

$$\lambda_o = \ln \sum_{m=n}^{2n-1} \exp - \lambda_1 m \qquad 5.31$$

and from the equation giving the mean (cf. eq. 5.26):

$$\sum_{n}^{2n-1} mx^m \Big/ \sum_{n}^{2n-1} x^m = n/(1 - T_{\infty,\, n}) \qquad 5.32$$

where we have put

$$\exp - \lambda_1 = x \qquad 5.33$$

For example, the correct root of x (i.e. $0 < x < 1$) in eq.5.32 has been found for the case n = 4, by successive approximations to be given by:

$$x = 0.6426 \qquad (n = 4) \qquad 5.34$$

By eliminating λ_o, λ_1 and x between eqs.5.30, 5.31, 5.33 and 5.34, one finally obtains

$$p_m = x^m \Big/ \sum_{n}^{2n-1} x^m \qquad 5.35$$

The distribution thus calculated was compared with that obtained experimentally by a Monte Carlo method on the Mercury Computer, and satisfactory agreement was obtained (Table 5.2). In this Monte Carlo experiment a bank of i = 400 counters was treated as a linear lattice, and blocks of n = 4 adjacent counters had their contents changed (from 0 to unity) at a time. The blocks were located on the linear lattice by the machine choosing a random number for location of the first counter of the block of four and verifying that the block in question was available, (i.e. all four counters showed zero). If the block was not

Table 5.2

Distribution of lengths m (eq.5.25)

m	n = 4 P_m (From maximization of entropy)	P_m (From Monte Carlo calculation)
4	0.4309	0.45
5	0.2769	0.25
6	0.1779	0.18
7	0.1143	0.12

available, the random number was rejected and another chosen. The machine stopped whenever no further blocks of four adjacent counters in the bank of 400 remained at zero. This always required fewer than 2000 trials (random numbers). The values of P_m, obtained from two successive runs, each run giving the average distribution from twenty such 'experiments' differed by less than 3%. Satisfactory agreement between the distributions derived from the Monte Carlo calculation, and from maximizing the entropy is shown in Table 5.2.

The limiting distribution obtained from eq.5.30 by letting n tend to infinity is of importance since this again refers to the case of a continuous line (instead of a linear lattice). As $n \to \infty$, one must let $\lambda_1 \to 0$ while

$$\lambda_1 n = c \qquad 5.36$$

with c finite. The probability p_m goes over into a probability density $p_j dj$ that a given composite segment (consisting of an unoccupied segment of length $0 < l' < 1$ coupled with its left neighbouring occupied segment of length 1) has a length between j and j + dj (where $1 < j < 21$). The distribution (eq.5.30) becomes in the limit

$$p_j dj = c(\exp - cr)dr/[(\exp - c) - (\exp - 2c)] \qquad 5.37$$

where we have put

$$j/1 = r \qquad (1 < r < 2) \qquad 5.38$$

The unoccupied segments on their own (not coupled with their left neighbours) are clearly distributed according to the truncated exponential distribution:

$$q_{l'}dl' = c(\exp - cu)du/(1 - \exp - c) \qquad 0 < u < 1 \qquad 5.39$$

with $u = l'/l$

and mean $l' = (1 - 2\exp - c)/(1 - \exp - c)$ 5.40

Thus, by comparison with eq.5.6, c can be found:

$$c = -\ln (1 - 2T_{\infty,\infty})/(2 - 3T_{\infty,\infty}) = 0.9198 \qquad 5.41$$

Application

Problem IIb, just solved, provides an interesting special case analogous to a well-known model for the liquid state, viz., the packing of hard spheres in one dimension (Taylor and Glasstone 1952). Thus, the line segments of constant length are interpreted (Fig.5.1 c) as diameters of spheres placed at random along a line. In the general model the mean packing density is left as a parameter, and no restriction is placed on the lengths of individual unoccupied segments. Our model, however, is strictly 'close-packed', i.e., no gap larger than a sphere diameter can occur (Bernal 1960). Furthermore, our model fixes the mean density of occupation of the line by spheres at the value:

$$1 - T_{\infty,\infty} = 0.74784$$

which arises from imagining the spheres placed on the line successively at random points (avoiding overlap). The three-dimensional close-packed-sphere model of Bernal (1960) leads to

a mean density of occupation of 0.61.

Solution of Problem III

Denoting the total number of sites on the linear lattice by i as before, we obtain the difference equation for the statistical fraction $t_{i,\ n}$ of the sites left empty:

$$t_{i,\ n} = [(i-1)t_{i-1,\ n} + 2t_{i-n-1,\ n}]/(i - n + 2) \qquad 5.42$$

which should be compared to eq.5.9.

The initial conditions are:

$$t_{0,\ n} = 0 \qquad 5.43$$

$$t_{i,\ n} = 1 \quad (0 < i \leqslant n) \qquad 5.44$$

For even values of n, a simple correspondence exists between problem IIIa and problem Ia:

$$1 - T_{\infty,\ n+1} = (1 + n)(1 - t_{\infty,\ n}) \qquad 5.45$$

(This is readily seen by flanking each occupied site in problem IIIa by n/2 fictitious occupants on each side as in Fig.5.1d. These merely block the corresponding sites against further occupation.)

The values of $t_{\infty,\ n}$ tabulated in Table 5.3 were compiled as follows:

n odd: by solving equations 5.42 - 5.44 by iteration on the Mercury Computer by the method for the previous problem.

Table 5.3

Empty Fraction $t_{\infty, n}$, and Statistical Wastage $W_{\infty, n}$ (eqs.5.42 and 5.46)

n	$t_{\infty, n}$	$W_{\infty, n}$
2	0.72545	0.21410
3	0.79903	0.24394
4	0.84154	0.26218
5	0.86923	0.27443
10	0.93022	0.30283
15	0.95242	0.31362
20	0.96390	0.31927
30	0.97567	0.32516
40	0.98164	0.32817
50	0.98526	0.32999
60	0.98769	0.33121
100	0.99258	0.33361
150	0.99504	0.33466
200	0.99627	0.33508

n even: from equation 5.45 using values of $T_{\infty,\, n+1}$ from Table 5.1.

For the present problem, the statistical wastage of accommodation is calculated as the proper fraction

$$W_n = (n + 1)\,(1 - t_{\infty,\, n})^{-1} - 1 \qquad 5.46$$

which is also tabulated in Table 5.3. The definition of $W_{\infty,\, n}$ is based on the fact that the maximum fraction of sites occupied is $(n + 1)^{-1}$, (when the placing of these occupied sites occurs regularly at intervals at n + 1 sites), while the fraction occupied by random placing is $1 - t_{\infty,\, n}$.

Solution of Problem IV

As n tends to infinity, the fraction of sites wasted owing to the randomness of placement is given by (eq.5.45, 5.46)

$$W_{\infty,\, n} = T_{\infty,\infty}/(1 - T_{\infty,\infty}) = 0.33718 \qquad 5.67$$

Application

The solution of problems III and IV are applicable to Hooley's model (1961) for the sorption of foreign molecules in graphite. Here the three dimensional graphite lattice is formally reduced to the linear spacing ($3.35\,\mathring{A}$) of the graphitic lattice planes. Penetration of foreign molecules into one such spacing is imagined to block occupation of n adjacent spacings on each side. The results in Table 5.3 could be evaluated in terms of the maximum amount of sorbate found experimentally.

REFERENCES

Avrami, M., 1939, J.Chem.Phys., 7, 1103.

Banks, W., Hay, J.N., Sharples, A. and Thomson, G., 1962, Nature, 194, 542.

Banks, W., Hay, J.N., Sharples, A. and Thomson, G., 1964, Polymer, in press.

Banks, W., Gordon, M., Roe, R.J., and Sharples, A., 1963a, Polymer, 4, 61.

Banks, W., Gordon, M. and Sharples, A., 1963b, Polymer, 4, 289.

Banks, W., and Sharples, A., 1963, Makromol.Chem., 59, 233.

Barnes, W.J., Luetzel, W.G. and Price, F.P., 1961, J.Phys.Chem., 65, 1742.

Bernal, J.D., 1960, Nature, 185, 68.

Boor, J. and Mitchell, J.C., 1963, J.Polymer Sci.A, 1, 59.

Bunn, C.W. and Holmes, D.R., 1958, Disc.Faraday Soc., 25, 95.

Chiang, R. and Flory, P.J., 1961, J.Amer.Chem.Soc., 83, 2857.

Eppe, R., Fischer, E.W. and Stuart, H.A., 1959, J.Polymer Sci., 34, 721.

Ferry, J.D., 1961, Viscoelastic Properties of Polymers, London, John Wiley and Sons Inc.

Fischer, E.W., 1957, Z.Naturforsch.A, 12a, 753.

Fischer, E.W. and Schmidt, G.F., 1962, Angew.Chem., 1, 488.

Fletcher R. and Powell, M.J.D., 1963, Publication T.P.100, A.E.R.E. England.

Flory, P.J., 1939, J.Amer.Chem.Soc., 61, 1518.

Flory, P.J., 1953, Principles of polymer chemistry, Ithaca: Cornell University Press.

Flory, P.J. and McIntyre, A.D., 1955, J.Polymer Sci., 18, 592.

Flory, P.J., 1962, J.Amer.Chem.Soc., 84, 2858.

Frank, F.C. and Tosi, M., 1961, Proc.Roy.Soc.A, 263, 323.

Geil, P.H., 1960, J.Polymer Sci., 47, 65.

Geil, P.H., 1962, Bull.Am.Phys.Soc., 7, 206.

Gordon, M., 1951, Proc.Roy.Soc.A, 204, 569.

Gordon, M., 1963, High Polymers, London, Illife Ltd.

Griffith, J.H. and Ranby, B.G., 1959, J.Polymer Sci., 38, 107.

Gubler, M.G. and Kovacs, A.J., 1959, J.Polymer Sci., 34, 551.

Ham, F.S., 1958, J.Physics.Chem.Solids, 6, 335.

Hammer, C.F., Brandt, W.W. and Peticolas, W.L., 1957, J.Polymer Sci., 24, 291.

Hildebrand, F.B., 1956, Introduction to numerical analysis, New York, McGraw-Hill.

Hirai, N. and Eyring, H., 1958, J.Appl.Phys., 29, 810.

Hoffman, J.D. and Lauritzen, J.I., 1961, J.Res.Nat.Bur.Stand.A, 65, 297.

Hoffman, J.D., Weeks, J.J. and Murphey, W.M., 1959, J.Res.Nat. Bur.Stand.A, 63, 67.

Hooley, G.J., 1961, Nature, 190, 530.

Jackson, J.B., Flory, P.J. and Chiang, R., 1963, Trans.Faraday Soc., 59, 1906.

Jacobs, P.W.H. and Tompkins, F.C., 1955, Chemistry of the solid state, London, Butterworths Sci.Publ., Chap.7.

Jaycock, M.J. and Parfitt, G.D., 1961, Trans.Faraday Soc., 57, 791.

Karasz, F.E. and Hamblin, D.J., 1963, National Physical Laboratory, Basic Physics Division, Report B.P.R.15.

Kargin, V.A., Bakeer, N.F., Li, Li-Shen and Ochapovskaya, T.S., 1960, Vysokomol. Soed., 2, 1280.

Kawai, T. and Keller, A., 1963, Phil.Mag., 8, 1203.

Keller, A., 1955a, J.Polymer Sci., 17, 291.
1955b, J.Polymer Sci., 17, 351.
1955c, J.Polymer Sci., 17, 447.

Keller, A., 1962, Polymer, 3, 393.

Keller, A. and Sawada, S., 1964, Makromol.Chem., in press.

Keller, A., 1964, Polymer Physics Meeting, Shrivenham.

Kenyon, R.C., Gross, R.C. and Wurstner, A.L., 1959, J.Polymer Sci., 40, 159.

Levy, H. and Lessman, F., 1959, Finite difference equations, London, Sir Isaac Pitman and Sons Ltd.

Mandelkern, L., 1956, Chem.Rev., 56, 903.

Mandelkern, L., 1958, Growth and perfection of crystals, London, Chapman and Hall, pp.467-497.

Mandelkern, L., Roberts, D.E. and Halpin, J.C., 1960, J.Amer. Chem.Soc., 82, 46.

Marker, L., Hay, P.M., Tilley, G.P., Early, R.M. and Sweeting, O.J., 1959, J.Polymer Si., 38, 33.

Matsuoka, S., 1960, J.Polymer Sci., 62, 511.

Morgan, L.B., 1954, Phil.Trans.A., 921, 13.

Natta, G., 1957, Chem.and Ind.(Paris), 77, 1009.

Padden, F.J. and Keith, H.D., 1959, J.Appl.Phys., 30, 1485.

Palmer R.P. and Cobbold, A.J., 1964, Makromol.Chem., in press.

Parrini, P. and Corrieri, G., 1963, Makromol.Chem., 62, 83.

Peterlin, A. and Roeckl, E., 1963, J.Appl.Phys., 34, 102.

Price, F.P., 1961, J.Chem.Phys., 35, 1884.

Price, F.P., 1964, Private communication.

Ranby, B.G., Morehead, F.F. and Walter, N.M., 1960, J.Polymer Sci., 44, 349.

Ree, T., Hahn, S.J. and Eyring, H., 1955, Proc.International Wool Textile Res.Conference, p.234.

Rényi, A., 1958, Magy.Tud.Akad.Mat.Kut.Intézetének Kozleményei, 3, 109.

Roe, R.-J., Smith, K.J. and Krigbaum, W.R., 1961, J.Chem.Phys., 35, 1306.

Rosenbrock, H.H., 1960, Computer J., 3, 175.

Sharples, A., and Swinton, F.L., 1963, Polymer, 4, 119.

Sharples, A., 1963, private communication.

Statton, W.O. and Geil, P.H., 1960, J.Appl.Polymer Sci., 3, 357.

Strand, T.G., Kohl, D.A. and Bonham, R.A., 1963, J.Chem.Phys., 39, 1307.

Stuart, H.A., 1959, Ann.N.Y.Acad.Sci., 83, 3.

Swan, P.R., 1960, J.Polymer Sci., 42, 525.

Taylor. H.S. and Glasstone, S., 1952, A treatise on Physical Chemistry, London: D.Van Norstrand Co.Inc., p.358.

Tribus, M., 1962, Thermostatics and Thermodynamics, London, D.Van Norstrand Co.Inc., p.77.

Tung, L.H. and Buckser, S., 1959, J.Phys.Chem., 63, 763.

Turnball, D. and Fisher, J.C., 1949, J.Chem.Phys., 17, 71.

APPENDIX A

The examiners of this thesis have suggested a further discussion of the "approximation" introduced on page 15 because of its serious effects on this work. This fragmentation problem appears first in the literature when Morgan (1954) discusses it in the case of fibrillar growth from predetermined nuclei. He states that the Avrami equation "is nearly correct however for the case where the growing end of the cylinder does not stop on meeting a crystallized locality but deviates from its straight-line growth into the surrounding amorphous regions and proceeds on a fresh course". Lauritzen, in private discussion at the Bristol Conference on High Polymers (1961), claimed to have obtained a first order approximation to the correct model for discs as well as rods.

Fragmentation.

The Avrami equation represents exactly a well-defined theoretical model, a space-filling one in which all the fragments (Fig.3.6) of the bodies are formed. This is unrealistic in the absence of forces causing re-nucleation over large distances. Some, but by no means all, of the space occupied by fragments of a given body, other than the original fragment (containing the primary nucleus), must in reality remain permanently amorphous. A volume element in any other fragment of the given body will permanently fail to crystallize only if an infinity of other bodies competing for this element fail to reach it without prior fragmentation. The successive bids by these bodies for this element of volume become less and less likely to succeed, because their primary nuclei are placed at successively greater

distances from the element (leading to an increasing chance of fragmentation).

Quantitative estimates of the effect of fragmentation are not available. This means that all the curve-fitting of experimental data to non-spherulitic Avrami models, both in this thesis and the literature, has to be viewed with caution. Fragmentation is likely to become serious at the point where the sum of the volume of the entities is equal to the volume of the sample. This occurs when (eq. 2.26) $Q\bar{V} = 1$, i.e. when $\chi/\chi_\infty = 1-1/e = 0.64$, which means when the crystallization experiment has reached 64% conversion. However, turning to practical applications, since generally only the ratio χ/χ_∞ is fitted, with χ_∞ taken from the measured total contraction, the experimental and theoretical curves are forced to agree again at infinite time. In effect this means that the result of fragmentation at infinite time has been eliminated by scaling χ_∞ to the observed value. It follows that if the fraction of the current crystallinity which (in the real sample) is lost owing to fragmentation is a constant (independent of χ) then it is correct to apply Avrami-type theories as exemplified in this thesis. The replacement of the time-variable fractional wastage due to fragmentation by its final value at infinite time constitutes the approximation mentioned in the text (p. 15).

The situation is further improved by the following consideration. The rate curves (χ/χ_∞ vs time) predicted on the Avrami model overestimate χ at all times, which thus at least provides an upper bound. Since fragmentation is asymptotically eliminated as the time origin is approached, the curves calculated from Avrami models are asymptotically correct.

More can be said about the severity in various cases of fragmentation effects in fitting Avrami-type models to experimental results. First, an experimental value of χ_∞ near unity would indicate that there can be little fragmentation. Accordingly, the closer the experimental values of χ_∞ to unity, the better the approximation will evidently be. The overriding factor is due to geometrical shape: the thinner the rods or discs (in relation to their dimensions in the directions of growth) the more serious the fragmentation to be expected. Although χ_∞ for polymethylene is much less than unity, being about 30%, (Table 3.1), when the secondary crystallization is present the limiting value of the crystallinity is increased to 55%. Some of the remaining amorphous material may be due to amorphous folds at the lamellar faces, rather than to fragmentation, although the existence of extensive amorphous folds in the case of solution grown lamellae is the subject of controversy at present, (p. 36). The "wafer-like" appearance (approximately 1μ long, 100-400Å thick) of polyethylene lamellae obtained from disintegration of bulk samples implies that serious fragmentation may result from the impingement of such lamellae.

The number of growing points per platelet.

Throughout the discussion of the single-crystal model in this thesis it is implicitly assumed that each growing body has only one growth front, but nothing is significantly changed provided the number of growth fronts remains at any other constant value during the whole process. It would seem likely that as the growing faces grow larger, additional growing fronts would inevitably be nucleated,

thereby changing the growth law. Theoretically, the additional growth fronts nucleated at random points on the growing faces are less likely to be in exact register (i.e. to be coherent) than is the case for the re-nucleation of growth fronts dealt with in our model. Thus we would expect branching and spherulitic growth when the faces get large enough. This is, in fact, observable outside the range of our experiments, as explained on p. 54-55. Therefore, the assumptions of the model seem acceptable in this respect.

Interference with growth due to impingement.

Apart from the fragmentation problem just discussed, there is a further related source of error, viz. due to interference of impingement with growth, which is inherent in the fitting of our folding-chain models. This differs from fragmentation in that it concerns the original (Fig 3.6; A) fragment of a body containing the primary nucleus. Growth has been assumed to depend on continuous deposition at one or more growth fronts. Impingement of the body under consideration with any other body may necessitate reflection of the growth front at the point of impingement. This would lead to a small but progressive acceleration of the growth. If there is no growth front between the regions of impingement of one body with [redacted] two others further deposition of chain pleats on this part of the surface is prevented. On the other hand a growth front situated between two such points of impingement will merely be reflected back and forth between these points. Geometrically, there are two types of contacts which arise with finite probability when two lamellar-like bodies impinge. These are the result of the impingement of the growing edges of two bodies (edge-edge contact) and the

impingement of a corner of one body with the face of another (face-corner contact). Although the relative occurence of these two contacts cannot be assessed, an edge-edge contact may affect the subsequent growth of both bodies, whilst the growth of only one body will be affected by the most common face-edge contact, i.e. one in which the face concerned is not a growing face. The interference by impingement with growth may be summed up as follows: while the Avrami model postulates that all bodies have, with finite probability at infinite time, only face-face contacts, all such contacts will in reality be arrested at or near an edge-edge or face-corner contact. This will again leave amorphous regions in the final structure not accounted for by the model, except through the averaging process implied in forcing the final degree of crystallinity to agree with experiment.

APPENDIX

In this appendix, all of the dilatometric runs analysed and discussed in this thesis are tabulated.

Polymethylene (cf.Table 3.2; Figs.3.2, 3.4, 3.14) 161

Polypropylene (cf.Table 4.1; Fig.4.2) 170

Polybutene (cf.Table 4.2) 177

Poly-(ethylene oxide) (cf.Table 4.3) 181

Polystyrene (cf.Tables 4.4, 4.5) 184

Polymethylene (127.61°C). S=6.9%.

H(o)-H(T)(CM.)	TIME(MIN.)	H(o)-H(T)(CM.)	TIME(MIN.)
0.060	3	2.123	61
0.114	5	2.166	63
0.174	7	2.206	65
0.244	9	2.246	67
0.315	11	2.287	69
0.398	13	2.319	71
0.478	15	2.355	73
0.559	17	2.388	75
0.638	19	2.467	80
0.727	21	2.548	86
0.817	23	2.600	90
0.904	25	2.659	95
0.994	27	2.711	100
1.074	29	2.762	105
1.160	31	2.802	110
1.244	33	2.843	115
1.322	35	2.881	120
1.403	37	2.918	125
1.477	39	2.948	130
1.552	41	2.981	135
1.618	43	3.064	150
1.682	45	3.110	160
1.747	47	3.152	170
1.809	49	3.187	180
1.869	51	3.221	190
1.924	53	3.400	260
1.975	55	3.458	300
2.028	57	3.476	315
2.074	59	3.476	405

Polymethylene (127.61°C) S=33.3%.

H(o)-H(T)(CM.)	TIME(MIN.)	H(o)-H(T)(CM.)	TIME(MIN.)
0.176	2	1.455	31
0.250	3	1.503	33
0.325	4	1.549	35
0.399	5	1.586	37
0.472	6	1.641	40
0.536	7	1.695	43
0.595	8	1.728	45
0.654	9	1.798	50
0.709	10	1.860	55
0.762	11	1.918	60
0.812	12	1.973	66
0.860	13	2.012	70
0.904	14	2.054	75
0.950	15	2.096	80
0.991	16	2.124	85
1.030	17	2.157	90
1.064	18	2.188	95
1.102	19	2.219	100
1.139	20	2.243	105
1.167	21	2.263	110
1.205	22	2.284	115
1.236	23	2.325	125
1.296	25	2.392	146
1.327	26	2.543	210
1.352	27	2.563	220
1.379	28	2.577	240

Polymethylene (127.61°C) S=0.2%.

H(o)-H(T)(CM.)	TIME(MIN.)	H(o)-H(T)(CM.)	TIME(MIN.)
0.032	5	1.611	74
0.079	10	1.657	76
0.148	15	1.705	78
0.234	20	1.753	80
0.339	25	1.796	82
0.400	28	1.843	84
0.447	30	1.885	86
0.502	32	1.930	88
0.553	34	1.976	90
0.611	36	2.016	92
0.666	38	2.072	95
0.717	40	2.172	100
0.766	42	2.264	105
0.831	44	2.352	110
0.886	46	2.434	115
0.946	48	2.511	120
0.993	50	2.580	125
1.044	52	2.643	130
1.100	54	2.706	135
1.156	56	2.761	140
1.204	58	2.811	145
1.263	60	3.304	220
1.313	62	3.320	225
1.362	64	3.362	235
1.417	66	3.405	245
1.462	68	3.576	305
1.511	70	3.578	325
1.561	72	3.578	450

Polymethylene (125.79°C) Run A.

H(o)-H(T)(CM.)	TIME(MIN.)	H(o)-H(T)(CM.)	TIME(MIN.)
0.024	5	2.197	40
0.041	6	2.247	41
0.056	7	2.296	42
0.074	8	2.343	43
0.093	9	2.395	44
0.113	10	2.432	45
0.141	11	2.477	46
0.173	12	2.522	47
0.211	13	2.556	48
0.255	14	2.599	49
0.307	15	2.633	50
0.424	17	2.670	51
0.495	18	2.704	52
0.575	19	2.738	53
0.650	20	2.775	54
0.734	21	2.807	55
0.821	22	2.837	56
0.910	23	2.869	57
1.000	24	2.896	58
1.087	25	2.935	59
1.176	26	2.949	60
1.270	27	2.980	61
1.354	28	2.998	62
1.439	29	3.017	63
1.524	30	3.039	64
1.603	31	3.061	65
1.667	32	3.164	70
1.755	33	3.254	75
1.825	34	3.327	80
1.892	35	3.447	90
1.963	36	3.507	100
2.026	37	3.608	120
2.084	38	3.657	140
2.141	39	3.673	180
2.197	40	3.673	1620

Polymethylene (125.92 C) Run B.

H(o)-H(T)(CM.)	TIME(MIN.)	H(o)-H(T)(CM.)	TIME(MIN.)
0.036	8	2.261	46
0.065	10	2.307	47
0.095	12	2.353	48
0.149	14	2.398	49
0.226	16	2.443	50
0.323	18	2.512	52
0.435	20	2.590	54
0.503	21	2.660	56
0.573	22	2.728	58
0.648	23	2.784	60
0.724	24	2.844	62
0.804	25	2.895	64
0.878	26	2.945	66
0.965	27	2.993	68
1.050	28	3.034	70
1.136	29	3.143	75
1.222	30	3.232	80
1.303	31	3.314	85
1.388	32	3.381	90
1.460	33	3.440	95
1.540	34	3.489	100
1.614	35	3.573	110
1.692	36	3.642	120
1.756	37	3.692	130
1.827	38	3.717	135
1.884	39	3.738	140
1.951	40	3.761	145
2.008	41	3.782	155
2.062	42	3.808	165
2.117	43	4.032	795
2.173	44	4.047	855
2.217	45	4.069	945
		4.069	1125

Polymethylene (127.18 C) Run C.

H(o)-H(T)(CM.)	TIME(MIN.)	H(o)-H(T)(CM.)	TIME(MIN.)
0.008	10	1.372	95
0.018	14	1.429	97
0.030	17	1.486	99
0.043	20	1.533	101
0.055	23	1.588	103
0.068	26	1.640	105
0.086	29	1.704	108
0.102	32	1.755	110
0.124	35	1.802	112
0.139	37	1.855	114
0.155	39	1.893	116
0.170	41	1.939	118
0.195	43	1.984	120
0.215	45	2.042	123
0.238	47	2.066	124
0.264	49	2.143	128
0.293	51	2.186	130
0.325	53	2.214	132
0.357	55	2.284	136
0.394	57	2.314	138
0.435	59	2.350	140
0.471	61	2.496	150
0.514	63	2.571	155
0.560	65	2.635	160
0.609	67	2.696	165
0.658	69	2.866	180
0.704	71	2.965	190
0.755	73	3.054	200
0.809	75	3.134	210
0.863	77	3.207	220
0.919	79	3.272	230
0.972	81	3.329	240
1.035	83	3.384	250
1.090	85	3.490	300
1.140	87	3.620	400
1.205	89	3.680	500
1.265	91	3.720	700
1.316	93	3.737	900
		3.737	1380

Polymethylene (127.61°C) Run D.

H(o)-H(T)(CM.)	TIME(MIN.)	H(o)-H(T)(CM.)	TIME(MIN.)
0.014	35	2.400	201
0.053	40	2.460	206
0.100	50	2.517	211
0.152	60	2.556	215
0.184	65	2.607	220
0.225	70	2.656	225
0.268	75	2.742	235
0.334	80	2.785	240
0.408	85	2.822	245
0.484	90	2.861	250
0.559	95	2.901	255
0.655	100	2.936	260
0.745	105	2.972	265
0.838	110	3.004	270
0.947	115	3.093	285
1.102	123	3.158	295
1.140	125	3.206	305
1.181	127	3.238	310
1.237	130	3.270	320
1.281	132	3.313	330
1.340	135	3.345	340
2.014	172	3.369	347
2.130	180	3.396	360
2.165	182	3.435	385
2.204	185	3.449	395
2.239	187	3.465	405
2.275	190	3.477	415
2.303	193	3.495	435
2.327	195	3.495	450
		3.495	540

Polymethylene (128.26 °C). Run E.

H(o)-H(T)(CM.)	TIME(MIN.)	H(o)-H(T)(CM.)	TIME(MIN.)
0.005	23	1.661	290
0.017	51	1.722	296
0.040	62	1.762	300
0.052	70	2.110	340
0.066	76	2.146	345
0.117	100	2.179	350
0.148	111	2.215	355
0.175	120	2.252	360
0.206	128	2.319	370
0.380	160	2.422	385
0.455	170	2.485	395
0.497	176	2.515	400
0.532	180	2.543	405
0.578	186	2.571	410
0.619	190	2.631	420
0.678	196	2.759	445
0.713	200	2.804	455
0.762	205	2.919	480
0.817	210	3.165	545
0.867	215	3.203	555
1.018	230	3.256	575
1.076	235	3.285	585
1.134	240	3.298	590
1.181	245	3.359	612
1.258	252	3.374	625
1.295	260	3.375	635
1.590	285	3.492	1425
		3.492	1675

Polymethylene (129.12 °C) Run F.

H(o)-H(T)(CM.)	TIME(MIN.)	H(o)-H(T)(CM.)	TIME(MIN.)
1.587	730	2.013	845
1.628	740	2.100	870
1.645	745	2.362	955
1.739	770	2.407	970
1.778	780	2.437	980
1.814	790	2.465	990
1.836	795	2.489	1000
1.871	805	2.552	1025
1.911	815	2.776	1120
1.947	825	2.804	1135
1.982	835	2.857	1160
2.013	845	3.551	2170

Polymethylene (127.18°C) (Fig 3.2A).

H(o)-H(T)(CM.)	TIME(MIN.)	H(o)-H(T)(CM.)	TIME(MIN.)
0.074	19	2.570	130
0.096	23	2.646	135
0.120	26	2.735	141
0.137	28	2.820	148
0.161	31	2.922	155
0.195	34	3.036	165
0.232	37	3.131	175
0.276	40	3.216	185
0.328	43	3.296	195
0.363	45	3.372	205
0.425	48	3.434	215
0.477	50	3.495	225
0.549	53	3.551	235
0.600	55	3.640	255
0.657	57	3.803	300
0.712	59	3.943	360
0.775	61	4.030	420
0.838	63	4.468	1170
0.895	65	4.515	1265
0.957	67	4.551	1412
1.024	69	4.585	1592
1.085	71	4.629	1807
1.155	73	4.734	2702
1.220	75	4.781	3042
1.280	77	4.826	3307
1.380	80	4.881	4147
1.471	83	4.977	5587
1.552	86	5.049	7057
1.648	89	5.104	8677
1.734	92	5.153	10297
1.822	95	5.190	11797
1.975	101	5.237	14257
2.051	104	5.298	17137
2.121	107	5.359	21457
2.210	111	5.395	25777
2.297	115	5.414	30097
2.408	121	5.422	35857
2.482	125	5.422	41617

Polymethylene (127.60°C). (Fig.3.12).

H(o)-H(T)(CM.)	TIME(MIN.)	H(o)-H(T)(CM.)	TIME(MIN.)
0.296	5	1.350	410
0.423	10	1.418	520
0.564	20	1.455	615
0.657	30	1.691	1450
0.791	50	1.741	1820
0.888	70	1.870	2900
0.941	90	1.959	4340
1.023	120	2.036	5810
1.101	165	2.137	8690
1.177	215	2.159	10130
1.250	280		

Polypropylene (134.08°C).

H(o)-H(T)(CM.)	TIME(MIN.)	H(o)-H(T)(CM.)	TIME(MIN.)
0.029	6	3.009	30
0.087	8	3.160	31
0.179	10	3.324	32
0.241	11	3.521	33
0.317	12	3.694	34
0.405	13	3.861	35
0.493	14	4.015	36
0.601	15	4.167	37
0.711	16	4.307	38
0.835	17	4.449	39
0.968	18	4.592	40
1.105	19	4.722	41
1.255	20	4.848	42
1.409	21	4.965	43
1.557	22	5.079	44
1.745	23	5.183	45
1.927	24	5.282	46
2.105	25	5.452	48
2.283	26	5.602	50
2.463	27	5.713	52
2.647	28	5.819	55
2.827	29	5.882	70

Polypropylene (143.54°C).

H(o)-H(T)(CM.)	TIME(MIN.)	H(o)-H(T)(CM.)	TIME(MIN.)
0.038	45	4.081	345
0.423	125	4.208	355
0.486	130	4.284	360
0.546	135	4.359	365
0.594	140	4.435	370
0.650	145	4.669	385
0.707	150	4.745	390
0.772	155	4.888	400
0.847	160	5.038	410
0.900	165	5.171	420
0.967	170	5.311	430
1.044	175	5.432	440
1.111	180	5.604	455
1.189	185	5.788	475
1.270	190	6.870	1435
1.429	200	6.946	2875
1.510	205		

Polypropylene (135.50°C).

H(o)-H(T)(CM.)	TIME(MIN.)	H(o)-H(T)(CM.)	TIME(MIN.)
0.023	5	2.607	40
0.096	10	2.727	41
0.118	11	2.859	42
0.149	12	2.985	43
0.180	13	3.110	44
0.222	14	3.225	45
0.264	15	3.355	46
0.309	16	3.470	47
0.361	17	3.581	48
0.417	18	3.717	49
0.477	19	3.946	51
0.537	20	4.051	52
0.608	21	4.154	53
0.681	22	4.273	54
0.769	23	4.375	55
0.846	24	4.473	56
0.933	25	4.568	57
1.030	26	4.648	58
1.121	27	4.734	59
1.224	28	4.816	60
1.324	29	4.889	61
1.426	30	4.963	62
1.530	31	5.037	63
1.653	32	5.109	64
1.765	33	5.236	66
1.879	34	5.339	68
1.999	35	5.418	70
2.116	36	5.554	75
2.231	37	5.706	97
2.364	38	5.751	120
2.479	39	5.768	135

Polypropylene (149.30°C).

H(o)-H(T)(CM.)	TIME(MIN.)	H(o)-H(T)(CM.)	TIME(MIN.)
0.019	120	5.021	1355
0.035	155	5.154	1385
0.057	185	5.270	1415
0.080	215	5.378	1445
0.112	245	5.498	1475
0.161	275	5.865	1695
0.216	305	6.166	1815
0.286	335	6.909	2895
0.362	365	6.929	3075
0.437	395	6.970	4335

Polypropylene (137.04 °C)

H(o) - H(T) (CM)	TIME (MIN.)	H(o) - H(T) (CM)	TIME (MIN.)
0.018	7	2.603	54
0.034	9	2.691	55
0.063	11	2.786	56
0.097	13	2.871	57
0.141	15	2.956	58
0.193	17	3.047	59
0.250	19	3.141	60
0.323	21	3.227	61
0.360	22	3.311	62
0.407	23	3.400	63
0.453	24	3.482	64
0.501	25	3.575	65
0.551	26	3.658	66
0.603	27	3.738	67
0.656	28	3.812	68
0.710	29	3.887	69
0.767	30	3.966	70
0.825	31	4.047	71
0.890	32	4.125	72
0.951	33	4.195	73
1.017	34	4.271	74
1.081	35	4.349	75
1.151	36	4.410	76
1.215	37	4.483	77
1.283	38	4.595	79
1.357	39	4.703	81
1.435	40	4.789	83
1.506	41	4.873	85
1.591	42	4.946	87
1.665	43	5.028	89
1.737	44	5.095	91
1.831	45	5.192	94
1.991	47	5.252	97
2.078	48	5.343	102
2.161	49	5.421	107
2.251	50	5.502	117
2.338	51	5.576	127
2.427	52	5.582	157
2.521	53	5.617	187
		5.771	1027

Polypropylene (138.98 °C)

H(o) - H(T) (CM)	TIME (MIN.)	H(o) - H(T) (CM)	TIME (MIN.)
0.011	10	2.632	82
0.025	13	2.738	84
0.077	19	2.868	86
0.120	22	2.978	88
0.216	26	3.107	90
0.253	28	3.217	92
0.304	30	3.344	94
0.357	32	3.459	96
0.468	36	3.577	98
0.530	38	3.694	100
0.598	40	3.810	102
0.743	44	3.924	104
0.817	46	3.996	106
0.981	50	4.101	108
1.117	52	4.217	110
1.163	53	4.323	112
1.201	54	4.434	114
1.251	55	4.531	116
1.332	57	4.635	118
1.386	58	4.720	120
1.477	60	4.810	122
1.525	61	4.908	124
1.573	62	5.046	126
1.674	64	5.141	128
1.723	65	5.219	130
1.831	67	5.299	132
1.882	69	5.367	134
1.943	70	5.446	136
2.000	71	5.514	138
2.042	72	5.578	140
2.111	73	5.676	143
2.167	74	5.821	148
2.221	75	5.966	153
2.335	77	6.043	158
2.395	78	6.232	203
2.506	80		

Polypropylene (140.20°C).

H(o)-H(T)(CM.)	TIME(MIN.)	H(o)-H(T)(CM.)	TIME(MIN.)
0.014	10	2.885	126
0.039	20	2.998	129
0.074	25	3.126	132
0.114	30	3.246	135
0.158	35	3.362	138
0.225	40	3.485	141
0.294	45	3.612	144
0.334	47	3.732	147
0.371	49	3.850	150
0.407	51	3.969	153
0.441	53	4.080	156
0.486	55	4.196	159
0.534	57	4.303	162
0.580	59	4.419	165
0.630	61	4.532	168
0.675	63	4.629	171
0.751	66	4.730	174
0.831	69	4.953	181
0.916	72	5.084	184
1.004	75	5.143	187
1.100	78	5.338	193
1.190	81	5.411	196
1.287	84	5.514	200
1.383	87	5.773	210
1.486	90	5.877	215
1.596	93	5.985	220
1.699	96	6.078	225
1.813	99	6.176	230
1.922	102	6.258	235
2.045	105	6.317	240
2.151	108	6.444	250
2.269	111	6.542	260
2.390	114	6.602	270
2.511	117	6.693	300
2.631	120	6.708	330
2.753	123		

Polypropylene (143.54 °C) S=9%.

H(o)-H(T)(CM.)	TIME(MIN.)	H(o)-H(T)(CM.)	TIME(MIN.)
0.013	10	1.903	50
0.036	15	2.005	51
0.063	18	2.099	52
0.090	20	2.195	53
0.132	22	2.292	54
0.173	24	2.389	55
0.235	26	2.481	56
0.302	28	2.585	57
0.384	30	2.684	58
0.428	31	2.786	59
0.478	32	2.885	60
0.532	33	2.982	61
0.588	34	3.075	62
0.651	35	3.259	64
0.719	36	3.439	66
0.784	37	3.611	68
0.856	38	3.767	70
0.934	39	3.914	72
1.010	40	4.051	74
1.093	41	4.174	76
1.173	42	4.399	80
1.259	43	4.679	85
1.341	44	4.906	90
1.429	45	5.122	95
1.522	46	5.317	100
1.617	47	5.463	105
1.715	48	5.592	110
1.807	49		

Polypropylene (147.94°C) S=14%.

H(o)-H(T)(CM.)	TIME(MIN.)	H(o)-H(T)(CM.)	TIME(MIN.)
0.008	10	2.562	90
0.025	20	2.687	92
0.051	25	2.813	94
0.091	30	2.942	96
0.138	34	3.072	98
0.188	38	3.196	100
0.223	40	3.309	102
0.262	42	3.422	104
0.310	44	3.531	106
0.350	46	3.630	108
0.409	48	3.737	110
0.469	50	3.829	112
0.530	52	3.921	114
0.592	54	4.008	116
0.665	56	4.096	118
0.742	58	4.176	120
0.831	60	4.251	122
0.917	62	4.336	125
1.018	64	4.481	130
1.118	66	4.607	135
1.219	68	4.725	140
1.329	70	4.829	145
1.441	72	4.907	150
1.554	74	5.017	160
1.677	76	5.101	170
1.795	78	5.164	180
1.919	80	5.215	190
2.045	82	5.255	200
2.180	84	5.386	210
2.310	86	5.598	700
2.424	88		

Polybutene (103.10°C).

H(o)-H(T)(CM.)	TIME(MIN.)	H(o)-H(T)(CM.)	TIME(MIN.)
0.016	35	1.310	245
0.031	55	1.357	250
0.059	70	1.391	255
0.133	90	1.436	260
0.182	100	1.481	265
0.588	165	1.523	270
0.766	185	1.584	280
0.818	190	1.656	295
0.871	202	1.709	310
0.943	205	1.760	325
0.984	210	1.853	365
1.031	215	1.875	375
1.074	220	1.893	385
1.116	225	2.002	495
1.209	235	2.018	555
1.259	240	2.066	1395

Polybutene (97.31°C).

H(o)-H(T)(CM.)	TIME(MIN.)	H(o)-H(T)(CM.)	TIME(MIN.)
0.024	15	0.894	52
0.058	20	0.972	54
0.083	22	1.063	56
0.101	24	1.149	58
0.125	26	1.235	60
0.160	28	1.323	62
0.197	30	1.399	64
0.247	32	1.476	66
0.284	34	1.533	68
0.333	36	1.582	70
0.288	38	1.691	75
0.444	40	1.763	80
0.507	42	1.855	90
0.576	44	1.890	100
0.653	46	1.938	135
0.721	48	1.946	170
0.809	50		

Polybutene (98.47 °C).

H(o)-H(T)(CM.)	TIME(MIN.)	H(o)-H(T)(CM.)	TIME(MIN.)
0.008	10	0.816	74
0.024	20	0.864	76
0.056	30	0.915	78
0.073	32	0.974	80
0.088	34	1.033	82
0.108	36	1.092	84
0.127	38	1.140	86
0.154	40	1.207	88
0.174	42	1.266	90
0.195	44	1.311	92
0.218	46	1.371	94
0.247	48	1.416	96
0.284	50	1.465	98
0.321	52	1.499	100
0.353	54	1.575	105
0.391	56	1.635	110
0.422	58	1.678	115
0.471	60	1.716	120
0.515	62	1.750	125
0.560	64	1.776	130
0.607	66	1.785	135
0.653	68	1.795	140
0.703	70	1.819	150
0.761	72		

Polybutene (98.88 °C).

H(o)-H(T)(CM.)	TIME(MIN.)	H(o)-H(T)(CM.)	TIME(MIN.)
0.011	10	0.939	90
0.019	20	0.993	92
0.052	30	1.032	94
0.071	35	1.089	96
0.086	40	1.136	98
0.145	45	1.189	100
0.177	50	1.240	102
0.214	53	1.288	104
0.246	56	1.356	107
0.272	58	1.429	110
0.303	60	1.467	112
0.330	62	1.504	114
0.375	64	1.540	116
0.418	66	1.571	118
0.463	68	1.603	120
0.494	70	1.673	126
0.526	72	1.710	130
0.574	74	1.784	140
0.627	77	1.858	155
0.695	80	1.891	165
0.748	82	1.908	180
0.791	84	1.928	205
0.847	86	1.937	250
0.886	88		

Polybutene (100.62°C).

H(o)-H(T)(CM.)	TIME(MIN.)	H(o)-H(T)(CM.)	TIME(MIN.)
0.003	35	I.384	I90
0.027	50	I.464	I95
0.061	65	I.598	205
0.III	75	I.667	210
0.I36	80	I.742	215
0.I6I	85	I.786	220
0.I93	90	I.84I	225
0.227	95	I.883	230
0.265	I00	I.9I4	235
0.309	I05	I.948	240
0.356	II0	I.979	245
0.400	II5	2.006	250
0.459	I20	2.02I	255
0.506	I25	2.058	265
0.578	I30	2.I56	360
0.63I	I35	2.223	4I0
0.684	I40	2.270	495
I.245	I80	2.285	555
I.3I5	I85	2.36I	I275

Polybutene (101.54°C).

H(o)-H(T)(CM.)	TIME(MIN.)	H(o)-H(T)(CM.)	TIME(MIN.)
0.027	45	I.32I	230
0.330	I35	I.385	235
0.470	I50	I.438	240
0.39I	I40	I.665	260
0.504	I55	I.72I	265
0.604	I65	I.768	270
0.663	I70	I.820	275
0.704	I75	I.868	280
0.756	I80	I.9II	285
0.807	I85	I.960	290
0.853	I90	I.993	295
0.9I5	I95	2.032	300
0.972	200	2.058	305
I.050	205	2.I02	3I5
I.099	2I0	2.I50	325
I.I55	2I5	2.I80	335
I.220	220	2.476	I385
I.266	225		

Polybutene (105.81°C).

H(o)-H(T)(CM.)	TIME(MIN.)	H(o)-H(T)(CM.)	TIME(MIN.)
0.009	60	0.684	585
0.015	90	0.725	600
0.022	120	0.771	620
0.031	150	0.804	630
0.078	240	0.845	645
0.109	270	0.865	650
0.137	300	0.894	660
0.169	330	0.919	670
0.197	350	0.954	680
0.218	370	0.984	690
0.257	390	1.022	702
0.306	420	1.045	710
0.369	452	1.075	720
0.397	470	1.114	735
0.506	516	2.435	1450
0.525	525	2.505	1510
0.554	540	2.529	1570

Polybutene (107.08°C).

H(o)-H(T)(CM.)	TIME(MIN.)	H(o)-H(T)(CM.)	TIME(MIN.)
0.023	55	1.100	1595
0.029	205	1.142	1620
0.042	430	1.175	1645
0.088	595	2.512	2935
0.111	655	2.567	3095
0.863	1435	2.595	3215
0.897	1465	2.614	3295
0.944	1495	2.690	4285
0.983	1525		

Poly-(ethylene oxide) (58.23°C) S=14%.

H(o)-H(T)(CM.)	TIME(MIN.)	H(o)-H(T)(CM.)	TIME(MIN.)
0.056	2	2.156	54
0.107	4	2.260	56
0.184	7	2.355	58
0.257	10	2.457	60
0.345	13	2.552	62
0.431	16	2.641	64
0.530	19	2.726	66
0.642	22	2.817	68
0.710	24	2.900	70
0.784	26	3.061	74
0.868	28	3.427	84
0.950	30	3.592	89
1.048	32	3.710	93
1.140	34	3.796	96
1.236	36	3.895	100
1.324	38	4.043	106
1.420	40	4.133	110
1.523	42	4.253	116
1.631	44	4.327	120
1.738	46	4.471	129
1.844	48	4.560	135
1.949	50	4.629	140
2.054	52	6.034	1580

Poly-(ethylene oxide) (53.77°C).

H(o)-H(T)(CM.)	TIME(MIN.)	H(o)-H(T)(CM.)	TIME(MIN.)
0.017	3	3.587	72
0.036	6	3.732	74
0.064	10	3.874	76
0.128	15	3.952	77
0.184	18	4.017	78
0.261	21	4.148	80
0.353	24	4.275	82
0.466	27	4.400	84
0.604	30	4.512	86
0.702	32	4.624	88
0.804	34	4.728	90
0.922	36	4.885	93
1.049	38	4.983	95
1.180	40	5.071	97
1.309	42	5.216	100
1.447	44	5.306	102
1.584	46	5.424	105
1.734	48	5.507	107
1.882	50	5.609	110
2.043	52	5.678	112
2.199	54	5.773	115
2.347	56	5.862	118
2.508	58	5.997	123
2.663	60	6.066	126
2.741	61	6.159	130
2.822	62	6.281	136
2.968	64	6.350	140
3.048	65	6.422	145
3.126	66	6.798	190
3.209	67	6.867	210
3.284	68	6.899	230
3.363	69	6.944	265
3.430	70	6.963	310

Poly-(ethylene oxide) (51.14°C).

H(o)-H(T)(CM.)	TIME(MIN.)	H(o)-H(T)(CM.)	TIME(MIN.)
0.025	3	4.657	39
0.114	6	4.722	40
0.164	7	4.779	40
0.223	8	4.831	41
0.296	9	4.898	41
0.474	11	4.954	42
0.583	12	5.010	42
0.699	13	5.059	43
0.822	14	5.116	43
1.121	16	5.172	44
1.272	17	5.215	44
1.425	18	5.265	45
1.505	19	5.310	45
1.590	19	5.357	46
1.670	20	5.485	47
1.751	20	5.561	48
1.828	21	5.719	50
1.920	21	5.792	51
1.998	22	5.858	52
2.086	22	5.922	53
2.422	24	5.981	54
2.511	25	6.038	55
2.595	25	6.087	56
2.677	26	6.142	57
2.756	26	6.189	58
2.840	27	6.234	59
2.926	27	6.325	60
3.010	28	6.413	61
3.095	28	6.453	62
3.174	29	6.481	63
3.339	30	6.515	64
3.487	31	6.546	65
3.642	32	6.575	66
3.717	32	6.598	67
3.788	33	6.643	69
3.857	33	6.713	72
3.929	34	6.758	75
3.993	34	6.815	79
4.065	35	6.858	85
4.140	35	6.893	90
4.206	36	6.917	95
4.277	36	6.964	115
4.474	38	6.985	140
4.527	38	7.007	185
4.594	39	7.046	300

Polystyrene (180.0°C).

H(o)-H(T)(CM.)	TIME(MIN.)	H(o)-H(T)(CM.)	TIME(MIN.)
0.026	23	0.936	98
0.056	28	1.011	103
0.098	33	1.099	110
0.148	38	1.139	113
0.193	43	1.188	118
0.241	48	1.240	123
0.299	53	1.287	128
0.368	58	1.336	133
0.433	63	1.384	138
0.499	68	1.431	143
0.579	73	1.464	148
0.651	78	1.491	153
0.884	94	1.674	893

Polystyrene (203.4°C).

H(o)-H(T)(CM.)	TIME(MIN.)	H(o)-H(T)(CM.)	TIME(MIN.)
0.077	60	0.551	315
0.106	75	0.634	347
0.138	100	0.672	360
0.168	115	0.757	393
0.185	125	0.793	406
0.234	165	0.834	420
0.285	195	0.859	430
0.310	210	0.881	440
0.409	255	0.912	450
0.439	270	2.061	1890
0.488	290		

Polystyrene (209.7°C).

H(o)-H(T)(CM.)	TIME(MIN.)	H(o)-H(T)(CM.)	TIME(MIN.)
0.905	885	1.580	1445
1.081	990	2.171	2315
1.121	1025	2.255	2375
1.265	1145	2.259	2435
1.322	1235	2.262	2525
1.503	1385	2.299	2630
1.537	1415	2.315	2705

Polystyrene (186.8°C).

H(o)-H(T)(CM.)	TIME(MIN.)	H(o)-H(T)(CM.)	TIME(MIN.)
0.025	25	0.944	110
0.053	30	1.008	115
0.084	35	1.063	120
0.116	40	1.314	145
0.148	45	1.356	150
0.188	50	1.403	155
0.236	55	1.574	183
0.703	92	1.626	195
0.741	95	1.643	205
0.809	100	1.645	210
0.879	105	1.656	1030

Polystyrene (200.4°C).

H(o)-H(T)(CM.)	TIME(MIN.)	H(o)-H(T)(CM.)	TIME(MIN.)
0.022	40	0.787	245
0.039	60	0.807	255
0.064	75	0.890	275
0.086	85	0.968	290
0.117	100	1.042	305
0.158	115	1.127	325
0.203	130	1.199	342
0.239	140	1.234	360
0.288	155	1.275	370
0.351	170	1.313	380
0.413	185	1.448	400
0.458	195	1.849	1160
0.504	205		

Polystyrene (175.0°C).

H(o)-H(T)(CM.)	TIME(MIN.)	H(o)-H(T)(CM.)	TIME(MIN.)
0.030	10	0.884	90
0.063	15	0.963	95
0.098	20	1.030	100
0.133	25	1.100	105
0.176	30	1.171	110
0.218	35	1.229	115
0.251	40	1.283	120
0.292	45	1.334	125
0.322	47	1.378	130
0.355	50	1.414	135
0.546	65	1.449	140
0.606	70	1.534	150
0.684	75	1.583	160
0.762	80	1.632	175
0.824	85		

Polystyrene (149.06°C).

H(o)-H(T)(CM.)	TIME(MIN.)	H(o)-H(T)(CM.)	TIME(MIN.)
0.018	20	0.614	155
0.043	30	0.971	205
0.100	40	1.027	215
0.128	50	1.089	225
0.155	60	1.264	260
0.189	70	1.319	275
0.429	125	1.371	300
0.492	135	1.494	360
0.550	145	1.526	390

Polystyrene (159.3°C).

H(o)-H(T)(CM.)	TIME(MIN.)	H(o)-H(T)(CM.)	TIME(MIN.)
0.040	30	0.861	130
0.088	40	0.972	140
0.141	50	1.075	150
0.198	60	1.164	160
0.285	71	1.243	170
0.357	80	1.320	180
0.448	90	1.391	190
0.540	100	1.440	200
0.589	105	1.483	210
0.643	110	1.519	220
0.700	115	1.553	230
0.755	120	1.575	260
0.801	125		

Polystyrene (171.18°C).

H(o)-H(T)(CM.)	TIME(MIN.)	H(o)-H(T)(CM.)	TIME(MIN.)
0.029	15	1.034	105
0.072	20	1.101	110
0.125	26	1.155	115
0.170	31	1.219	120
0.214	35	1.286	125
0.272	40	1.332	130
0.323	45	1.379	135
0.362	50	1.425	140
0.412	55	1.468	145
0.462	60	1.517	150
0.529	65	1.546	155
0.582	70	1.570	160
0.650	75	1.619	170
0.705	80	1.677	180
0.773	85	1.695	190
0.841	90	1.720	200
0.908	95	1.729	210
0.969	100		

I. Hillier Ph.D.
1964.

(*Reprinted from Nature, Vol.* 198, *No.* 4877, *pp.* 257–258, *April* 20, 1963)

QUANTUM EFFECTS IN DILUTE SOLUTIONS

By IAN H. HILLIER and DR. JOHN WALKLEY
Department of Chemistry, Imperial College of Science and Technology, London, S.W.7

THE possibility that quantum effects are observed in the thermodynamic solubility properties of hydrogen and deuterium is suggested by two recent investigations. The first of these[1] is the examination of the saturation solubility properties of the two gases in a wide range of non-polar solvents. The second[2] is the measurement of their partial molar volumes, but in a more restricted solvent range. The data pertinent to these investigations are given in Table 1, and it may be seen that even at room temperatures a measurable difference in properties is found for the two gases in a given solvent.

Table 1. MOLE FRACTION SATURATION SOLUBILITY (x_2) AND PARTIAL MOLAR VOLUME ($\bar{V}_2$ C.C./MOLE)

	Hydrogen		Deuterium	
Solvent	$x_2 \times 10^4$	$\bar{V}_2$	$x_2 \times 10^4$	$\bar{V}_2$
C_7F_{16}	14·007	54·4	14·427	52·9
CCl_4	3·193	—	3·280	—
C_6H_6	2·578	35·3	2·655	32·7

In the fluorocarbon solvent the two solutes exhibit a relatively high solubility and a large partial molar volume whereas in benzene solvent the lower saturation solubility is accompanied by a smaller partial molar volume. Such differences are in accord with the concept that the gas molecule sits in a 'cavity' in solution, such a model having been exploited recently in the application of a classical free volume[3] or cell theory[4] to the prediction of the solubility properties of a wide range of solutes in non-polar solvents. The theories were necessarily restricted to classical systems as the prediction of the properties of a solute molecule of sufficiently small mass as to exhibit quantum behaviour awaits the evaluation of a cell model for a system obeying quantum statistical mechanics. The evaluation of the approximate uniform potential model for a single component quantum system shows this to be possible[5] and the extension to the full Lennard-Jones cell model is now in hand. It is useful, however, to investigate the theoretical likelihood of quantum behaviour in dilute solutions, and the recent investigation of the cell model for a system of quantum hard spheres[6] allows this to be done.

In a recent paper, Smith and Walkley[7] have considered the mixing process for a dilute solution to take place through the formation of a hypothetical solute liquid of internal pressure identical to that of the solvent. The analogy to the Hildebrand regular solution process[8] for dilute solutions is obvious and will be discussed in a subsequent paper. The advantage of the proposed 'equivalent internal pressure' theory is that the formation of the solution, the mixing of the hypothetical liquid solute with the solvent, requires no further volume change of the system. It follows, then, that the molal volume of the solute in the hypothetical liquid state must be identical with that of the partial molar volume of the solute in the final solution, and this equivalence acts as a good criterion for the validity of the model. An exceptionally good agreement between the theoretical molal volume and the experimentally measured partial molar volume was observed for a wide range of (classical) solute-solvent system[7].

The equation of state for this hypothetical 'equivalent internal pressure' liquid solute was developed from a uniform potential model and may be written:

$$p = NkT(\partial \ln V_f/\partial v)_T - [T(\partial p/\partial T)_v - p]$$

where the internal pressure of the solvent is defined as:

$$(\partial E/\partial V)_T = [T(\partial p/\partial T)_v - p]$$

The full derivation of the classical equation of state is discussed elsewhere[7], the free volume integral (V_f) reduces to that for a system of molecules of hard sphere diameter σ confined to a cell by neighbouring molecules equilibrium distance a apart:

$$V_f = \int_0^{(a-\sigma)} 4\pi r^2 dr = 4\pi(a-\sigma)^3/3$$

The final equation of state may be written:

$$(V/V_0) = \left[1 - \frac{R}{V}(\partial p/\partial T)_v^{-1}\right]^{-3}$$

where the definitions $V_0 = N\sigma^3$ and $V = Na^3$ are used. It is obvious that as V_0 and $(\partial p/\partial T)_v$ are uniquely defined by the chosen solute-solvent system then the molal volume (V) may be calculated.

The foregoing equation of state may be obtained by balancing $T(\partial p/\partial T)_v$ against the pressure generated by a system of hard sphere molecules[7]. If this is done for a system of hard spheres behaving quantum mechanically the free volume integral must be replaced by the Slater sum:

$$Q_{Qu} = \sum_i g_i \exp[-Ei/kT]$$

where $H_i\psi_i = E_i\psi_i$, H_i being the total Hamiltonian for the given molecule confined to its cell, and E_i the total energy of the molecule in the i^{th} eigen-state. The equation of state for the system becomes[7]:

$$[v(\partial p/\partial T)_v/Nk] = \left\{ \frac{\sum_i 2[An_i^2/T(V^{*\frac{2}{3}} - 1)]\,(V^*)^{\frac{1}{3}}\,[\exp - An_i^2/T(V^{*\frac{2}{3}} - 1)^2}{\sum_i \exp - An_i^2/T(V^{*\frac{2}{3}} - 1)^2} \right\}$$

The derivation of this equation of state was given in a recent paper[6], where it was shown that it was a valid approximation to replace the spherical cell by a cubical cell of equivalent free volume, that is, of side-length L where:

$$L^3 = (4\pi/3)\,(V^{\frac{1}{3}} - V_0^{\frac{1}{3}})^3$$

allowing the quantum partition function to be written:

$$Q_{Qu} = \left[\sum_i \exp\,[-An_i^2/TL^2]\right]^3$$

where $A = (h^2/8\ mk)$ and $n_i = 1, 2, 3 \ldots \infty$.

The equation of state given here for a hypothetical liquid (quantum) solute may be solved for V, ($V^* = V/V_0$), for given values of $(\partial p/\partial T)_v$ and V_0 at any required temperature. Assuming the hard sphere diameter of hydrogen and deuterium to be $\sigma = 2{\cdot}92$ Å the classical equation of state may be solved to give the molal volume (V_{Cl}) at 25° C as 39·7 c.c./mole in the fluorocarbon and 30·5 c.c./mole in benzene solvent. It is possible to regard V_0 as the volume of the solid at a low temperature, given as 23 c.c./mole for hydrogen and 20 c.c./mole for deuterium. From the classical equation of state using these values of V_0, that is to introduce a quantum difference through V_0, the molal volume values (V_{v_0}) for hydrogen and deuterium are predicted as 51 and 48 c.c./mole, in the fluorocarbon and 40 and 37 c.c./moles in benzene, respectively. From the quantum equation of state, assuming $V_0 = N\sigma^3 = 15{\cdot}11$ c.c./mole for both hydrogen and deuterium, the molal volumes are 45·7 and 44·3 c.c./mole in the fluorocarbon and 35·8 and 33·4 c.c./mole in benzene solvent. The foregoing results are given in Table 2 together with the experimental partial molar volume data.

The good agreement between the predicted molal volume (V_{Cl}) and the experimental partial molar volume ($\overline{V}_2$) for solutes behaving according to classical statistics[7]

Table 2. Molal Volume and Partial Molar Volume Data for Hydrogen and Deuterium at 25° C

System	V_{Cl}	V_{v_0}	V_{Qu}	$\overline{V}_2$ (exp)
H_2–C_7F_{16}	39·7	51	45·7	54·4
D_2–C_7F_{16}	39·7	48	44·3	52·9
H_2–C_6H_6	30·5	40	35·8	35·3
D_2–C_6H_6	30·5	37	33·4	32·7

contrasts sharply with the complete lack of agreement between V_{Cl} and $\bar{V}_2$ (exp) for the solutes hydrogen and deuterium. The possibility of quantum behaviour is emphasized by the comparison of both V_{r_0} and V_{Qu} with $\bar{V}_2$. The agreement of V_{Qu} with the experimental partial molar volume for the two gases in benzene solvent lies within the experimental error and in the fluorocarbon solvent the somewhat lower V_{Qu} values reflect a tendency noted for classical systems that in this solvent the predicted molal volume is observed to be somewhat smaller than the experimental partial molar volume.

It is to be expected that quantum effects of this nature are more likely to occur at lower temperatures, and in investigation of the thermodynamic properties of hydrogen and deuterium in liquid argon, Halsey has again showed possible quantum differences to exist[9]. An accurate value of the internal pressure of liquid argon is not available, but an estimate of this may be obtained from the energy of vaporization[8]. Assuming the energy of vaporization to be 1·39 kcal at 87° K a value for $T(\partial p/\partial T)$ of 49 cal/c.c. is obtained at this temperature. Using the quantum equation of state, the predicted molal volumes of the hypothetical liquid solute are 31·2 c.c./mole for hydrogen and 29·4 c.c./mole for deuterium. These values compare most favourably with the reported experimental partial molar volume value of 30 c.c./mole for both hydrogen and deuterium, as it is unlikely that the difficulties of the experimental measurement at these low temperatures would allow the predicted quantum differences to be observed.

We thank the University of London Computer Unit for the use of the Ferranti *Mercury* Computer on which the quantum equation of state calculations were made.

[1] Cook, M. W., Hanson, D. N., and Alder, B. J., *J. Chem. Phys.*, **26**, 748 (1957).
[2] Hildebrand, J. H., and Walkley, J., *J. Amer. Chem. Soc.*, **81**, 4439 (1959).
[3] Kobatake, Y., and Alder, B. J., *J. Chem. Phys.*, **66**, 720 (1962).
[4] Walkley, J. (to be submitted to *Trans. Faraday Soc.*).
[5] Hillier, I. H., and Walkley, J. (unpublished results).
[6] Hillier, I. H., and Walkley, J., *Trans. Faraday Soc.* (in the press).
[7] Smith, E. B., and Walkley, J., *J. Phys. Chem.*, **66**, 597 (1962).
[8] Hildebrand, J. H., and Scott, R. L., *Regular Solutions* (Prentice Hall, Inc., 1962).
[9] Volk, H., and Halsey, G. D., *J. Chem. Phys.*, **33**, 1132 (1960).

Printed in Great Britain by Fisher, Knight & Co., Ltd., St. Albans.

I. Hillier.
Ph.D. 1964.

A QUANTUM HARD-SPHERE EQUATION OF STATE

By

I. Hillier and J. Walkley

Offprinted from the *Transactions of The Faraday Society*,
No. 485, Vol. 59, Part 5, May, 1963

A Quantum Hard-Sphere Equation of State

By Ian Hillier and John Walkley

Dept. of Chemistry, Imperial College, London, S.W.7

Received 16*th August*, 1962

Compressibility data for hydrogen, deuterium, neon and argon have been computed using a quantum hard-sphere cell model over a wide range of temperature and density. Values for the exact spherical cell model and for the more easily computed, though approximate, cubical cell model have been obtained and compared. A comparison is also made with the classical hard-sphere cell model.

The investigation of a cell-model quantum equation of state for a system of hard-sphere molecules arises as part of a more general study of the P—V—T and thermodynamic behaviour of molecules obeying quantum-statistical mechanics. Previous investigations have been confined to the development of a quantum virial equation of state [1] and are thus limited to a region of low density. Recently, Levelt and Hurst [2] have investigated the possibility of developing a quantum-mechanical cell model for particles interacting with a Lennard-Jones 6 : 12 potential. Hillier and Walkley [3] have examined both a uniform potential model and a similar model but with a perturbation term, both models through their simplicity allowing thermodynamic data to be obtained over a wide range of temperature and density.

The imposition of a formal interaction potential and the limitation to pair-wise interactions greatly restricts the value of equation-of-state data developed from a cell model. Smith and Alder [4] have shown that such models may be improved by the use of a perturbation theory which relates the equilibrium properties of one system to those of a system whose molecules interact with a slightly different potential. For the high density region it is pertinent to use a free volume theory and apply some appropriate perturbation potential to this. The free-volume theory for a system of hard spheres is exact under conditions of high density [5] and so acts as a good basis potential for a perturbation calculation. The present calculations are concerned only with the evaluation of the free-volume theory for a system of quantum hard spheres as this allows an examination of the assumptions to be used in the extension of the model and indicates the range of conditions over which it is necessary to use quantum-statistical mechanics.

The solution for the energy levels from the wave equation describing a particle moving in a potential field in a spherical cell can be complicated and it is often not possible to obtain an analytical solution. A simplification by Hamann [6] is to replace the spherical cavity by a square-potential box of equivalent volume thus simplifying the evaluation of the energy levels. For any realistic potential it is difficult to assess the validity of this approximation as superimposed upon the difficulty of determining the effective spherical potential cell size is the use of a different expression for energy eigenvalues and the possibility that the use of a cubic box limits the accessible volume giving rise to a higher pressure term. The hard-sphere model allows not only an exact solution of both the spherical and cubical approximations but also the same free volume can be used in both cases and a comparison over a wide range of temperature and density can be made.

FUNDAMENTAL THEORY

For a classical system of molecules the kinetic energy $\sum_i p_i^2/2m$ and the potential energy $\phi(r^N)$ contributions to the overall Hamiltonian may be considered separately, only the latter term depending upon the configuration of all the particles of the system. Integrating over the momenta, the configurational partition function becomes

$$Q_N = (N!)^{-1} \int \exp\left[-\phi(r^N)/kT\right] \mathrm{d}\tau^N,$$

allowing the complete partition function for a system of classical particles to be written

$$Z_{\mathrm{Cl}} = (2\pi mkT/h^2)^{3N/2} Q_N.$$

The theory fundamental to the development of the quantum partition function is discussed in the study of the uniform potential model;[3] only the necessary outlines will be mentioned here. For a system obeying quantum-statistical mechanics, it is not possible to separate the total Hamiltonian for the system into a kinetic and potential energy term. The system can only be represented by a wave function $\psi(r^N, t)$ defined by the appropriate Schroedinger equation, and the partition function must be formulated in terms of the total Hamiltonian operator. If, however, the energy eigenfunctions are so chosen that $H\psi_i = E_i\psi_i$, where E_i is the total energy of the ith eigen state, then the partition function can be written as the simple " sum-over-states ",

$$Z_{\mathrm{Qu}} = \sum_i g_i \exp\left(-E_i/kT\right),$$

where g_i is the degeneracy factor.[7]

The equation of state for the system can be developed from the volume derivative of the partition function,

$$p_{\mathrm{cl}} = kT(\partial \ln Q_N/\partial V)_T.$$

The quantum pressure term, evaluated similarly, is

$$p_{\mathrm{Qu}} = kT(\partial Z_{\mathrm{Qu}}/\partial V)_T/Z_{\mathrm{Qu}}.$$

the volume derivative, for the present quantum model, being evaluated from the functional expression for the energy levels.

FREE-VOLUME EQUATION OF STATE

For a system of hard sphere molecules of diameter σ, the interaction potential energy $\phi(r)$ of a molecule within a spherical cell with its environment is given by

$$\phi(r) = 0, \quad 0 \leqslant r < (a-\sigma),$$
$$\phi(r) = \infty, \quad r > (a-\sigma),$$

where r is the distance of the molecule from the centre of the cell. a is the equilibrium distance between neighbours, related to the volume per molecule by $v = a^3$, and $v_0 = \sigma^3$.

With the usual assumptions of a cell theory [8] the partition function for a system of classical particles is

$$Q_N = (4\pi/3)(v^{\frac{1}{3}} - v_0^{\frac{1}{3}})^3$$

and the hard-sphere equation of state may be written as

$$pV/NkT = 1 + (v^{*\frac{1}{3}} - 1)^{-1},$$

where v^* is the reduced volume defined for a system of hard spheres, viz., $v^* = v/v_0$.[11]

In the above development the configurational integral is considered as the product of one-particle integrals, evaluated for one particle per cell. For the development of the quantum equation of state, a similar one-particle theory will be assumed and the Schroedinger equation for one particle restricted to a spherical cell solved for the necessary expression for the energy levels. For the hard-sphere model, by transforming the wave function to appropriate polar co-ordinates, the solutions to the equation may be written $\psi = AP_\rho^{|m|}(\cos\theta)\exp(im\phi)(1/r)J_{(\rho+\frac{1}{2})}(Kr)$, where $K = (2mE)^{\frac{1}{2}}/\hbar$, $P_\rho^{|m|}$ is an associated Legendre function and $J_{(\rho+\frac{1}{2})}$ is a Bessel function. The further condition that at the walls of the cell $\psi = 0$ (when $r = R$) imposes the restriction upon K that $J_{(\rho+\frac{1}{2})}(KR) = 0$. The energy levels are thus given by

$$E = (h^2C_\rho/8mR^2),$$

where R is the radius of the effective cavity and C_ρ is obtained numerically from the zeros of the half-integral order Bessel function.[12] The degeneracy of each level is $(2\rho+1)$, each value of ρ giving rise to an infinite number of energy levels. In practice, it was sufficient to include only 10 secondary quantum levels for any given ρ value, the convergence in these levels being extremely rapid.

The quantum partition function for a hard-sphere molecule in a spherical cavity can thus be written as

$$Z_{Qu} = \sum_{\rho=1}^{\infty}(2\rho+1)\exp(-h^2C_\rho/8mkTR^2),$$

where the radius of the effective quantum cell is given by

$$R = (v^{\frac{1}{3}} - v_0^{\frac{1}{3}}).$$

Rewriting the partition function in the form

$$Z_{Qu} = \sum_{\rho=1}^{\infty}(2\rho+1)\exp[-AC_\rho/T(V^{\frac{1}{3}} - V_0^{\frac{1}{3}})^2],$$

the compressibility term becomes

$$\frac{pV}{NkT} = \frac{\sum_\rho (2/3)(2\rho+1)(AC_\rho/T)(V^{\frac{1}{3}} - V_0^{\frac{1}{3}})^{-3}(V^{\frac{1}{3}})\exp[-AC_\rho/T(V^{\frac{1}{3}} - V_0^{\frac{1}{3}})^2]}{\sum_\rho (2\rho+1)\exp[-AC_\rho/T(V^{\frac{1}{3}} - V_0^{\frac{1}{3}})^2]}.$$

This expression is most easily evaluated in terms of the reduced parameters $T^* = kT/\varepsilon$ and $V^* = V/V_0$;

$$\frac{pV}{NkT} = \frac{\sum_\rho (2/3)(2\rho+1)(D^*C_\rho/T^*)(V^{*\frac{1}{3}} - 1)^{-3}(V^{*\frac{1}{3}})\exp[-D^*C_\rho/T^*(V^{*\frac{1}{3}} - 1)^2]}{\sum(2\rho+1)\exp[-D^*C\rho/T^*(V^{*\frac{1}{3}} - 1)^2]}$$

where D^* is a dimensionless parameter defined as $D^* = (h^2/8m\varepsilon)(V_0)^{-\frac{2}{3}}$, where ε is an energy reduction parameter, not strictly applicable to a hard-sphere system, but used to give a suitable temperature scale for computational purposes. This equation of state refers to a particle restricted to a spherical cavity but the model does not lend itself easily to mathematical manipulation.[3] A considerable simplification is obtained by replacing the free-volume spherical cavity by an equivalent cubical cavity, that is, to assume the particle is restricted to a cubical box of volume L^3, where L is defined as

$$L^3 = 4\pi(a-\sigma)^3/3 = 4\pi(V^{\frac{1}{3}} - V_0^{\frac{1}{3}})^3/3.$$

For a hard-sphere particle in a cubical box, again assuming that $\psi_i = 0$ at the walls of the box, the energy levels of the system are

$$E = E_x + E_y + E_z = (n_x^2 + n_y^2 + n_z^2)A/L^2,$$

where

$$A = (h^2/8m), \text{ and } n_{i(i=x,y,z)} = 1, 2, 3, 4, \ldots \infty.$$

Assuming symmetry within the box the quantum partition function can be written in a form analogous to that for a spherical cavity and is given in reduced parameters as

$$\mathcal{Z}_{\text{Qu}} = \{\sum_i g_i \exp\left[-C^* n_i^2/T^*(V^{*\frac{1}{3}} - 1)^2\right]\}^3,$$

where

$$C^* = (h^2/8m\varepsilon)\,(4\pi V_0/3)^{-\frac{1}{3}}.$$

The equation of state for a particle in a square cavity thus becomes

$$\frac{pV}{NkT} = \frac{\sum_i 2g_i[C^* n_i^2/T^*(V^{*\frac{1}{3}} - 1)^3](V^*)^{\frac{1}{3}} \exp\left[-C^* n_i^2/T^*(V^{*\frac{1}{3}} - 1)^2\right]}{\sum_i g_i \exp\left[-C_i^* n_i^2/T^*(V^{*\frac{1}{3}} - 1)^2\right]}.$$

The difference between this and the similar expression for a particle in a spherical cavity lies, essentially, in the degeneracy factory and the spacing of the energy levels.

RESULTS

The difference in the compressibility factor evaluated for the two models is illustrated in fig. 1, where a series of isotherms are plotted against $1/V^*$ for a quantum gas of mass 2 (hydrogen). In the evaluation of all data the force constant (ε/k) for a 6 : 12 Lennard-Jones intermolecular potential and the molecular diameter σ values are those listed by Hirschfelder, Curtiss and Bird.[9] In particular, the values used for hydrogen and deuterium are $\varepsilon/k = 37°\text{K}$, and $V_0 = N\sigma^3 = 15{\cdot}12$ cm^3/mole.

To evaluate the compressibility term, it is necessary to include sufficient energy levels in the " sum-over-states " that the addition of further terms does not appreciably alter the resulting value of pV/NkT. For the cubical cell model the formulation of the energy levels allows an accurate value of this term to be obtained over the whole temperature and density range studied. For computation, terms up to $n = 100$ were used, and all values of the compressibility factor are thus accurate to the fourth decimal place.

The difficulty in obtaining the zero-order values for the half-integral Bessel functions restricted the use of the spherical cavity model to a more limited temperature range. All data were evaluated for this model up to and including energy levels $\rho = 14$, $n = 10$, this limit being chosen such that convergence of the PV/NkT factor correct to four places of decimal for a particle of mass 2 was obtained for $V^* < 2{\cdot}0$ for temperatures $T^* < 10$, that is, for densities appropriate to the region in which the cell theory can itself be considered valid. For a particle of mass 4 (deuterium), an accurate evaluation to four decimal places can be claimed only for $V^* < 2{\cdot}0$ at temperatures $T^* < 5$. For values outside this range, the convergence becomes worse for increasing temperature and volume, and for the higher values of T^* and V^* studied, because of the lack of convergence, the compressibility factor for the spherical cavity model is too small by approximately 4 %.

The approach to classical behaviour with increase of temperature can also be seen from fig. (1) as the temperature-independent classical compressibility factor is also included. A plot of the compressibility factor against the reduced temperature for three values of the reduced volume (fig. 2), again illustrates the approach to

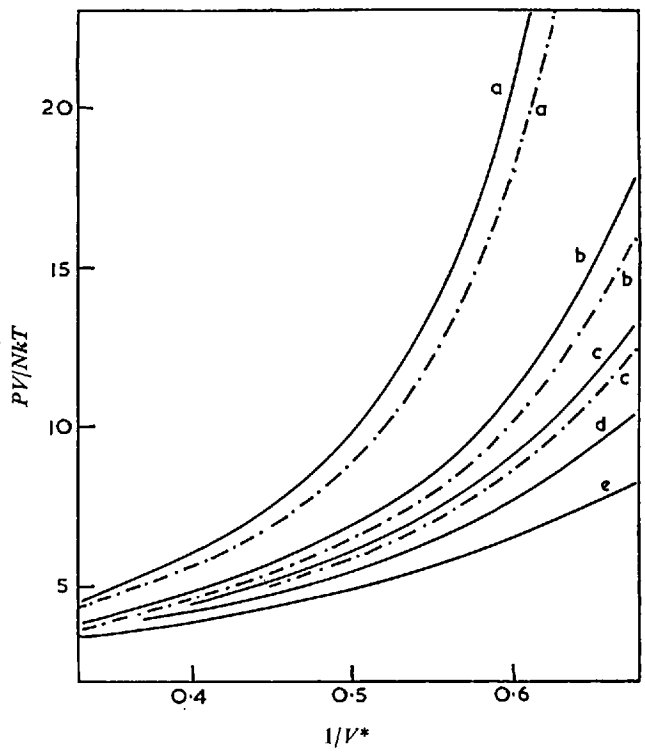


FIG. 1.—Quantum hard-sphere cell model. pV/NkT isotherm as a function of the reciprocal reduced volume. Cubical cavity approximation: full curve; spherical cavity: dash-dot curve.

Curve (*a*) hydrogen, 100°K;
(*b*) hydrogen, 300°K;
(*c*) hydrogen, 600°K;
(*c*) deuterium, 300°K;
(*d*) deuterium, 1000°K;
(*e*) classical hard-sphere cell model.

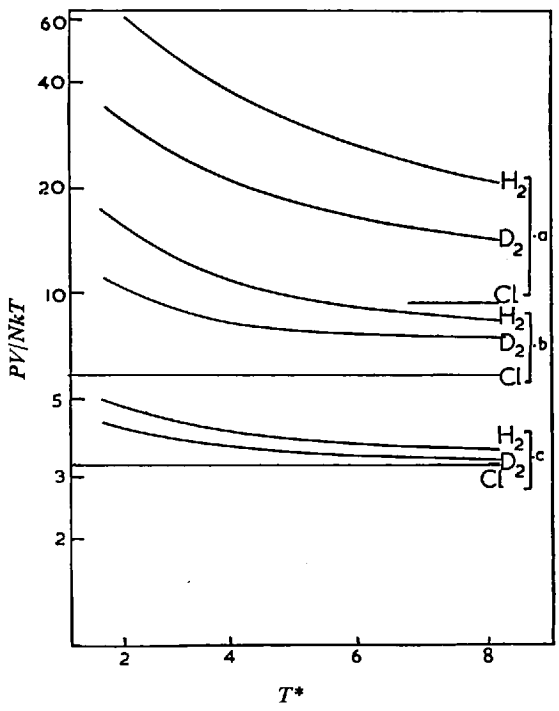


FIG. 2.—Comparison of quantum and classical hard-sphere cell model.
pV/NkT (constant volume) as function of the reduced temperature.

Curve (*a*) V^*, 1·398; (*b*) V^*, 1·701; (*c*) V^*, 2·970.

classical behaviour with increase of temperature. This plot also shows the " quantum difference " apparently existing between hydrogen and deuterium as evaluated for the spherical cavity model.

The slow convergence to classical behaviour (for a particle of mass 4 a considerable deviation from the classical term exists even at 1000°K for densities of about $V^* = 1{\cdot}6$) suggested an investigation of the quantum equation of state for a particle of mass sufficiently large as to be normally considered classical in its behaviour. The quantum-mechanical compressibility factor was evaluated for both a particle of mass 14 (neon) and of mass 40 (argon), and a plot of this term against $1/V^*$ over a small range of temperature and density is given in fig. 3 and 4 respectively. The

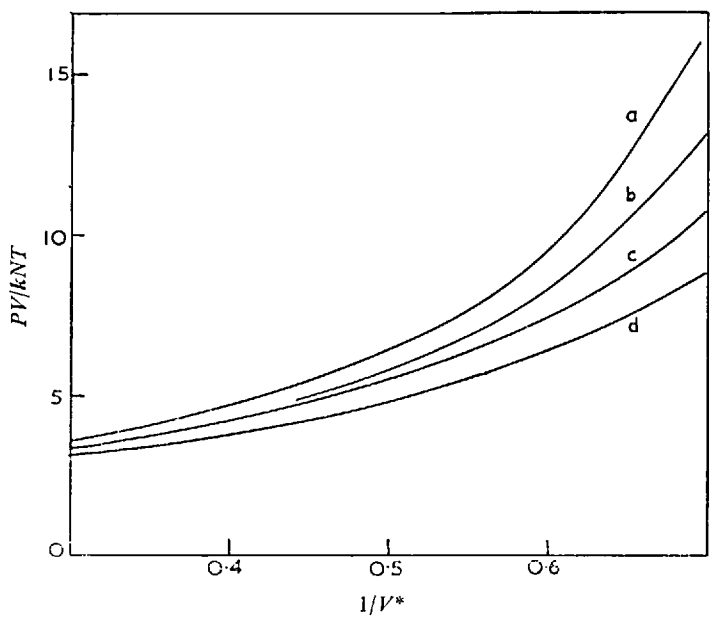


FIG. 3.—Quantum hard-sphere compressibility isotherms as functions of the reciprocal reduced volume; neon; (cubical cavity).
Curve (*a*) 50°K; (*b*) 100°K; (*c*) 200°K; (*d*) classical hard-sphere cell model.

density range covered for the argon data ($1{\cdot}2 < V^* < 2{\cdot}0$) is higher than for neon. The mass term for these gases was sufficiently large so that the equation-of-state data were evaluated for only the equivalent cubical cavity model, using energy levels to $n = 200$. For neon, a convergence for the pV/NkT term was obtained for the spherical cavity model at $T^* = 1{\cdot}5$; the agreement between this isotherm and the one derived from the cubical cavity model was better than for the lighter gases, suggesting that the use of the cubical cavity model was justified for the heavier gases at the higher temperatures.

DISCUSSION

From the comparison of the cubical and spherical cavity models in fig. 1, agreement between the two models is best at high temperature and low density and it is only where the low energy levels are heavily populated that a restrictive difference between the two models occurs. The close agreement between the two models coupled with the far greater ease of evaluation particularly under conditions of high

temperature (since the low density conditions are not suited to the use of a cell model) suggests that the cubical cell model may be regarded as a valid, and useful, approximation.

The distinction between the quantum and the classical expressions for the compressibility factor is that whereas the former is temperature dependent, through the construction of the energy levels, the latter is not. It is expected for an ideal gas that the quantum-mechanical " sum-over-states " approaches the classical integral at high temperatures. In the density region suitable to the use of a cell

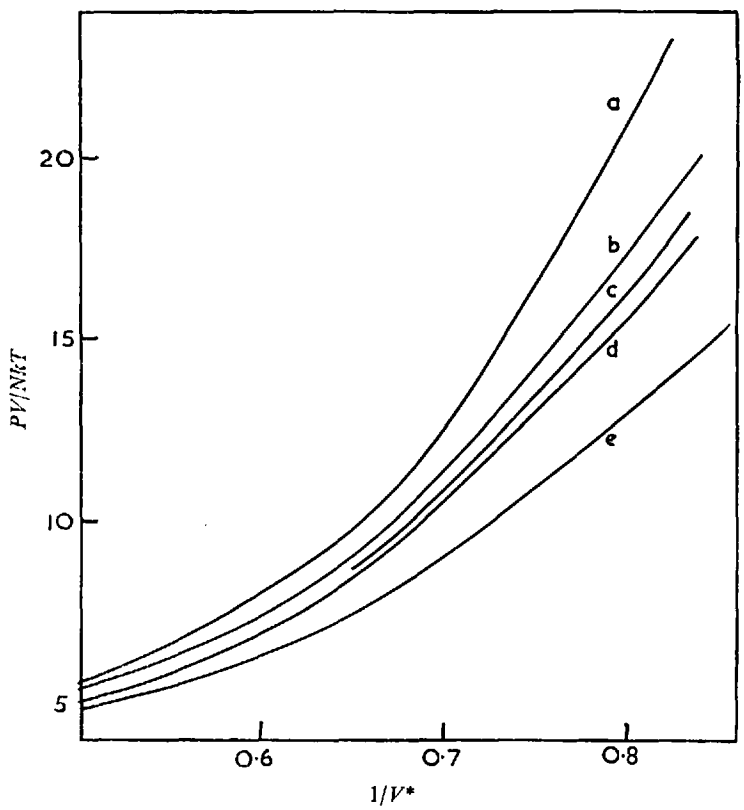


FIG. 4.—Quantum hard-sphere compressibility isotherm as a function of the reciprocal reduced volume; argon; (cubical cavity).

Curve (*a*) 50°K; (*b*) 100°K; (*c*) 150°K; (*d*) 200°K; (*e*) classical hard-sphere cell model.

model (roughly, liquid densities and greater) the compressibility factor for both hydrogen and deuterium does not fall to the classical value at temperatures even as high as 1000°K. The equation of state for a quantum system has been developed through the use of the Slater sum but no account has been taken of quantum statistics, that is, a Boltzmann distribution of energy has been assumed. At high density where the distance between the centres of molecules is of the order of a de Broglie wavelength the effect of the symmetry of the wave functions could be appreciable at even moderate temperatures (e.g., 100°K). At the temperatures considered here, the effect of quantum statistics is negligible and in no way invalidates the differences observed at high densities between the quantum and classical models. No comparison to experimental data has been made as it is not expected that the hard-sphere

model is sufficiently realistic over the temperature and density range covered by the experimental data at present available.

Quantum deviations for molecules of mass far greater than hydrogen and deuterium are usually ignored. The compressibility isotherms presented for neon and argon in fig. 3 and 4, respectively, show that a deviation from classical behaviour becomes significant even at liquid densities. For neon a considerable excess quantum pressure appears at temperatures as high as 200°K. This is not unexpected as the recent study by Bernardes [10] of the zero-point energies for the rare gases, based on a quantum-mechanical variational calculation using a Lennard-Jones 6 : 12 potential, suggests that appreciable quantum effects should be found in the equation-of-state data for these gases. Such effects have not previously been tested by an adequate theory or by experimental data, but the application of new high-pressure techniques, particularly shock-wave studies at low temperatures, should produce P—V—T data in the high-density region where deviations from classical behaviour should, apparently, become appreciable.

In the present use of a cell theory to obtain a quantum equation of state, the convergence to classical behaviour is less rapid than is predicted by the traditional expansion of the Slater sum as a power series in h^2. The data quoted in the present communication must be regarded as exact only for the model considered, that is, a system of hard-sphere molecules in which any given molecule is restricted to a cell formed by its neighbours. The general problem of the convergence to classical behaviour will be considered in a further communication, both for hard-sphere molecules and for molecules interacting with a more realistic potential.

The calculations were performed on the Mercury Computer of the University of London Computer Unit.

[1] Kirkwood, *Physic. Rev.*, 1933, **44**, 31.
[2] Levelt and Hurst, *J. Chem. Physics*, 1960, **32**, 96.
[3] Hillier and Walkley, submitted to *J. Chem. Physics*.
[4] Smith and Alder, *J. Chem. Physics*, 1959, **30**, 1190.
[5] Alder and Wainwright, *J. Chem. Physics*, 1957, **27**, 1208.
[6] Hamann, *Trans. Faraday Soc.*, 1952, **48**, 303.
[7] de Boer, *Reports Progr. Physics*, 1948, **12**, 305.
[8] Lennard-Jones and Devonshire, *Proc. Roy. Soc. A*, 1937, **163**, 53.
[9] Hirschfelder, Curtiss and Bird, *Molecular Theory of Gases and Liquids* (J. Wiley and Sons Inc., New York, 1954).
[10] Bernardes, *Physic. Rev.*, 1958, **112**, 1357.
[11] Wood, *J. Chem. Physics*, 1952, **20**, 1334.
[12] Kauzmann, *Quantum Chemistry* (Academic Press Inc., New York, 1957).

PRINTED IN GREAT BRITAIN AT
THE UNIVERSITY PRESS
ABERDEEN